THE DEVELOPMENT OF MASS SPECTROMETRIC METHODS FOR THE DETERMINATION OF THE CHEMICAL COMPOSITION OF COMPLEX MIXTURES RELEVANT TO THE ENERGY SECTOR AND THE DEVELOPMENT OF A NEW DEVICE FOR CHEMICALLY ENHANCED OIL RECOVERY FORMULATION EVALUATION

by

Katherine Elisabeth Wehde

A Dissertation

Submitted to the Faculty of Purdue University

In Partial Fulfillment of the Requirements for the degree of

Doctor of Philosophy

Department of Chemistry

West Lafayette, Indiana

December 2019

THE PURDUE UNIVERSITY GRADUATE SCHOOL

STATEMENT OF COMMITTEE APPROVAL

Dr. Suzanne Bart, Co-Chair

Department of Chemistry

Dr. Cliff Johnston, Co-Chair

Department of Agronomy

Dr. Gozdem Kilaz

School of Engineering Technology and Aviation Technology

Dr. Weiguo (Andy) Tao

Department of Biochemistry

Approved by:

Dr.Christine A. Hrycyna

Head of the Graduate Program

To my parents, Tom and Betsy, for unending love and inspiration

To my siblings, Samantha and Brian, for the best confidants I could ask for

To my best friend, Sean, for endless encouragement and laughs throughout the years

ACKNOWLEDGMENTS

First, I would like to express my gratitude to my first advisor, Professor Hilkka I. Kenttämaa, for giving me the opportunity to be a part of such an amazing research group, she has made me a better person and researcher. I would like to express my thanks for her trust in me to pursue many of my own ideas in my research projects and every opportunity she gave me. It was truly an honor to be her student. Next, I would like to acknowledge Dr. Suzanne Bart for her support and aid in the final months of my tenure at Purdue. Without her guidance, I would not have been able to complete this work. Additionally, I would like to thank Dr. Gozdem Kilaz for her unending encouragement and joyful research collaboration, Dr. Cliff Johnston who provided me challenging research projects and stretched my thinking process, and Dr. Rituraj Borgohaun, Timothy Henderson, Dr. Thomas Everett, and Dr. Nathan Schultheiss who provided unwavering support and guidance in all things petroleum. In addition to my graduate advisors, I would like to thank my undergraduate mentors Dr. J. Clay Harris and Dr. Noel Paul for teaching me to love the pursuit of knowledge in the face of research failures and setbacks. They changed how I viewed success and showed me how to enjoy failures and embrace all the things I do not know… yet. Also, to my undergraduate research group, thank you for supporting and encouraging me as I found myself as a scientist. Last but never least, my first chemistry teacher, John C. Cerauli at Warren Township for showing me the beauty of chemistry and the fun. I do not know any other teacher who jumps around the room like a ninja while teaching significant figures, creates a fireball that nearly lights the posters on the wall on fire, or who says “that stain was always there” when exploding Diet Coke with Mentos inside the classroom. Your enthusiasm encouraged me to take AP chemistry and, as they say, the rest is history.

There have been numerous Kenttämaa group members, past and present, that have been instrumental to my success. Dr. Joann Max, Dr. Xueming Dong, and Dr. Mark Romanczyk are truly people I have strived to exemplify in my research efforts. I have enjoyed collaborating on research and undertaking the challenges of graduate school with Leah Easterling, Dr. Edouard Niyonsaba, Jeremy Manheim, Jacob Milton, Lan Xu, Brent Moderager, Jorge Rameriez, Dr. Petr Vozka, Jeff Zhang, Tianru Jiang, Ethan Hillman, Alyssa Stiving and the other members of the Wysocki lab at The Ohio State University. I would like to express special gratitude to Dr. Edouard Niyonsaba who joined the Kenttämaa group alongside me from the Purdue PULSe program. We

have made it through hurdles alongside each other and I will always be grateful for the support and friendship you have given me. Finally, I need to thank others in lab for their contributions to my development as a scientist and a person, Dr. Mckay Easton, Dr. Yuan Jiang, Dr. Chunfen Jin, Dr. John Kong, Dr. Ravikiran Yerabolu, Laurance Cain, Rashmi Kumar, Xin Ma, Yuyan Zhang, Duanchen Ding, Dr. Josh Yu, Ben Lei, Jifa Zhang, Erlu Feng, Judy Liu, Wanru Li, Kawthar Zeyad Alzarieni, Nancy Fu, and all Kenttämaa members past and present.

To Stefan Irby, my love, it has truly been a blessing meeting you. I cannot imagine my life without you, you are my favorite. It has been a dream seeing our relationship and love grow over these crazy years and I cannot wait to see what the future holds for us. Together I know we can take on anything. Thank you for your unwavering support and the endless supply of laughs and joy. I would also like to thank the friends that I have made outside and within the research group during my time at Purdue University, Dr. Nicole Vike (my work wife), Dr. Joann Max (my work mom), Cynthia Alvardo, Dr. Franziska Lang and the Lang family, Kathryn Jacobson, Dr. Ezra Coughlin, Sarah Elder, Patrick Sweet (sweetie), Emma Lendy, Liesl Krause, Alex Clarissa, Greg Puckett, Elijah Roth, Dr. Kathleen Jeffery, and Juliet Prieto. Your friendship and the memories we made together were irreplaceable in getting me through these last years, you are all responsible for the fun and enjoyable moments during my time at Purdue. This experience would not have been the same without all of you and I will truly miss you. Mindy, Mark, and Keegan (K pup) Irby you have encouraged me since the day we met. I am grateful for the wonderful relationship and friendship we have developed; I look forward to more vacation adventures and Indy 500 trips together.

I must also thank my close friends for all their support and help, Brooke Anderson, Bryanne Vollmer, Abigail Grabile, Ariel Balske, Aubrey Meyer, Karen and Nina Silvasy, Patricia Capone, Clayton Casper, my Devilette dance family and Coach Stepek. Without all your encouragement, I would never have been able to reach my personal and educational goals. A special thanks to Sean Katherine MacLennan my soul sister and best friend. Words cannot accurately describe my gratitude for your love and support since we were 11 years old. You have been the key to me believing in myself and pushing the boundaries of what I believe I am capable of accomplishing both personally and professionally. You always seem to know how to keep me smiling and the best way to help no matter what was going on and how far away you were at the time. I am truly indebted to your kind soul, honest words, and mostly for the laughter and joy you bring to my life.

To the Lang family, thank you for housing me during the last months of this crazy adventure. Your support and guidance have helped me stay strong in the final hours of completing this work. I will always look back at our time as Roomies fondly and remember the laughs and visits to the park with the boys. Thank you for sharing your home with me.

Finally, my crazy, big, loving family both blood and extended. You have provided me with unlimited support throughout my life. Although sometimes you have no idea what I am talking about, when I chat about work, I appreciate you smiling and watching me talk about something I am passionate about. My parents, Tom and Betsy, thank you for showing me that it is possible to do anything if I set my mind to it and for pushing me to take a leap when needed. A big thank you to my brother Brian, sister Samantha, brother-in-law Derek, niece Addison, and nephew Grant for making time to visit and see me during my crazy schedule these past years. Thank you for always making me feel loved and important. A great appreciation for my extended family, aunts, uncles, cousins, my godmother Loraine, and those I choose to call family, Aunt Heidi, Uncle Ricky, Aunt Cynthia, and my godfather Harry for planning events and holidays around my schedule and making me always feel loved and supported.

I could likely fill ten more pages with the gratitude and love I feel, but I will stop myself and apologize to anyone I may have missed. Know that I am overwhelmed with joy and appreciation for all the people in my life. Whether you have played a brief role in my life or have been here for the long haul, I appreciate every moment that has made me into the woman I am today. I dedicate this work and my future accomplishments to all of you.

TABLE OF CONTENTS

LIST OF TABLES 11
LIST OF FIGURES 12
List of Equations 17
List of Abreviations 18
ABSTRACT 19
CHAPTER 1. INTRODUCTION AND THESIS OVERVIEW 20
1.1 Introduction 20
1.2 Thesis Overview 21
1.3 References 22
CHAPTER 2. INSTRUMENTAL AND EXPERIMENTAL ASPECTS OF TIME-OF-FLIGHT AND QUADRUPOLE MASS SPECTROMETERS INTRODUCTION 23
2.1 Introduction 23
2.2 Instrumentation and Experimental Aspects of Two-Dimensional Gas Chromatography/Electron Ionization High-Resolution Time-of-Flight Mass Spectrometry (GC×GC/(EI)TOF MS) 24
2.2.1 Two-Dimensional Gas Chromatography (GC×GC) 24
2.2.1.1 Components of Comprehensive GC×GC 25
2.2.1.2 Separation of Analytes in the GC Columns 26
2.2.1.3 Thermal Modulator 27
2.2.2 Mass Spectrometry 29
2.2.2.1 Electron Ionization 29
2.2.2.2 Time-of-Flight Mass Spectrometer 31
2.3 Instrumentation and Experimental Aspects of Gas Chromatography (GC)/Electron Ionization (EI) Quadrupole Mass Spectrometry (Q MS) 34
2.3.1 Ion Motion in the Quadrupole Mass Analyzer 34
2.3.2 Ion Detection 37
2.4 References 38
CHAPTER 3. GC×GC/(EI) TOF MS METHOD DEVELOPMENT FOR THE ANALYSIS OF FUELS AND BASE OILS INTRODUCTION 41

3.1 Introduction 41
3.2 Experimental 43
3.3 Results and Discussion 45
3.3.1 Development of an appropriate separation method for aviation fuels and fuel blending components 45
3.3.2 Determination of the chemical composition of aviation fuels and fuel blending components 58
3.3.3 Determination of the chemical composition of light base oils 61
3.4 Conclusions and Future Directions 63
3.5 References 65
CHAPTER 4. ASTM D2425 METHOD VERIFICATION: A FIRST LOOK AT BIAS, LIMIT OF DETECTION, AND LIMIT OF QUANTITATION FOR ASTM D2425 2019 UPDATED INSTRUMENTATION AND SAMPLE TYPE 68
4.1 Introduction 68
4.2 Experimental section 70
4.2.1 Instrumentation hardware 70
4.2.2 Methods 71
4.2.2.1 GC method conditions 71
4.2.2.1.1 Aromatic compound fraction of RJF 71
4.2.2.1.2 Saturated compound fraction of RJF and both saturated and aromatic compound fractions of GO 71
4.2.2.2 MS conditions 72
4.2.2.3 Data analysis 72
4.2.3 Samples 73
4.2.3.1 Sample sets for evaluation of instrument performance 73
4.2.3.2 Sample fractionation 74
4.2.3.3 Sample sets for evaluation of the 2019 updated ASTM D2425 method 74
4.2.4 Modifications to ASTM D2549-17 76
4.3 Results and Discussion 78
4.3.1 Instrument evaluation 78
4.3.1.1 MS tuning validation 78

4.3.1.2 Magnitude of the instrument signal as a function of the wt % of analyte 79
4.3.1.3 Instrument ruggedness 82
4.3.2 Method evaluation 86
4.3.2.1 Limit of detection 86
4.3.2.2 Limit of quantitation 87
4.3.2.3 Bias 88
4.4 Conclusions and Future Directions 89
4.5 References 91
CHAPTER 5. CREATION AND VALIDATION OF A TRANSPARENT MINIATURE COREFLOOD DEVICE FOR CHEMICALLY ENHANCED OIL RECOVERY (CEOR) FORMULATION TESTING 92
5.1 Introduction 92
5.2 Experimental 94
5.2.1 Materials 94
5.2.2 Methods 95
5.3 Results and Discussion 97
5.3.1 TMCF Device Design 97
5.3.2 TMCF Device Performance 100
5.3.2.1 TMCF Device Performance: Volume of Oil Recovered from Multiple Operators.. 103
5.3.2.2 TMCF Device Performance: Volume of Oil Recovered from Multiple Rockcores. 104
5.3.3 Semi-automated TMCF device 106
5.4 Conclusions and Future Directions 110
5.5 References 111
CHAPTER 6. MONITORING OILS' VOLATILE COMPOUND COMPOSITIONS DURING CHEMICALLY ENHANCED OIL RECOVERY FORMULATION TESTING ON BEREA ROCKCORES BY USING TWO-DIMENSIONAL GAS-CHROMATOGRAPHY WITH FLAME IONIZATION DETECTION (GC×GC-FID) 113
6.1 Abstract 113
6.2 Introduction 114

6.3 Experimental 116
6.3.1 Materials 116
6.3.1.1 Test One: Testing of Formulation One, Polymer 3230 and Surfactants S13-D, A-6, and L4-2 117
6.3.1.2 Test Two: Testing of Formulation Two, Polymer 3330 and Surfactant S13-C 118
6.3.2 Methods 118
6.3.2.1 Instrumentation Methods 119
6.3.2.2 Principal Component Analysis (PCA) 121
6.4 Results 122
6.4.1 CF Test: Oil Volume Recovery 122
6.4.2 GC×GC-FID Analysis 123
6.4.3 PCA results 125
6.5 Conclusions and Future Work 130
6.6 References 131
VITA 134
PUBLICATIONS 136

LIST OF TABLES

Table 3.1. Model compound retention times for the polar (x) primary GC column and nonpolar (y) secondary GC column compared to retention times for compounds in Jet-A which were determined to be the same compounds. 60

Table 3.2. Retention times in the primary (polar) column and the secondary (nonpolar) column for standard linear alkanes that have similar retention times as compounds in Base Oil A and Base Oil B. N/A denotes "not applicable" as a compound with this retention time was not found in the base oil samples. 63

Table 4.1. An internal standard, PFTBA, was used as the calibrant for targeted automatic tuning. The MS was tuned automatically five times and each time reached the ion abundances in the ranges specified below. 83

Table 4.2. Kurtosis values 84

Table 4.3. Skewness. Highly skewed: $x < -1$ or $x > 1$, Moderately skewed: $x < -0.5$ or $x > 0.5$, Approximately normal: $-0.5 < x < 0.5$ 85

Table 4.4. HOV test. If *p*-value > alpha, then the variance in the different groups are the same, accept the null hypothesis. An alpha of 0.01 was chosen to reduce the chance of Type I errors (false positives). 86

Table 5.1. Compilation of results obtained for a formulation containing surfactants S13D, A6, and L4-2 and polymer 3330 by using a TMCF device and the CF device. Each result was determined in comparison to the original oil in place (OOIP), except the percentage of the rockcore that was saturated with oil (%OOIP) which was determined in comparison with the rockcore's pore volume. Therefore, the results are given as a percent opposed to a volume so that the test parameters from the differently sized rockcores can be compared. 103

Table 6.1. Rockcore characteristics of the Berea rockcores used in this research. 117

Table 6.2. Experimental conditions of GC×GC-FID analysis. 121

Table 6.3. Oil distillate recovery volumes for each cEOR formulation CF test. 122

Table 6.4. The carbon atom range observed for each oil distillate sample in the GC×GC-FID. 124

LIST OF FIGURES

Figure 2.1. A schematic of the GC×GC/(EI) TOF MS instrument, Pegasus GC-HRT 4D, which features a folded flight path MS. The instrument parts are described in Section 2.2. 24

Figure 2.2. Components in the Agilent GC×GC system. 26

Figure 2.3. A) The thermal modulator with all components turned off. The eluates, blue dots, will flow freely through the modulator section. B) When a jet is turned on, the shape representing the jet will appear in green. New eluates marked in red and black are introduced as reference points for the four steps of thermal modulation. Step 1 of thermal modulation: Stage 1: The first cold jet is on, trapping and cryo-focusing the eluent coming from the primary column; Stage 2: The second hot jet is on, desorbing any eluates from the second stage of the modulator. C) Step 2 of thermal modulation: Stage 1: The first hot jet is on, releasing the partially cryo-focused eluent from stage 1 into the stage 2 of the modulator; Stage 2: The second cold jet is on to trap the incoming eluent and to cryo-focus the eluent. D) Step 3 of thermal modulation: Stage 1: The first cold jet is on, preventing any additional eluent from moving past stage 1; Stage 2: The second cold jet is on to further cryo-focus the eluent. E) Step 4 of thermal modulation: The first cold jet remains on preventing any additional eluent from moving past stage 1; Stage 2: The second hot jet is on and therefore it is releasing the cryo-focused eluent from the second stage of the modulator onto the second column for further chromatographic separation. The eluate marked with a red dot has now moved onto the secondary column for further chromatographic separation and is no longer in the modulator section of the instrument. 28

Figure 2.4. Electron ionization source where e- are fast moving electrons, A are analytes, $M^{+\bullet}$ are molecular radical cations, $F^{+\bullet}$ are fragment radical cations and F^{+} are fragment cations. 31

Figure 2.5. Schematic of the TOF section. The blue line represents the beam of ions on the flight path (20 m flight length). The first flight section is labeled in detail. The gridless mirrors are used to turn the ions flight trajectories, and the periodic lenses guide the ions through the proper flight path to the detector. 33

Figure 2.6. Schematic of the GC/Q MS, including an EI source, and an example of two ion trajectories, one that is detected (blue line) and one that will collide with one of the electrodes and is not detected (red line). 34

Figure 2.7. Graphic of quadrupole rods shown with alternating applied voltages such that one rod pair is positively charged, and one rod pair is negatively charged. The directional axes are also labeled: x-, y-, and z-axis. 35

Figure 2.8. The Mathieu stability diagram. The colored circles represent ions of different sizes. The *q*- and *a*-values of the ions are indicated on the x- and y-axis, respectively. All the ions indicated have stable trajectories in the quadrupole as their *a*- and *q*-values are shown in the stable region of the diagram, the checkered region (A). Therefore, the ions would successfully travel down the quadrupole towards the detector. If any ions had *a*- and *q*-values in the unstable region (B), they would not successfully reach the detector. 37

Figure 3.1. Jet-A sample analysis using normal-column configuration. The sample exhibits a phenomenon known as wrap-around, highlighted in the red box. Wrap-around is noted because the analytes appear to elute before the solvent line, marked with a black line for clarity. This phenomenon implies the method was unsuccessful..... 46

Figure 3.2. Chromatogram of normal-phase GC×GC separation of Jet-A. The lack of baseline separation of small alkane compounds is highlighted by the black box..... 47

Figure 3.3. 3D GC×GC chromatogram of Jet-A fuel with three chemical classes outlined: 1) n-alkanes, iso-alkanes, and cycloalkane compounds, 2) alkyl benzene compounds, and 3) alkyl naphthalene compounds. Compounds were identified based on their EI MS match to the NIST library..... 49

Figure 3.4. GC×GC chromatogram of Jet-A where each elution peak apex is labeled with a dot marker. The n- and iso-alkanes are marked in black, cycloalkanes are in red, alkyl benzenes are in purple, and alkyl naphthalenes are in brown. Compound class elution regions were determined by model compound studies. The orange line notes an elution trend line in which all the compounds are of a specific carbon number. This elution trend is present throughout the chromatogram of the saturated compounds..... 51

Figure 3.5. A)GC×GC chromatogram of Jet-A zoomed in on the smaller analytes eluting before 2,000 seconds primary column elution time and 5.5 seconds secondary column elution time. B) The 3-D representation of the same GC×GC chromatogram shown in A. The z-axis represents intensity, and the color intensity scale, which represents counts, is noted on the left. C) A further zoomed-in GC×GC chromatogram of 720 ± 100 seconds primary column elution time and 3.5 ± 0.5 seconds secondary column elution time. The tooth-like mountains with multiple apexes (pink circle) are undesired co-elution of compounds while only one elution peak, with one apex (black circle), should ideally be observed for all compounds. D) A closer look at the undesired co-eluting compounds noted in the pink circle shown in C. It can be observed that no baseline separation is achieved for many compounds. 52

Figure 3.6. Jet-A GC×GC chromatogram obtained by using longer column sets. Each elution peak apex is labeled with a dot marker. The n- and iso-alkanes are marked in black, cycloalkanes are in red, alkyl benzenes are in purple, and alkyl naphthalenes are in brown..... 54

Figure 3.7. Compounds are classified in colors: black- *n*- and *iso*-alkane compounds, red-cycloalkane compounds, purple- aromatic compounds, and brown- naphthalene compounds. Each mark on the figure is a unique compound with a specific chemical structure assigned to it. The heat map of color indicates the intensity (counts) of the compound peak. All x-axis denotes elution time from the primary column (seconds) and y-axis denotes elution time from the secondary column (seconds). A) FT-S8 aviation fuel additive diluted 1:100 for analysis. B) 50/50 Jet-A/ HEFA aviation fuel diluted 1:100 for analysis. C) SIP alternative fuel additive diluted 1:500 for analysis, consisted of one analyte: 2, 6, 10-trimethyldodecane. D) CHCJ alternative pathway aviation fuel diluted 1:100 for analysis..... 56

Figure 3.8. EI (70 eV) TOF mass spectrum from a GC×GC/(EI)TOF MS and NIST library mass spectrum for tetradecane (n-C14) (top) and pentadecane (n-C15) (bottom), similarity score 928. 59

Figure 3.9. 2D-Gas chromatograms measured for Base Oil A (left) and Base Oil B (right) at mass fractions of 4550 ppm and 11400 pm in n-hexane, respectively, by using GC×GC/EI TOF MS. Each orange square represents a different linear alkane, each black dot represents a different iso-alkane, each red dot represents a different mono-, di-, or tricyclic alkane, and each brown dot represents a different tetra- or pentacyclic alkane. The internal standard, n-butylbenzene, that was spiked into each base oil is noted by the purple circle. 62

Figure 4.1. ASTM D2425-2019 analysis workflow 69

Figure 4.2. Scheme for the preparation of renewable jet fuel (RJF) sample for LOD, LOQ, and bias investigation. Samples are named as fuel type_spiked (S) or neat (0)_sample number. 75

Figure 4.3. A) The average response for RJF linearity samples. B) The average response for gas oil linearity samples. 81

Figure 4.4. Renewable jet fuel (RJF) and gas oil (GO) samples residual plots. There is no observable correlation between the average residuals and the analyte concentration. 82

Figure 5.1. Miniature coreflood device prototype 1.0 from A) top view and B) side view. 97

Figure 5.2. Miniature coreflood device prototype 1.0 system and its components assembled: 1) fluid accumulator, injection cylinder, 2) isolation valves, 3) core holder (core size: 4” length x 0.75” diameter), 4) collection tube 98

Figure 5.3. Second-generation TMCF device with three coreflood devices. 1) pump fluid; 2) pumping lines; 3) injection pump; 4) valve; 5) piston plate; 6) injection vessel where cEOR formulations are placed; 7-9) TMCF devices; 10) collection tube. Only one TMCF device can be used for cEOR formulation testing at a time. One TMCF device (7) is shown connected to the system in the figure. Flow direction is indicated by arrows on the pumping lines..... 99

Figure 5.4. A. Miniature coreflood device prototype 2.0, TMCF, and its components in use with a rockcore inside the inner chamber: 1) fluid accumulator, injection cylinder 2) isolation valves, 3) core holder (core size: 6” length x 1” diameter) B. Miniature coreflood prototype 2.0, TMCF, schematic and its components: A) inner chamber injection port, B) outer chamber injection port, C) end cap, D) inner chamber tubing (PVC Tygon), and E) outer chamber transparent case (polycarbonate). 100

Figure 5.5. The new TMCF device design allows oil migration to be monitored during the initial oil saturation process to ensure an even and complete oil distribution..... 101

Figure 5.6. Percent oil recovery for each step of three TMCF tests carried out by three different operators. Core 1 was completed by the senior graduate student, core 2 by the graduate student, and core 3 by the undergraduate student over three days by using a cEOR formulation of three surfactants (S13D, A6, and L4-2) and a polymer (3230). Step 1 corresponds to the initial waterflood (IWF), followed by cEOR (a surfactant and polymer mixture flood (SP) followed by a polymer solution flood (P)), and finally an ending waterflood (EWF). The oil recovered from the cEOR process is shown, as well as the overall oil recovery, which includes the oil volume recovered upon both IWF and cEOR. 104

Figure 5.7. Percent oil recovery for each step of five TMCF tests using five different rockcores (1 – 5) flooded using a cEOR formulation containing one surfactant (S13D) and one polymer (3330). Step 1 corresponds to the initial waterflood (IWF), followed by cEOR (a surfactant and polymer mixture flood (SP) followed by a polymer solution flood (P)), and finally an ending waterflood (EWF). The oil recovered from the cEOR process is shown, as well as the overall oil recovery, which includes the oil volume recovered upon both IWF and cEOR..... 105

Figure 5.8. The core on the left exhibits formulation fingering, red box, seen during cEOR process on TMCF core 1. The proper oil migration is shown in red brackets on the rockcore on the right. No breakthrough of formulation fingering was observed. The color was augmented for ease of viewing in both pictures..... 106

Figure 5.9. (A) Front view: 1. Formulation fluid accumulator holder; 2. Open space for future expansion to include more fluid accumulators or TMCF devices; 3. cEOR TMCF device holder; 4. Automatic valves; 5. Automatic valve controllers; 6. Backpressure transducer electronic reader, (B) Side view, and (C) Back view. 107

Figure 5.10. Front view of the Tri-TMCF device stand with all of its components: 1. Formulation fluid accumulator; 2. Open space for future expansion to include more fluid accumulators or TMCF devices; 3. cEOR TMCF device with rockcores inserted; 4. Automatic valves; 5. Automatic valve controllers; and 6. Backpressure transducer electronic reader. 110

Figure 6.1. A graphic of the cEOR miniaturized-CF testing process. Each orange-highlighted box represents an oil distillate sample that was recovered for GC×GC-FID analysis, totaling six samples from each of the cEOR CF testing process. 119

Figure 6.2. Oil recovered for each formulation as a function of the percentage of original oil in place (OOIP) and pore volume (PV) equivalents injected. Green dashed lines represent different CF steps: initial waterflood (IWF), surfactant and polymer flood (SP), polymer flood (P), and ending waterflood (EWF). Formulation two recoverd more oil overall but does not surpass the oil volume recovered over formulation one until the EWF injection. 123

Figure 6.3. A chromatogram of the original oil distillate. The chromatogram has three dimensions of information: the elution times of the primary and secondary GC columns, as well as abundance or signal intensity (z-axis represented by heat mapping colors noted on the right-hand side scale). Each chemical class is marked and color-coded. The apex of each elution peak is marked with a colored dot. The *n*-alkanes are marked in black with the associated carbon numbers, *iso*-alkanes are red, monocycloalkanes are white, dicycloalkanes are green, tricycloalkanes are light green, alkylbenzenes are peach, cycloalkanes are maroon, alkylnaphthalenes are yellow, biphenyls are orange, phenanthrenes and anthracenes are off-white, and pyrenes are light purple. 125

Figure 6.4. PCA plot of the entire oil distillate data set. Each sample was grouped according to the cEOR formulation as well as the step in the CF process in which the oil distillate was recovered, including the original oil distillate. PC-1 accounts for 98% of the explained variance in the data set and PC-2 accounts for another 1% of data variance..... 126

Figure 6.5. Correlation loadings plot of each data component (X) used to define each PC. The closer a data component's correlation loading value is to one, the more of an influence that value has on that component. There are two clusters of highly correlated variables that define the PC-1. 127

Figure 6.6. Correlation loading values categorized according to molecular size: small molecules have carbon numbers 6-10, medium molecules have carbon numbers 11-15, and large molecules have carbon numbers greater than 16. 128

Figure 6.7. Correlation loading values categorized according to molecular size: small carbon numbers 6-10 can be seen to the right of the plotting area and large carbon numbers greater than 16 are on the left side. Note medium range carbon numbers (11-14) are not shown but are included in Figure 6.6. 129

LIST OF EQUATIONS

Equation 2.1 Radio frequency (RF) voltage, where V is the amplitude of the RF voltage, ω is the angular frequency of the RF potential, and t is time 36

Equation 2.2 Direct current (DC) voltage 36

Equation 2.3 Where φ is the potential, x and y are rectangular Cartesian coordinates of the ion, $r0$ is the radius of the central space created by the quadrupole rods, and the remaining terms have the same meaning as previously defined 36

Equation 2.4 Where φ is the potential, x and y are rectangular Cartesian coordinates of the ion, $r0$ is the radius of the central space created by the quadrupole rods, and the remaining terms have the same meaning as previously defined 36

Equation 2.5 Where $\xi = \omega t/2$; $u = x\ or\ y$; for $u = x$ then $ax = 8eU/m\omega 2r02$; $qx = 4eV/m\omega 2r02$; and for for $u = y$ then $ay = -8eU/m\omega 2r02$; $qy = -4eV/m\omega 2r02$; and the remaining terms have the same meaning as previously defined 36

Equation 4.1 Residual calculation 80

Equation 4.2 RJF linear regression fit line equation used to solve for y which is equal to vi 82

Equation 4.3 Gas oil linear regression fit line equation used to solve for y which is equal to vi . 82

Equation 4.4 Relative spiked recovery percentage calculation 88

Equation 5.1 Initial oil saturation 102

Equation 5.2 Initial waterflood oil recovery 102

Equation 5.3 cEOR oil recovery 102

Equation 5.4 Overall oil recovery 102

Equation 5.5 Oil left in place 102

LIST OF ABREVIATIONS

Acronyms	Meaning
%OOIP	Percentage of Original Oil in Place
ASTM	American Standard Test Method
B MS	magnetic sector mass spectrometer
BF HOV	Brown-Forsythe Homogeneity of Variance
cEOR	Chemically Enhanced Oil Recovery
CF	Coreflood
CHCJ	Catalytic Hydrothermal Conversion Jet
DC	Direct Current
DCM	Dichloromethane
EI	Electron Ionization
EOR	Enhanced Oil Recovery
EWF	Ending Waterflood
FID	Flame Ionization Detector
FT-S8	Fischer-Tropsch Synthetic-8
GC	Gas Chromatograph
GC/Q MS	Gas Chromatograph/ Quadrupole Mass Spectrometer
GC×GC	Comprehensive Two-Dimensional Gas Chromatograph
GC×GC/(EI) TOF MS	Comprehensive Two-Dimensional Gas Chromatograph/Electron Ionization Time-of-Flight Mass Spectrometer
GO	Gas Oil
HEFA	Hydroprocessed Esters and Fatty Acids
HOV	Homogeneity of Variance
IWF	Initial Waterflood
Jet-A	Petroleum-based Jet Fuel
LOD	Limit of Detection
LOQ	Limit of Quantitation
m/z	Mass-to-Charge Ratio
mEOR	Microbially Enhanced Oil Recovery
MS	Mass Spectrometer
NIST	National Institute of Standards and Technology
OOIP	Original Oil In Place
P	Polymer
PFTBA	Perfluorotributylamine
Q	Quadrupole
RF	Radio Frequency
RJF	Renewable Jet Fuel
SIP	Synthetic Iso-Paraffins
SP	Surfactant/Polymer
TIC	Total Ion Chromatogram
TMCF	Transparent Miniature Coreflood
TOF	Time-of-Flight
TOF MS	Time-of-Flight Mass Spectrometer
XIC	Extracted Ion Chromatogram

ABSTRACT

This dissertation focused on the development of mass spectrometric methodologies, separation techniques, and engineered devices for the optimal analysis of complex mixtures relevant to the energy sector, such as alternative fuels, petroleum-based fuels, crude oils, and processed base oils. Mass spectrometry (MS) has been widely recognized as a powerful tool for the analysis of complex mixtures. In complex energy samples, such as petroleum-based fuels, alternative fuels, and oils, high-resolution MS alone may not be sufficient to elucidate chemical composition information. Separation before MS analysis is often necessary for such highly complex energy samples. For volatile samples, in-line two-dimensional gas chromatography (GC×GC) can be used to separate complex mixtures prior to ionization. This technique allows for a more accurate determination of the compounds in a mixture, by simplifying the mixture into its components prior to ionization, separation based on mass-to-charge ratio (*m/z*), and detection. A GC×GC coupled to a high-resolution time-of-flight MS was utilized in this research to determine the chemical composition of alternative aviation fuels, a petroleum-based aviation fuel, and alternative aviation fuel candidates and blending components as well as processed base oils.

Additionally, as the cutting edge of science and technology evolve, methods and equipment must be updated and adapted for new samples or new sector demands. One such case, explored in this dissertation, was the validation of an updated standardized method, ASTM D2425 2019. This updated standardized method was investigated for a new instrument and new sample type for a quadrupole MS to analyze a renewable aviation fuel. Lastly, the development and evaluation of a miniaturized coreflood device for analyzing candidate chemically enhanced oil recovery (cEOR) formulations of brine, surfactant(s), and polymer(s) was conducted. The miniaturized device was used in the evaluation of two different cEOR formulations to determine if the components of the recovered oil changed.

CHAPTER 1. INTRODUCTION AND THESIS OVERVIEW

1.1 Introduction

This dissertation focusses on the development of analysis techniques for energy-related samples, including fuels and oils to better understand the chemical composition of fuels and oils to utilize and process them more effectively. Throughout this dissertation, mass spectrometry (MS) techniques were employed to study these complex mixtures.

The first mass spectrometer was invented by J.J. Thomson in 1913.[1] Since then, MS has evolved into a versatile analytical technique used in many scientific fields such as fuels research, petroleomics, proteomics, environmental studies, and forensics.[2-14] The main advantage of MS and different ionization techniques is the ability to provide molecular weight and structural information for unknown compounds in complex mixtures. This ability has been improved over the past 20 years, through advances in new technologies such as those that increase the resolution of a number of mass spectrometers to over a million resolution.[15] This has enabled the ability to determine the composition of increasingly complex mixtures.

A mass spectrometer generally consists of an inlet system, an ionization source, a mass analyzer, and a detector.[16] The sample must first be vaporized into the gas phase, and subsequently ionized to create analyte ions. The analyte ions are then introduced into the mass analyzer section where they are separated by their mass-to-charge ratios (*m/z*). Finally, the mass-separated ions are detected, and their abundancies determined. From these data, mass information can be gained, and using certain ionization methods or fragmentation techniques, structural information can also be gained.

Electron ionization (EI) followed by time-of-flight (TOF) MS as well as EI followed by quadrupole (Q) MS analysis were the main MS techniques used in this research to determine the chemical compositions of fuels and oils. Additionally, a new miniaturized analytical device was created and tested for chemically enhanced oil recovery (cEOR) formulation testing and compared to a considerably larger commercially-available device. The device was also used to compare oil's chemical composition after during recovery from a rockcore using two different cEOR formulations.

1.2 Thesis Overview

Chapter 2 discusses the fundamental principles of mass spectrometry, as well as the experimental aspects of these studies. The aforementioned TOF MS and Q MS, as well as preparative methods, such as chromatographic separation techniques, are discussed in detail in this chapter.

Chapter 3 discusses the development of a two-dimensional gas chromatography (GC×GC) method followed by electron ionization and high-resolution TOF MS (GC×GC/(EI)TOF MS) detection for the chemical analysis of fuels, fuel blending components, and light lubricant base oils. Structural information was used from this analysis to determine the chemical compositions of the samples. The developed method is a universal analysis method which does not rely on the chemical composition or structure of a molecule to detect it. Therefore, this analysis method was shown to be useable for petroleum-based fuels, alternatively sourced fuels and fuel additives, and even light lubricant base oils of various origins and processing procedures.

Chapter 4 investigates the recently updated American Standard Test Method (ASTM) D2425, "Standard Test Method for Hydrocarbons Types in Middle Distillates by Mass Spectrometry."[17] New instrumentation, a gas chromatograph connected to a quadrupole mass spectrometer (GC/Q MS), and sample type, renewable jet fuel, were introduced in the 2019 method. While the method update is a proper step towards modernization, it still lacked validation parameters. Therefore, the limit of detection, limit of quantitation, and bias were determined in an intra-laboratory study completed during a collaboration project in Porvoo, Finland, with the Neste Corporation's research and development department.

Chapters 5 outlines studies on crude oil recovery techniques and analysis. This chapter details the development of a new transparent miniaturized coreflood (TMCF) device for high-throughput screening of cEOR formulations. The performance of the new TMCF device was compared to that of a commercially-available coreflood (CF) device through comparison of the oil volume recovery by various cEOR formulations. Each cEOR formulation was found to perform comparably on the newly designed TMCF device as compared to the traditional CF device. Chapter 6 then discusses the use of the TMCF device to conduct CF experiments on two different cEOR formulations. The chemical composition of the recovered oil was monitored throughout the CF experiments by using a GC×GC with a flame ionization detector (GC×GC-FID) to analyze the oils. This allowed direct comparison of the oils recovered at different times point throughout the experiments to determine

if the chemical composition was changing throughout the CF experiment as well as if the two different cEOR formulations recovered oils of different chemical compositions.

1.3 References

(1) Thomson, J. J. *Rays of Positive Electricity and Their Application to Chemical Analyses*; Longmans, Green and Co.: London, **1913**.

(2) Rathsack, P., Wollmerstaedt, H., Kuchling, T., Kureti, S. *Fuel*. **2019**, 248, 178-188.

(3) Machado, M.E. *Talanta*. **2019**, 198, 263-276.

(4) Dong, X., Wang, F., Fan, X. et al. *Fuel*. **2019**, 245, 392-397.

(5) Gajdosechova, Z., Mester, Z., Pagliano, E. *Anal. Chim. Acta*. **2019**, 1064, 40-46.

(6) Hsu, C.S., Hendrickson, C.L., Rodgers, R.P., McKenna, A.M., Marshall, A.G. J *Mass Spectrom.* **2011**, 46, 337-343.

(7) Marshall, A.G., Rodgers, R.P. *Proc. Natl. Acad. Sci*. **2008**, 105, 18090-18095.

(8) Marshall, A.G., Rodgers, R.P. *Acc. Chem. Res*. **2004**, 37, 53-59.

(9) Ma, J., Tang, S., Syed, J.A., Meng, X. *RSC Adv*. **2016**, 6, 82995-83002.

(10) Hoffmann, W.D., Jackson, G.P. *Annu. Rev. Anal. Chem*. **2015**, 8, 419-440.

(11) Busardò, F.P., Pacifici, R., Pichini, S. *Clin. Chem. Lab. Med*. **2017**, 55, e236-e237.

(12) Viant, M.R., Sommer, U. *Metabolomics*. **2013**, 9, 144-158.

(13) Beauchemin, D. *Mikrochim. Acta*. **1989**, 99, 273-281.

(14) Hourani, N., Andersson, J.T., Möller, I., Amad, M., Witt, M., Mani-Sarathy, S. *Rapid Commun. Mass Spectrom.* **2013**, 27, 2432-2438.

(15) Marshall, A.G., Hendrickson, C.L. *Annu. Rev. Anal. Chem.* **2008**, 1, 579-599.

(16) de Hoffmann, Mass Spectrometry: Principles and Applications, 3rd Edition; Wiley, Brussels, Belgium, **2007**.

(17) ASTM Standard D2425, "Standard Test Method for Hydrocarbons Types in Middle Distillates by Mass Spectrometry," ASTM International, West Conshohocken, PA, **2019**, www.astm.org.

CHAPTER 2. INSTRUMENTAL AND EXPERIMENTAL ASPECTS OF TIME-OF-FLIGHT AND QUADRUPOLE MASS SPECTROMETERS INTRODUCTION

2.1 Introduction

Mass spectrometry (MS) is one of the most versatile analytical tools for analyzing mixtures of organic compounds. This technique is therefore used in a wide variety of fields, such as fuels research, petroleomics, proteomics, environmental studies, and forensics.[1-13] The continuous development of new MS techniques and applications enables many different types of experiments to be performed using the same basic methodology.

MS typically involves three steps: 1) vaporization and ionization of the analytes of interest, 2) separation of the resulting gas-phase ions based on their mass-to-charge ratios (*m/z*), and 3) detection and measurement of the ions' abundances. This final step produces a mass spectrum. There are many different ionization methods that can be used for optimal ionization of a given analyte. In this research, electron ionization (EI) was used to ionize the analytes before separation and detection of those ions. EI is a useful ionization technique because it is a universal ionization method that ionizes all organic compounds independent of their structure.[14] EI can also induce fragmentation of ionized analytes. Fragment ions of analytes can be useful for identification of the chemical structure of the analyte because ionized analytes of a given structure fragment into specific *m/z*-ratios and of particular relative abundances which results in a reproducible mass spectrum. Because of the uniqueness and reproducibility of these fragmentation mass spectrum, commercial libraries have been developed which contain hundreds of thousands of standard EI mass spectra (collected at 70 eV ionization energy) that can be used to identify the structure of the analyte. If the EI mass spectrum of the analyte is not in a database, the fragmentation pattern can still be used to determine the chemical structure by identifying the chemical compositions of characteristic fragment ions observed in the mass spectrum.

For this research, two mass spectrometers were used and will be discussed in detail: a quadrupole (Q) mass spectrometer and a time-of-flight (TOF) mass spectrometer. Theoretical, fundamental, and experimental aspects of Q MS and TOF MS are discussed below.

2.2 Instrumentation and Experimental Aspects of Two-Dimensional Gas Chromatography/Electron Ionization High-Resolution Time-of-Flight Mass Spectrometry (GC×GC/(EI)TOF MS)

In this research, an Agilent 7890A two-dimensional gas chromatograph (GC×GC) system and Leco Pegasus GC-HRT 4D high-resolution time-of-flight mass spectrometer equipped with electron ionization (GC×GC/(EI)TOF MS) were used to develop methodologies to determine the chemical compositions of complex mixtures, including fuels and fuel blending components as well as processed light base oils. The compositions of many of these complex mixtures were unknown and have not been previously reported in the literature. A general schematic for the GC×GC/(EI)TOF MS is shown in Figure 2.1. Each component of the system will be discussed in detail below. First, the gas chromatography system and the separation method are discussed, followed by the mass spectrometry method, including the ionization method, and finally, the high-resolution time-of-flight mass analyzer and detector.

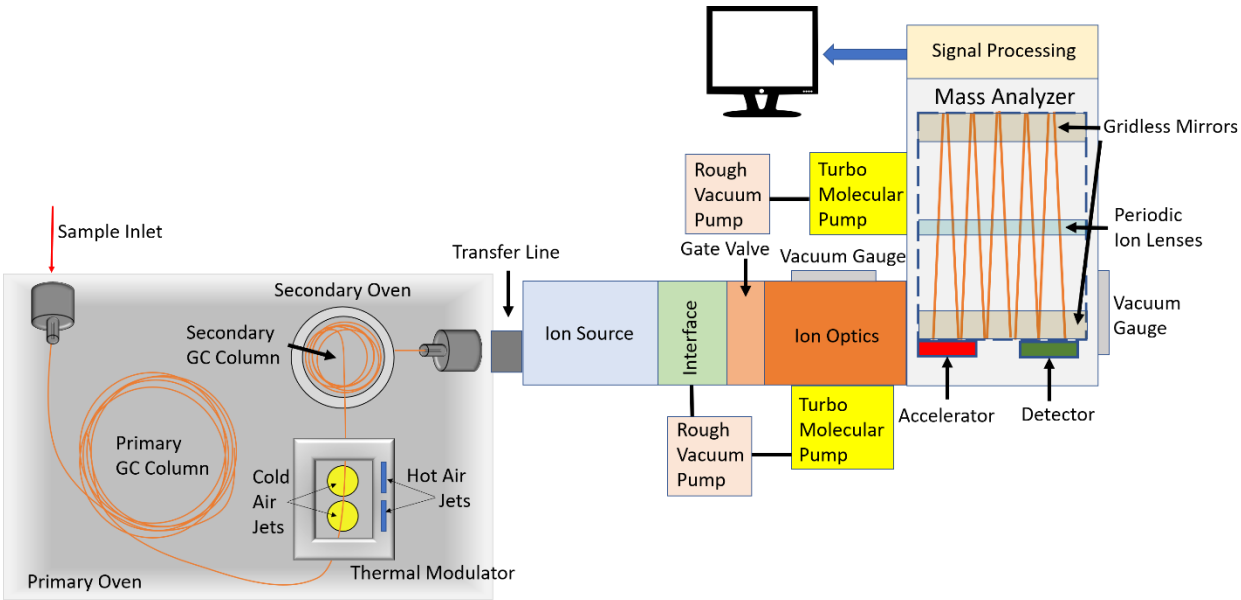

Figure 2.1. A schematic of the GC×GC/(EI) TOF MS instrument, Pegasus GC-HRT 4D, which features a folded flight path MS. The instrument parts are described throughout Section 2.2.

2.2.1 Two-Dimensional Gas Chromatography (GC×GC)

Two general types of two-dimensional gas chromatographs exist: comprehensive two-dimensional gas chromatography (GC×GC), first discussed in 1991,[15] and multidimensional GC, first discussed

in 1952.[16] In comprehensive GC×GC, a modulator is used to partition the eluent from the first column into discrete portions prior to injection onto the second column.[15] As such, all analytes that enter the first column pass through to the second column and then on to the detector. In contrast, multidimensional GC uses a technique called heart-cutting to divert a portion of the eluent from the first column onto the second column (or multiple columns) and then on to independent detectors.[16,17] Multidimensional GC is best suited for a targeted analytical approach because it must be known ahead of time when to divert the sample matrix flow to the appropriate column(s) and detector(s). In contrast, comprehensive GC×GC can be used for untargeted analysis of unknown mixtures by using a single detector such as a MS. Comprehensive GC×GC also has a greater resolving power,[18] and therefore it better separates mixtures into individual components. In this research, comprehensive GC×GC was utilized.

2.2.1.1 *Components of Comprehensive GC×GC*

The samples were injected into the GC×GC with an auto injector (Agilent G4513A). The injection port was heated to vaporize the analyte mixture before continuing on to the first GC column called the primary column. A modulator connected the primary column to the secondary column. A schematic of the GC×GC used in this research is presented below (Figure 2.2). The primary column employed in this research was located in the primary oven, and the secondary column was located in the secondary oven. The temperature of each oven was controlled in such a manner that the secondary oven temperature was positively offset from the primary oven temperature. Specific experimental procedures, including temperature settings, will be discussed in detail in later sections where appropriate.

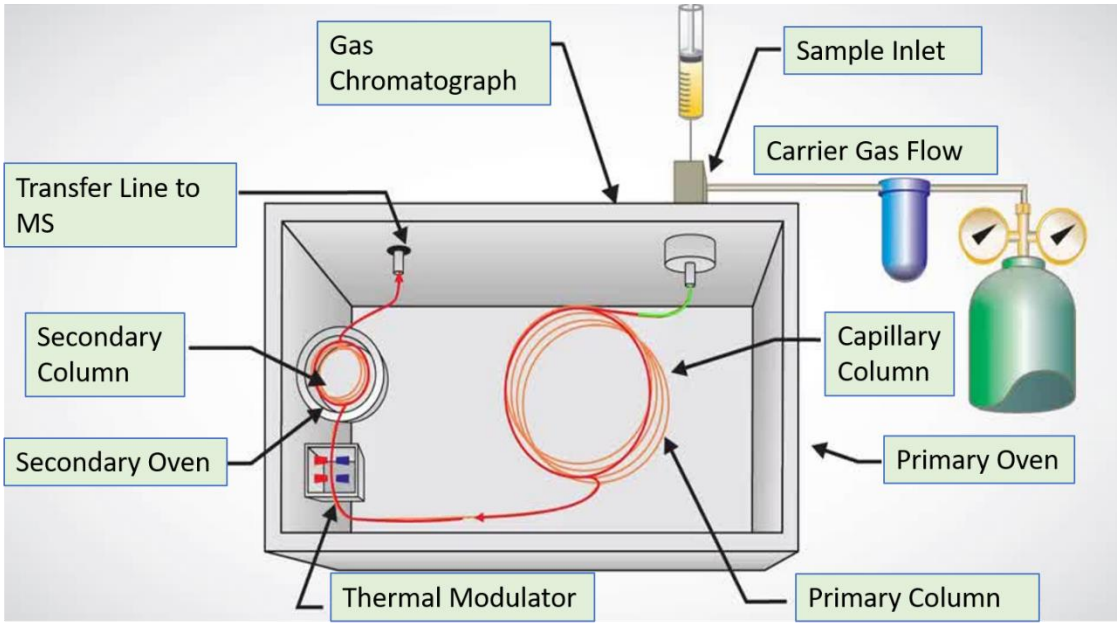

Figure 2.2. Components in the Agilent GC×GC system.

2.2.1.2 *Separation of Analytes in the GC Columns*

The GC columns were composed of fused silica. The inner walls of the GC columns were coated with a thin layer of a nonvolatile stationary phase. Many different stationary phases can be used in different GC columns to achieve a range of polar to non-polar phase properties that can be used for separation of different types of mixtures. Stationary phases of three different polarities were considered to determine optimal separation methods: a nonpolar stationary phase (Rxi-1ms Restek column, 100% dimethylpolysiloxane stationary phase), a low polarity stationary phase (Rxi-5ms Restek column, 95% dimethylpolysiloxane:5% diphenyl stationary phase), and a polar stationary phase (Rxi-17Sil ms Restek column, proprietary stationary phase).

When a gaseous sample passes through a polar GC column, the polar and polarizable analytes will have stronger interactions with the polar stationary phase than the nonpolar analytes. Therefore, nonpolar analytes will pass through faster than more polar analytes. This begins to separate analytes in a complex mixture based on partitioning differences in the stationary phase. In a GC×GC system, the two columns are typically chosen to exhibit orthogonal properties. Analytes of varying polarities were efficiently separated in this research with two columns of opposite stationary phase properties, one column was polar, while the other was nonpolar or had a

low polarity.[19] In addition to the separation of the analytes based on their polarity, the boiling point of the compounds can also facilitate separation of the analytes.[20]

The GC columns were housed in two ovens whose temperatures were increased as separation progressed. This facilitated the separation of the analytes based not only on their polarities but also their boiling points, leading to another dimension of separation. As the temperature increases, analytes with lower boiling points move faster through the column. By employing this separation approach, thermally stable complex mixtures can be separated by using comprehensive GC×GC at a substantially greater resolution than traditional GC.[18]

2.2.1.3 *Thermal Modulator*

A thermal modulator resided between the two GC columns. The thermal modulator preserves the separation of the analytes from the primary column while acting as an injector for the secondary column.[21] The thermal modulator uses a cold and a hot jet of nitrogen gas to accomplish these things. The cold jet utilizes cryo-cooled nitrogen gas and the hot jet utilizes heated nitrogen gas to momentarily slow down and gather eluent from the primary column and then to heat and release those discrete portions of eluent onto the secondary column[21-24] (eluent shown by colored dots in Figure 2.3).

It must be ensured that the modulation period of the thermal modulator is long enough for analytes to elute from the secondary column before the next portion of analytes is released from the modulator onto the secondary column. If the modulation period is too short, a phenomenon called wrap-around will occur in which the analyte appears to elute before the solvent, which is theoretically impossible as the solvent is chosen to have a boiling point significantly lower than any analytes in the mixture.[25] Two methods are used to resolve this issue: 1) increase the secondary oven temperature-offset such that analytes move through this column faster or 2) increase the modulation time to allow analytes sufficient time to move through the secondary column. Given that the modulation time controls the size of the aliquot delivered onto the secondary column from the primary column, it is desirable to keep this time short to maintain the separation of analytes resolved by the primary column prior to entering the secondary column. If the modulation time is too long, the separation of analytes achieved in the primary column may be lost, and the secondary column may be overloaded, or exceed the peak capacity of the column. The peak capacity of a GC column refers to the maximum number of analytes that can be separated by that column.[26]

After the analytes passed through the secondary GC column and were further separated, they entered a transfer line that directed the analytes into the ionization chamber of the mass spectrometer. The ionization technique will be discussed in the following section.

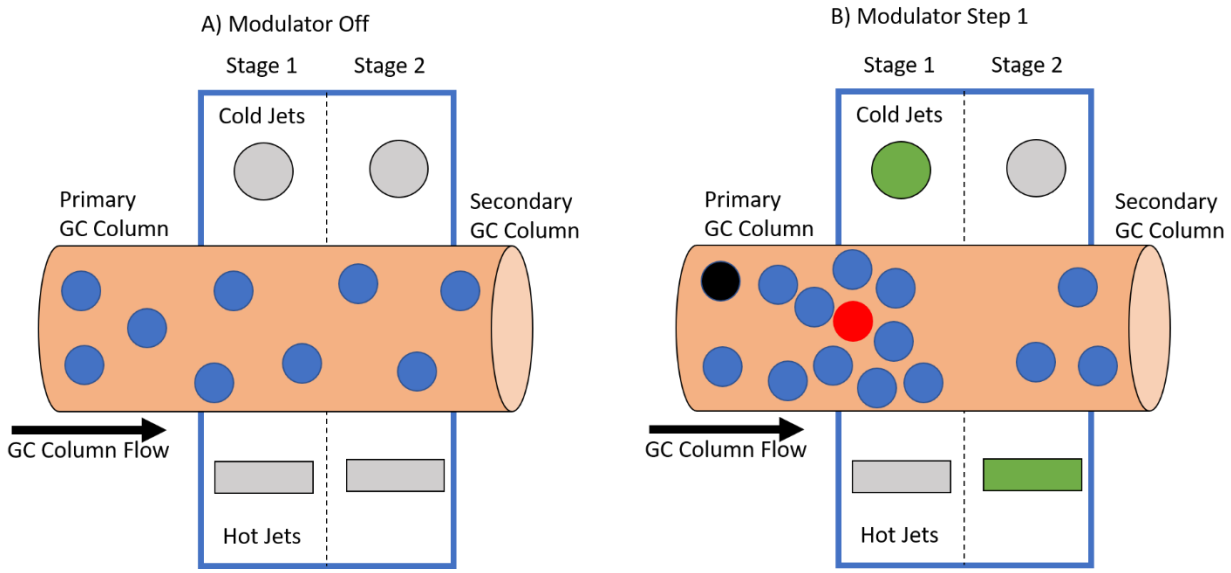

Figure 2.3. A) The thermal modulator with all components turned off. The eluates, blue dots, will flow freely through the modulator section. B) When a jet is turned on, the shape representing the jet will appear in green. New eluates marked in red and black are introduced as reference points for the four steps of thermal modulation. Step 1 of thermal modulation: Stage 1: The first cold jet is on, trapping and cryo-focusing the eluent coming from the primary column; Stage 2: The second hot jet is on, desorbing any eluates from the second stage of the modulator. C) Step 2 of thermal modulation: Stage 1: The first hot jet is on, releasing the partially cryo-focused eluent from stage 1 into the stage 2 of the modulator; Stage 2: The second cold jet is on to trap the incoming eluent and to cryo-focus the eluent. D) Step 3 of thermal modulation: Stage 1: The first cold jet is on, preventing any additional eluent from moving past stage 1; Stage 2: The second cold jet is on to further cryo-focus the eluent. E) Step 4 of thermal modulation: The first cold jet remains on preventing any additional eluent from moving past stage 1; Stage 2: The second hot jet is on and therefore it is releasing the cryo-focused eluent from the second stage of the modulator onto the second column for further chromatographic separation. The eluate marked with a red dot has now moved onto the secondary column for further chromatographic separation and is no longer in the modulator section of the instrument.

Figure 2.3 Continued

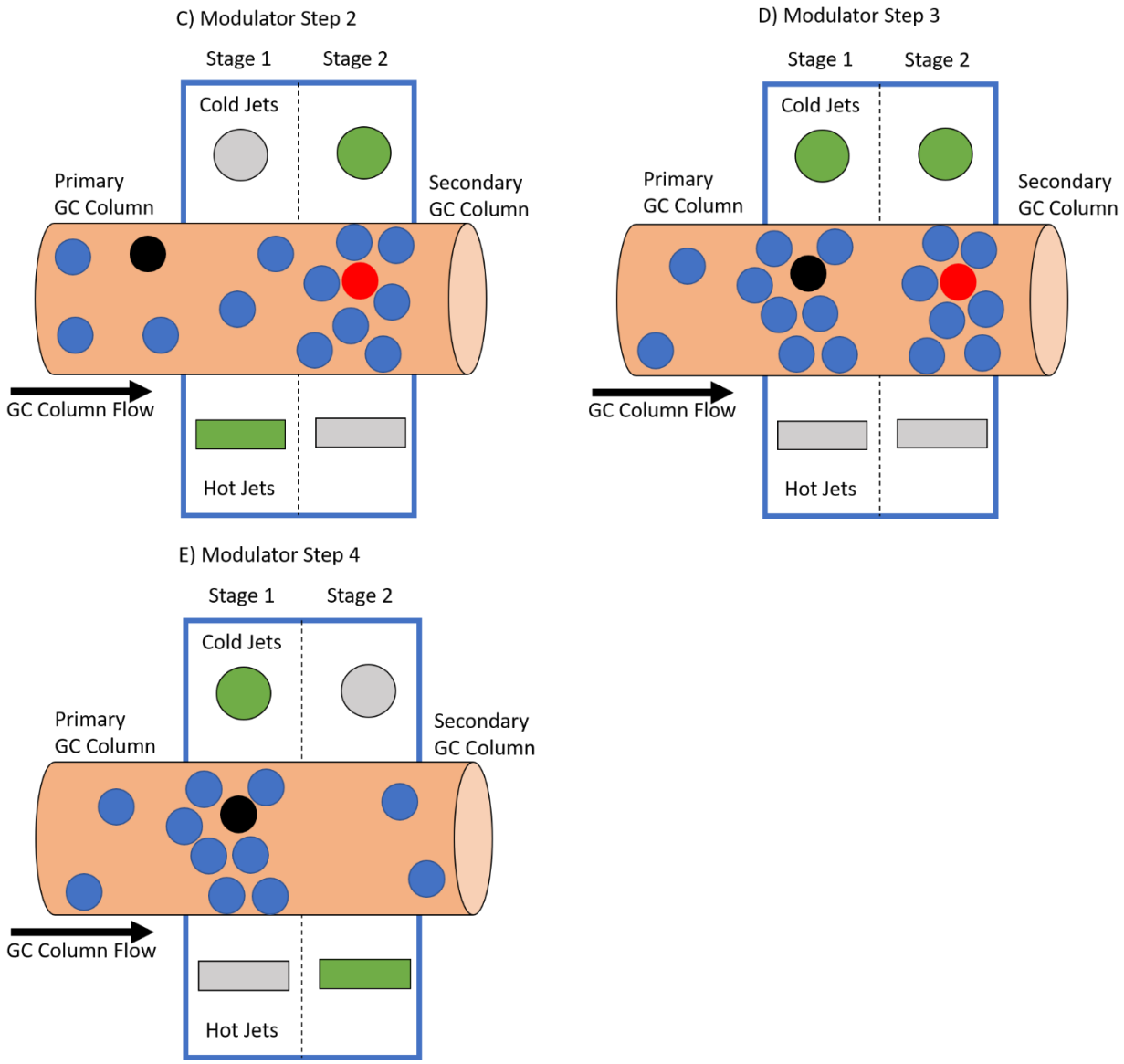

2.2.2 Mass Spectrometry

2.2.2.1 *Electron Ionization*

As the analytes traveled from the GC×GC into the ionization chamber of the mass spectrometer, they are already in the gas phase. These gaseous analytes are then ionized via electron ionization (EI), where fast-moving electrons impact the neutral gas-phase analytes, inducing ionization and fragmentation (Figure 2.4). EI begins when a large electric voltage is applied to a wire filament which is consequently heated and produces electrons through thermionic emission.[27,28] This

process releases slow-moving electrons which are then accelerated through a 70-V electric field which results in electrons with high kinetic energies (70 eV). The released fast moving electrons and the neutral analytes undergo high-energy collisions in the ionization chamber which causes the ejection of an electron from the analytes to produce radical cations (molecular ions).[29,30] The ionization chamber is maintained at low pressure (1 × 10-4 Torr) to minimize ion/molecule collisions and side reactions.

Additionally, part of the kinetic energy of the bombarding electrons are converted into internal energy of the analyte ions. If the added internal energy exceeds the fragmentation threshold of the ion, fragmentation takes place.[31,32] This fragmentation can be helpful for identifying the structure of the analyte ions because EI fragmentation patterns, caused by electrons with a kinetic energy of 70 eV, are highly reproducible and are inventoried in large, searchable libraries. However, sometimes isomers may produce similar fragmentation patterns making a library match to the EI MS difficult to determine. Furthermore, fragmentation can be so extensive that no molecular ions are detected, and thus, no molecular weight information can be determined for the analyte. This makes an EI MS library match more difficult to determine. However, if the EI mass spectrum of the analyte is not in a database or is hard to match to the database, the fragmentation pattern can still be used to determine the chemical structure by identifying the chemical compositions of characteristic mass fragments observed in the mass spectrum.

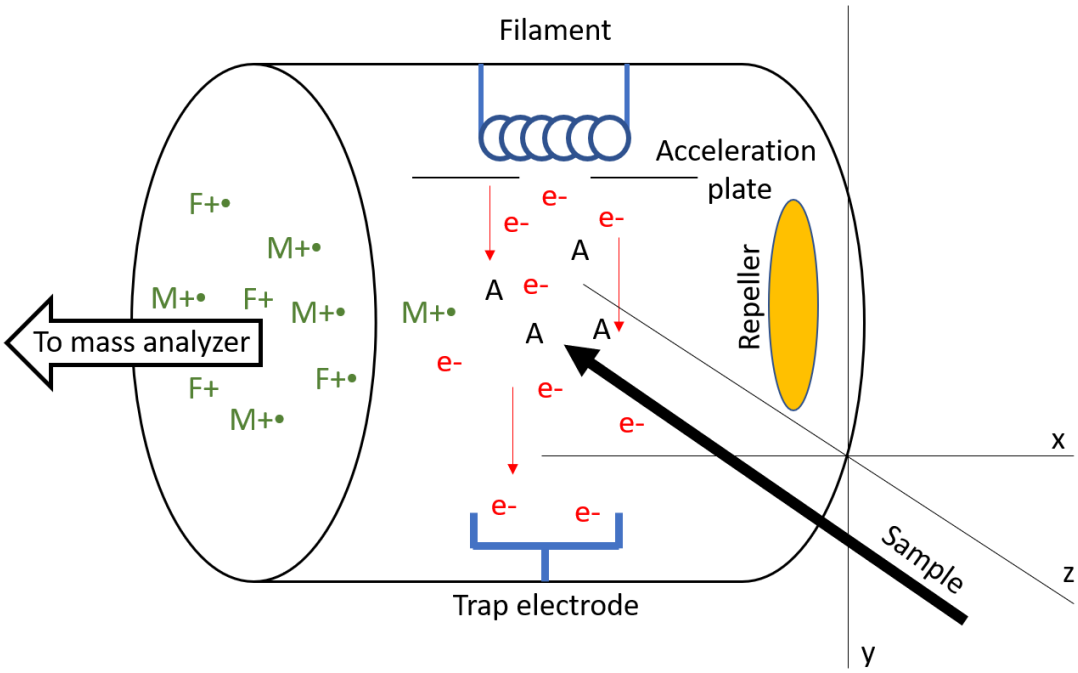

Figure 2.4. Electron ionization source where e- are fast moving electrons, A are analytes, $M^{+\bullet}$ are molecular radical cations, $F^{+\bullet}$ are fragment radical cations and F^{+} are fragment cations.

2.2.2.2 *Time-of-Flight Mass Spectrometer*

A time-of-flight mass spectrometer (TOF MS) contains a field-free flight region instead of a scanning type mass analyzer. In these instruments, the ions are emitted by a repulsive voltage applied to the push plate to theoretically achieve a uniform kinetic energy as they enter the flight region. Since kinetic energy is equal to one-half mass times velocity squared, the lower the mass of an ion, the greater its velocity and the shorter its flight time.[33] By measuring the flight time of the ions from the push plate to the detector, their mass-to-charge (*m/z*) ratios can be determined. TOF MS is well-suited for untargeted analysis because all ions are detected.[34] TOF MS also offers fast acquisition rates and a large dynamic range, making it ideal for pairing with chromatography techniques for complex mixture analysis.[35,36] Figure 2.5 details parts of the TOF MS used in this research, which are described in detail below.

After the ions were accelerated into the mass analyzer by the push plate, the ions were focused by a focusing lens before entering the flight region. As ions entered the flight region, deflection plates removed any unwanted low mass ions (as dictated by the mass range of analysis determined by the user). This was achieved via a positive potential applied to one deflection plate,

with no potential on the parallel deflection plate. Because the ions in this research were positively charged, the unwanted low mass ions were deflected by the positively charged deflection plate. As larger ions began to pass, an equal positive potential was applied to the parallel deflection plate, enabling the remaining ions to continue into the flight region.

Next, an Einzel lens and steering plates were used to focus and direct the ions. Additionally, gridless mirrors were incorporated into the flight sections to enhance resolution by allowing ions with the same *m/z*-ratios but with more kinetic energy to penetrate deeper into the gridless mirror. This allowed the ions with lower kinetic energies of the same *m/z*-ratio to catch up before they were all detected at the end of the flight path. Gridless mirrors are used because the kinetic energy imparted into the ions by the push plate should theoretically be equal, but in reality, there are small variations. For example, not all ions that are accelerated by the push plate are located in the same place in the accelerator section. This allows some ions to get a "head start" traversing the flight path. A gridless mirror, therefore, compensates for this energy spread and increases the resolving power of TOF MS.[37] Although this provision was taken to rectify ions with improperly high kinetic energy, a spread in low kinetic energy may still remain. Therefore, as a last safeguard, a barrier grid is located before the detector to catch ions traveling with low kinetic energy. A smaller ion traveling with less kinetic energy would travel with a flight time characteristic of a larger ion. Therefore, to remove slow traveling, small ions, the barrier grid had a varying potential applied to it as time progressed such that smaller ions were attracted to the grid and removed before detection while larger ions were unaffected and continued to the detector.[37]

The detector was a microchannel plate with a negatively charged conversion dynode and was located at the focal point at the end of the flight path. When the positive ions struck the conversion dynode, electrons and negative ions were emitted, called secondary ions. These secondary ions were focused by the concaved surface of the dynode and accelerated into the electron multiplier by an attractive electric field between the dynode and the electron multiplier. The electron multiplier is composed of a cathode and an anode. The cathode has a V-shape, and the anode is a wide bowl located at the bottom point of the V-shaped cathode. The secondary ions from the dynode strike the inside of the cathode, releasing electrons. This process is repeated numerous times resulting in a cascade of electrons which generate an electrical current. The electrical current is collected by the anode and is proportional to the abundance of ions that originally struck the dynode. Hence, the current detected by the anode was proportional to the

abundance of ions with that specific flight time and therefore *m/z*-ratio.[38] The mass spectrum is then generated based on 1) the flight time of the ions from the push-plate to the detector, which is used to determine the *m/z*-ratio of the ion and 2) the strength of the signal current collected by the anode which is proportional to the ion's abundance. The determined *m/z*-ratios of the ions are plotted on the x-axis and their relative abundance is plotted as the y-axis of the MS.

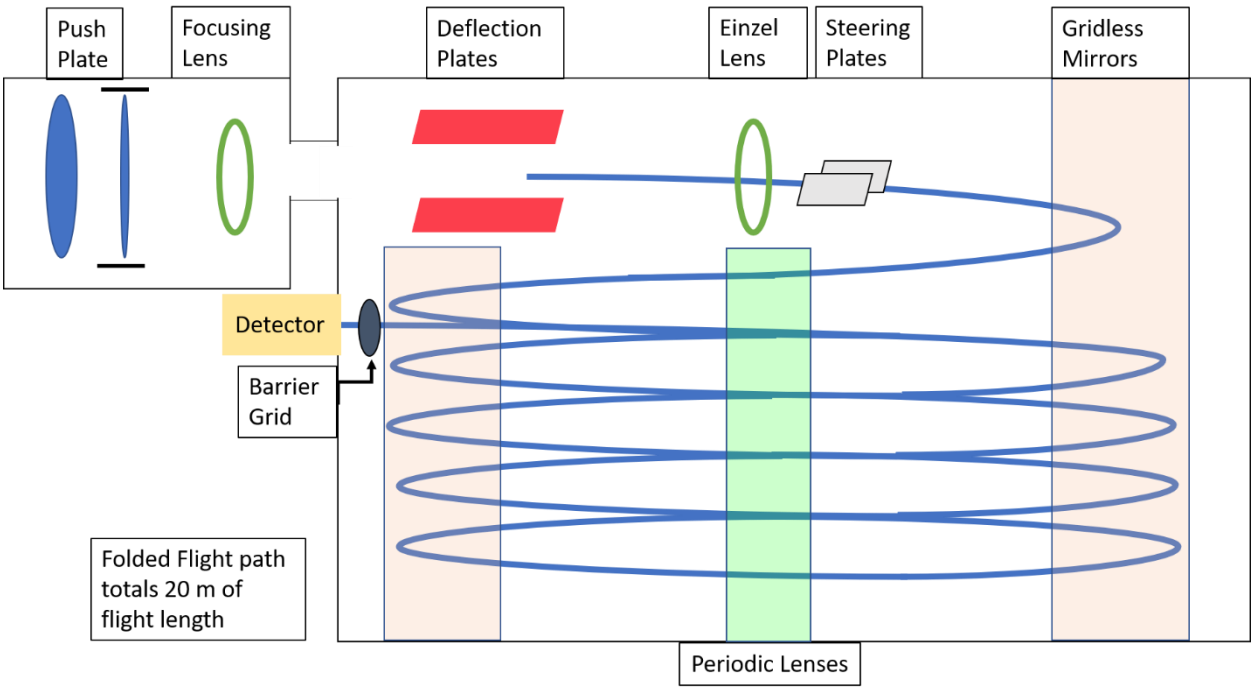

Figure 2.5. Schematic of the TOF section. The blue line represents the beam of ions on the flight path (20 m flight length). The first flight section is labeled in detail. The gridless mirrors are used to turn the ions flight trajectories, and the periodic lenses guide the ions through the proper flight path to the detector.

The TOF system requires high vacuum (1 × 10-7 Torr) as any collisions in the flight region would cause unreliable and inconsistent flight times. Data were reported to the computer system at a rate up to 500 mass spectra/second (LECO Corp. KADAS® system). Each mass spectrum reported to the computer system was a sum of 10 mass spectra. A high reporting rate is important for proper analysis of the analytes. The manufacturer has suggested that approximately 18-20 mass spectra should be collected for each GC peak. This will allow the optimal performance of the data analysis software. To accomplish this, data in this research were collected using an acquisition rate of 200 Hz (200 mass spectra/second).

2.3 Instrumentation and Experimental Aspects of Gas Chromatography (GC)/Electron Ionization (EI) Quadrupole Mass Spectrometry (Q MS)

Quadrupole mass spectrometers (Q MS) contain scanning type mass analyzers. A quadrupole mass analyzer uses ion trajectories in oscillating electric fields to separate the ions according to their mass-to-charge (*m/z*) ratios.[39] An Agilent quadrupole mass spectrometer equipped with an EI source and gas chromatograph was used in the research presented here. The instrument was located and used in Porvoo, Finland at the Neste Corporation research and development center. The components of the gas chromatograph/electron ionization quadrupole mass spectrometer (GC/(EI) Q MS) are shown in Figure 2.6. After ions were generated in the ion source, they were drawn into the quadrupole via a pressure and voltage differential. The ion source slit was placed off-center to the exit of the EI source to prevent neutral analytes from entering the quadrupole region. Ions that entered were focused into a beam and moved towards the detector by an accelerator plate (Figure 2.6). To maintain proper ion trajectories without collisions with neutral analytes in the quadrupole, the instrument contained differentially pumped areas: the atmospheric pressure injection site, the EI source region held in vacuum (0.5 Torr to 0.1 Torr), and the quadrupole region held in an even higher vacuum (1 × 10-5 Torr).

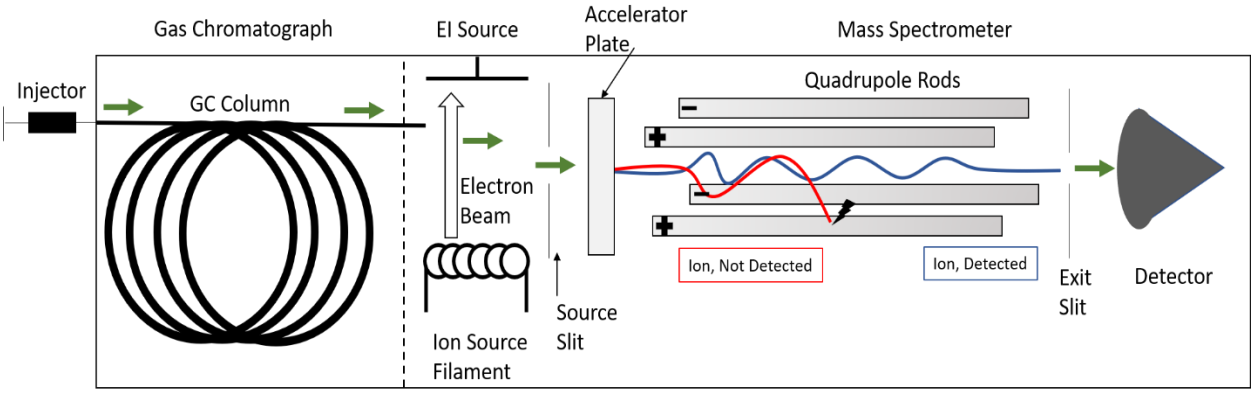

Figure 2.6. Schematic of the GC/Q MS, including an EI source, and an example of two ion trajectories, one that is detected (blue line) and one that will collide with one of the electrodes and is not detected (red line).

2.3.1 Ion Motion in the Quadrupole Mass Analyzer

The quadrupole mass analyzer consists of four parallel hyperbolic electrodes (referred to as rods) to which a direct current (DC) potential is applied as well as an alternating radio frequency (RF)

potential. The RF is superimposed over the DC potential on each rod pair. The rods are operated in pairs such that the rods opposite to one another on a diagonal are operated in the same way. While one pair of rods is positively charged, one pair is negatively charged (Figure 2.7). The combination of DC and RF potentials dictates the motion of the ions in the x-y plane.[39] These potentials cause no acceleration along the z-axis (towards the detector). Therefore, a plate, referred to as an acceleration plate, is located before the quadrupole and is charged with a voltage to accelerate the ions in the z-direction towards the detector. Typically, the DC and RF potentials are adjusted such that only ions with one specific *m/z*-ratio can go through the quadrupole at a given time while all others will have unstable trajectories, collide with the electrodes, and are neutralized and pumped out.[40] Thus, to detect ions of various *m/z*-ratios, the amplitude, V, of the RF potential (Equation 2.1) and the voltage, U, of the DC potential (Equation 2.2) are scanned such that the ratio V/U remains constant to detect ions with different *m/z*-ratios.

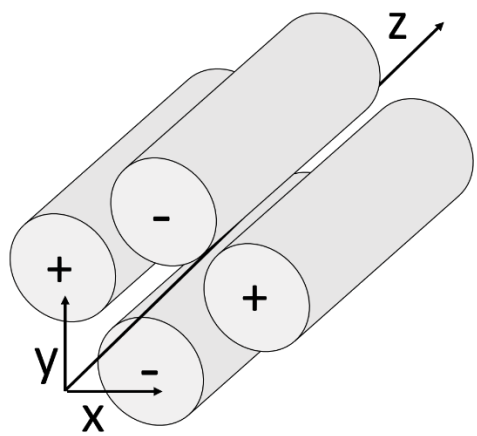

Figure 2.7. Graphic of quadrupole rods shown with alternating applied voltages such that one rod pair is positively charged, and one rod pair is negatively charged. The directional axes are also labeled: x-, y-, and z-axis.

Ions in the quadrupole will oscillate in the electric field, which can be defined by Equation 2.3. Equation 2.3 can also be expressed as an infinite series, (Equation 2.4) or in a canonical form, also known as the Mathieu's equation (Equation 2.5), by satisfying the Laplace's equation.[41,42] The Mathieu's equation can be used to construct a diagram to indicate stable and unstable trajectories of ions, also known as the Mathieu's stability diagram (Figure 2.8) for defined values

of a and q. The Mathieu's stability parameters, a and q, describe the motion of ions and the overall stability of the ion's motion inside the quadrupole such that a_x and q_x describe the motion in the x-direction and a_y and q_y describe the motion in the y-direction. Because the ion's motion in the x- and y-direction are independent of each other, ions that travel down the quadrupole must have a stable trajectory in both the x- and y-directions. Furthermore, based on Equation 2.5, the mass of the ions is inversely related to the Mathieu's stability parameters such that a larger mass ion will have a lower a and/or q value than a smaller mass ion. An example of the stable trajectories for ions of various masses can be seen in Figure 2.8 A.

Equation 2.1. Radio frequency (RF) voltage, where V is the amplitude of the RF voltage, ω is the angular frequency of the RF potential, and t is time

$$\text{Radio Frequency (RF) voltage} = V \cos \omega t$$

Equation 2.2. Direct current (DC) voltage

$$\text{Direct Current (DC) Voltage} = U$$

Equation 2.3. Where φ is the potential, x and y are rectangular Cartesian coordinates of the ion, r_0 is the radius of the central space created by the quadrupole rods, and the remaining terms have the same meaning as previously defined

$$\varphi = [(x^2 - y^2)/r_0^2](U + V \cos \omega t)$$

Equation 2.4. Where φ is the potential, x and y are rectangular Cartesian coordinates of the ion, r_0 is the radius of the central space created by the quadrupole rods, and the remaining terms have the same meaning as previously defined

$$\varphi = (U + V \cos \omega t) \sum_{n=0}^{\infty} C_m \left({}^{r}/_{r_0}\right)^m \cos m\theta$$

Equation 2.5. Where $\xi = \omega t/2$; $u = x \text{ or } y$; for $u = x$ then $a_x = 8eU/m\omega^2 r_0^2$; $q_x = 4eV/m\omega^2 r_0^2$; and for for $u = y$ then $a_y = -8eU/m\omega^2 r_0^2$; $q_y = -4eV/m\omega^2 r_0^2$; and the remaining terms have the same meaning as previously defined

$$0 = \frac{d^2u}{d\xi^2} + (a_u + 2q_u \cos 2\xi)u$$

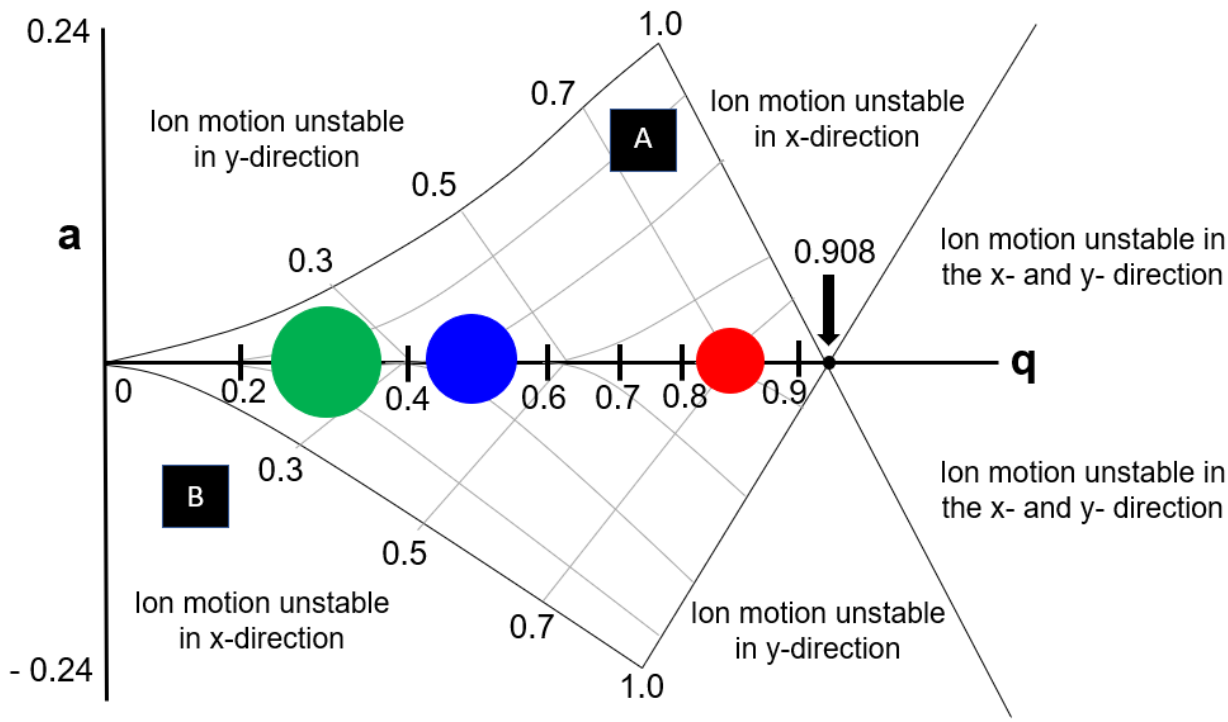

Figure 2.8. The Mathieu stability diagram. The colored circles represent ions of different sizes. The *q*- and *a*-values of the ions are indicated on the x- and y-axis, respectively. All the ions indicated have stable trajectories in the quadrupole as their *a*- and *q*-values are shown in the stable region of the diagram, the checkered region (A). Therefore, the ions would successfully travel down the quadrupole towards the detector. If any ions had *a*- and *q*-values in the unstable region (B), they would not successfully reach the detector.

Ions with stable trajectories, or *a*- and *q*-values located in the checkered region (A) of Figure 2.8, can successfully travel down the quadrupole in the x- and y-direction to the detector. If an untargeted analysis is performed, the DC and RF potentials are scanned to allow ions with different *m*/z-ratios to have stable x- and y-direction trajectories and be sent to the detector.[43]

2.3.2 Ion Detection

After ions go through the quadrupole, they are detected. Ions are attracted to the detector by a large DC potential (-15 kV for positive ions). The detector system is a conversion dynode and an electron multiplier which is composed of a cathode and an anode. The ions first hit the surface of a conversion dynode that generates secondary particles of electrons and negatively charged ions, which are then attracted to the electron multiplier by a voltage gradient between the conversion

dynode and the electron multiplier. When the secondary particles strike the inner walls of the electron multiplier, which is a cathode, additional electrons are generated. The ejected electrons travel down the funnel-shaped cathode and repeatedly hit its inner walls, each time emitting a cascade of electrons. The cascade of electrons produces an electrical current at the terminating anode which is located at the base of the funnel-shaped cathode. The electric current generated at the anode is proportional to the number of secondary particles that initially hit the cathode; this is translated into an abundance for the ion packet that originally traversed the quadrupole. The ions' *m/z*-ratios are obtained by scanning the RF voltage (Equation 2.5). By relating the amplitude of the measured current at the anode and the timing of the RF voltage scan, a mass spectrum is acquired with the ions' *m/z*-ratios as the x-axis and the ions' relative abundance as the y-axis.

2.4 References

(1) Rathsack, P., Wollmerstaedt, H., Kuchling, T., Kureti, S. *Fuel*. **2019**, 248, 178-188.

(2) Machado, M.E. *Talanta*. **2019**, 198, 263-276.

(3) Dong, X., Wang, F., Fan, X. et al. *Fuel*. **2019**, 245, 392-397.

(4) Gajdosechova, Z., Mester, Z., Pagliano, E. *Anal. Chim. Acta*. **2019**, 1064, 40-46.

(5) Hsu, C.S., Hendrickson, C.L., Rodgers, R.P., McKenna, A.M., Marshall, A.G. J *Mass Spectrom.* **2011**, 46, 337-343.

(6) Marshall, A.G., Rodgers, R.P. *Proc. Natl. Acad. Sci*. **2008**, 105, 18090-18095.

(7) Marshall, A.G., Rodgers, R.P. *Acc. Chem. Res*. **2004**, 37, 53-59.

(8) Ma, J., Tang, S., Syed, J.A., Meng, X. *RSC Adv*. **2016**, 6, 82995-83002.

(9) Hoffmann, W.D., Jackson, G.P. *Annu. Rev. Anal. Chem*. **2015**, 8, 419-440.

(10) Busardò, F.P., Pacifici, R., Pichini, S. *Clin. Chem. Lab. Med*. **2017**, 55, e236-e237.

(11) Viant, M.R., Sommer, U. *Metabolomics*. **2013**, 9, 144-158.

(12) Beauchemin, D. *Mikrochim. Acta*. **1989**, 99, 273-281.

(13) Hourani, N., Andersson, J.T., Möller, I., Amad, M., Witt, M., Mani-Sarathy, S. *Rapid Commun. Mass Spectrom.* **2013**, 27, 2432-2438.

(14) Fenn, J.B., Mann, M., Meng, C.K., Wong, S.F. *Mass Spectrom. Rev.* **1990**, 9, 37-70.

(15) Liu, Z., Phillips, J.B. *J. Chromatogr Sci.* **1991**, 29, 227-231.

(16) James, A.T., Martin, A.J.P. *Biochem. J.* **1952**, 50, 679–690.

(17) Simmons, M.C., Snyder, L.R. *Anal. Chem.* **1958**, 30, 32-35.

(18) Liu, Z., Phillips, J.B. *J. Chrom. Sci.* **1991**, 29, 227-231.

(19) Ryan, P., Morrison, P.M. *J. Chromatogr. A.* **2005**, 1071, 47-53.

(20) Vendeuvre, C., Ruiz-Guerrero, R., Bertoncini, F., Duval, L., Thiébaut, D., Hennion, M.C. *J. Chromatogr. A.* **2016**, 1086, 21-28.

(21) Phillips, J.B., Luu, D., Pawliszyn, J.B., Carle, G.C. *Anal. Chem.* **1985**, 57, 2779-2787.

(22) Liu, Z., Phillips, J.B. *J. Microcol. Sep.* **1989**, 1, 159-162.

(23) Liu, Z., Phillips, J.B. *J. Microcol. Sep*. **1989**, 1, 249-256.

(24) Liu, Z., Phillips, J.B. *J. Microcol. Sep*. **1990**, 2, 33-40.

(25) Chow, H.Y.J., Górecki, T. *Anal. Chem*. **2017**, 89, 8207-8211.

(26) Bertsch, W. *J. High Res. Chrom.* **1990**, 22, 647-665.

(27) Dempster, A.J. *Phys. Rev*. **1918**, 11, 316-325.

(28) Amirav, A., Fialkov, A., Gordin, A. *Rev. Sci. Instrum*. **2002**, 73, 2872-2876.

(29) Wolfgang, L. *Z. Phys*. **1968**, 216, 241-247.

(30) Rapp, D., Englander-Golden, P. *J. Chem. Phys*. **1965**, 43, 1464-1479.

(31) Schulz, G. *Rev. Mod. Phys.* **1973**, 45, 423-486.

(32) Hwang, W., Kim, Y.K., Rudd, M.E. *J. Chem. Phys.* **1996**, 104, 2956-2966.

(33) Guilhaus, M. J *Mass Spectrom.* **1995**, 30, 1519-1532.

(34) Verentchikov, A., Ens, W., Standing, K.G. *Anal. Chem*. **1994**, 66, 126-133.

(35) von Mühlen, C., Zini, C.A., Caramão, E.B., Marriott, P.J. *J. Chromatogr. A.* **2008**, 1200, 34-42.

(36) von Mühlen, C., Khummueng, W., Zini, C.A., Caramão, E.B., Marriott, P.J. *J. Sep. Sci.* **2006**, 29, 1909-1921.

(37) Räther, O., Michelmann, K., Franzen, J. (**2011**) *US 8,013,290 B2*

(38) Verentchikov, A., Yavor, M., Mitchell, J.C., Arteav, V. (**2008**) *US 7,385,187 B2*.

(39) Kaiser, R.E., Cooks, R.G., Stafford, G.C., Syka, J.E.P., Hemberger, P.H. *Int. J. Mass. Spectrom*. **1991**, 106, 79-115.

(40) Miller, P.E., Denton, M.B. *J. Chem. Educ*. **1986**, 63, 617-623.

(41) Barber, M., Gordon, D.B., Woods, M.D. *Rapid Commun. Mass. Sp.* **1990**, 10, 442-446.

(42) Goeringer, D.E., Whitten, W.B., Ramsey, J.M., McLuckey, S.A., Glish, G.L. *Anal. Chem*. **1992**, 64, 1434-1439.

(43) March, R.E. *Rapid Commun. Mass. Spectrom.* **1998**, 12, 1543-1554.

CHAPTER 3. GC×GC/(EI) TOF MS METHOD DEVELOPMENT FOR THE ANALYSIS OF FUELS AND BASE OILS INTRODUCTION

3.1 Introduction

There is a global push to develop renewable/alternative fuels to reduce our reliance on fossil fuels, enhance energy security, and decrease adverse effects on the environment. However, in contrast to other fuels, aviation fuels simultaneously serve as hydraulic fluids, a cooling medium, and the power source of an aircraft;[1,2] thus, the approval process for such fuels is much more stringent than that for, for example, ground transportation fuels.[3,4] The multi-tier protocol used to test a fuel's ability to perform is defined by the American Standard Testing Methods (ASTM) D4054.[3] This method presents a significant hurdle to the development of alternative fuels due to its demands in terms of both cost and time, including the enormous volumes of fuel required to complete testing.[5] Ideally, a new test method should be created that requires small volumes of fuel to determine whether or not a fuel is fit-for-purpose based on its chemical composition. By using a fuels composition to predict the fuel's physical properties, if the physical properties of a given fuel could be predicted based on its chemical composition, such a test would save time and resources by eliminating unlikely alternative fuel candidates before they are tested by using ASTM D4054. Developing a method to determine the chemical compositions of successful aviation fuels would be the first step to predicting how the chemical components of fuels' affect their physical properties.

However, there is currently no definition for a "standard composition" of a successful fuel, leading to difficulties associated with analyzing such mixtures—no methods have been developed that can fully characterize petroleum fuels due to their complexity. For instance, carbon-13 NMR, proton NMR, and FTIR techniques have been previously used to chemically characterize fuels but have required the use of supplementary statistical models to analyze them successfully.[6-11] Additionally, such methods only provide knowledge of chemical bond types of compounds in the fuels, not details on the exact structures of these compounds. Thus, such methods do not present a good starting point for developing a new method for analyzing aviation fuels. Instead, a universal analysis method for determining the compositions of aviation fuels would allow abundances of different hydrocarbon classes to be determined and a "standard composition" for successful aviation fuels to be established. Additionally, any new testing method should be usable for both petroleum-based fuels and alternately sourced fuels, which is challenging because the success of

many analysis methods depends on the chemical composition of the compounds analyzed. It is possible that future alternative fuels could contain compounds not typically found in petroleum. Thus, an ideal analysis method must function for a wide variety of chemicals. Gas chromatography (GC) coupled with mass spectrometry (MS) represents one possible universal method.

The compositions of fuels have been previously analyzed with gas chromatography followed by electron ionization (EI) and mass analysis with a mass spectrometer (GC/(EI) MS). Such analysis has been conducted using both quadrupole[12,13] and time-of-flight (TOF) mass spectrometers,[14] offering low-resolution and high-resolution mass analysis, respectively. GC/(EI) MS couples an efficient separation method with mass spectrometry, which is advantageous because the mass spectra collected are simpler to interpret than a single mass spectrum produced from an unseparated mixture. However, using GC/(EI) MS, only 170 compounds (out of thousands) in the petroleum-based fuel Jet-A, could be resolved.[15] Therefore, since the mixture is exceptionally complex, the use of a two-dimensional separation method may be necessary to efficiently separate all of the compounds before detection. This can be achieved by comprehensive two-dimensional gas chromatography (GC×GC), which has a higher resolving power than one-dimensional gas chromatography.[16] Furthermore, GC×GC coupled to an electron ionization (EI) source followed by TOF MS analysis is a universal analysis method which does not rely on chemical composition or structure to ionize or detect chemical compounds. Thus, GC×GC/(EI) TOF MS was chosen as the combination separation-analysis method for analyzing the jet fuels studied in this research.

However, GC×GC separation must be optimized before the separation of a mixture as complex as a jet fuel can be performed. For instance, GC×GC separation can be performed with either a normal or reverse-phase column configuration. A normal configuration has a primary capillary column with a nonpolar stationary phase and secondary column with a polar stationary phase, while the reverse-phase configuration has the columns in the reverse order. It is advantageous to have the longer, primary column with a stationary phase polarity that best separates compounds in the mixture;[17] thus, the first step in developing a successful GC×GC separation method is to determine which configuration offers the best separation. If the content of the mixture is unknown, this must be determined empirically. Once the optimal configuration is determined, optimal temperature programming of the injection port, primary and secondary ovens, modulator, transfer line, and ionization chamber must be performed. This chapter will discuss the

GC×GC method development for analyzing petroleum-based fuels, alternative fuels, and fuel additives. The developed method was also found to be successful for separating and analyzing another processed petroleum-based mixture, light base oils. The methodology used to analyze the base oils will also be discussed at the end of this chapter.

3.2 Experimental

Method parameters developed over the course of these experiments, and the resulting mixture analysis will be discussed below in the results section (Section 3.3). Each method, however, had several components in common. First, all samples were analyzed using a GC×GC/(EI) TOF MS (Pegasus GC-HRT 4D from Leco; Saint Joseph, MI), as follows. An auto-injector (Agilent G4513A) was used to inject 0.5 μL of each sample into a split/splitless injector with a split ratio of 1:20 held at 260 °C with a constant flow (1.25 mL/min) of ultra-pure helium (99.9999%) carrier gas. An acquisition delay of 350 seconds was employed to prevent the ionization of solvent, which would have saturated the detector and potentially harmed the EI filament. The transfer line from the GC×GC to the MS was held at 300 °C throughout the analysis. The MS ion source was held at 250 °C throughout the analysis. Eluted compounds were ionized by EI using 70 eV kinetic energy electrons, and all ions were transferred into a TOF MS for high-resolution analysis (20 m flight path; 25,000 resolution at *m/z* 219). Mass spectra were collected at an acquisition rate of 200 Hz. Data collection, processing, and analysis were performed by using LECO's Visual Basic Scripting (VBS) software, ChromaTOF version 5.10.58.0.52262. The Wiley (2011) and NIST (2011) mass spectral databases were used for compound identification with a match factor threshold of > 800 (on a scale of 0-999). Daily mass calibration and tuning were performed using perfluorotributylamine (PFTBA) as the calibrant.

Different gas chromatography columns were employed throughout to optimize the column configuration for analysis. First, a normal-phase configuration was investigated for separating fuels and fuel additives. The nonpolar primary column was 30 m in length (Rxi-5ms, Restek; Bellefonte, PA) and the polar secondary column was 1 m in length (Rxi-17Sil ms, Restek; Bellefonte, PA). Next, a reverse-phase configuration was investigated using polar primary column 30 m in length (Rxi-17Sil ms, Restek; Bellefonte, PA) and a nonpolar secondary column 2 m in length (Rxi-1ms, Restek; Bellefonte, PA). Finally, a reverse-phase column configuration was tested with a longer polar primary column, 60 m in length (Rxi-17Sil ms, Restek; Bellefonte, PA),

and a nonpolar secondary column of 2 m in length (Rxi-1ms, Restek; Bellefonte, PA). Various temperature settings were investigated for sample separation and ion detection and will be discussed where appropriate. The separation was considered suitable when peaks were baseline separated, and no coelution was detected (no shouldering peaks, or peaks marked with more than one compound identification marker). After the column configuration was determined, the resulting method was then expanded to include analysis of light base oils, and the temperatures were adjusted as discussed below.

All fuel and fuel additive samples were diluted in *n*-hexane (≥ 97% pure, Sigma Aldrich) at a dilution factor of 1:100 before analysis. Petroleum-based jet fuel (Jet-A) was tested in addition to alternative fuels and fuel additives including synthetic iso-paraffins (SIP), Fischer-Tropsch synthetic-8 (FT-S8), hydroprocessed esters and fatty acids (HEFA), and catalytic hydrothermal conversion jet (CHCJ).

Linear alkane model compounds for the light base oils, carbon numbers *n*-C14 to *n*-C28 (>99% pure), and *n*-butylbenzene (>99% pure) were purchased from Sigma Aldrich and used without further purification. Model compound mixtures were prepared by performing serial dilutions of the model compounds with *n*-hexane (≥ 97% pure, Sigma Aldrich). The total volume of each model compound solution studied was 1 mL and the model compound concentrations were 1,000 ppm. Each base oil sample and model compound mixture was doped with 20 µL of a 3,034 ppm stock solution of *n*-butylbenzene, which served as an internal standard.

The concentration of the base oils used for these studies differed due to the varying amounts of linear alkanes present in them. The base oils are simply defined as Base Oil A and Base Oil B based on request from the funding agency. The concentrations for the base oils were chosen based on the observed GC×GC peak areas for linear alkanes. It was desired that the linear alkanes produce a signal with a signal to noise ratio above 3:1, with peak areas below the saturation limit of the detector for proper quantification. Therefore, the final concentration used of Base Oil A was 4,552 ppm, and the concentration of Base Oil B was 11,380 ppm in 1 mL of *n*-hexane.

3.3 Results and Discussion

3.3.1 Development of an appropriate separation method for aviation fuels and fuel blending components

First method development was performed for Jet-A, a petroleum-based aviation fuel. Jet-A is currently utilized by commercial aviation companies world-wide and is used as a standard fuel to start building the separation method. The GC×GC/(EI) TOF MS instrument used to analyze the fuels is described in Chapter 2 (Section 2.2). The first GC×GC column configuration tested, was a normal-phase column configuration. The boiling point of Jet-A (176 °C),[3] served as a guideline for the inlet temperature and the maximum temperature of the primary GC oven (which were both kept above 176 °C). The inlet temperature was set to 260 °C to ensure complete vaporization of all the compounds in Jet-A. The initial oven heating parameters were as follows: the primary oven (containing the nonpolar column) was set to 40 °C and held there for 0.2 minutes after sample injection. After this, the oven was heated to a maximum temperature of 200 °C at a rate of 1.5 °C /min. The oven was then held at 200 °C for 4 minutes. Increasing the temperature of the GC ovens over the course of analysis separates components of the sample by boiling point in addition to polarity. The secondary oven was offset by + 10 °C from the primary oven and followed the same temperature program (i.e., the heating rate and times were the same, but the temperatures were 10 °C higher). The dual-stage thermal modulator, Figure 2.3, had a total modulation time of 4 s, split between two stages of thermal modulation (2 s each): 0.5 s was used for the hot jet pulse and 1.5 s for the cold jet pulse. The modulator hot jet was offset by + 15 °C from the secondary oven containing the polar column and used heated nitrogen gas; the cold jet used cryo-cooled nitrogen gas. Data were collected over an *m/z* range of 45-510 and analyzed, as discussed in the experimental section. The chromatogram resulting from the analysis of Jet-A is shown in Figure 3.1.

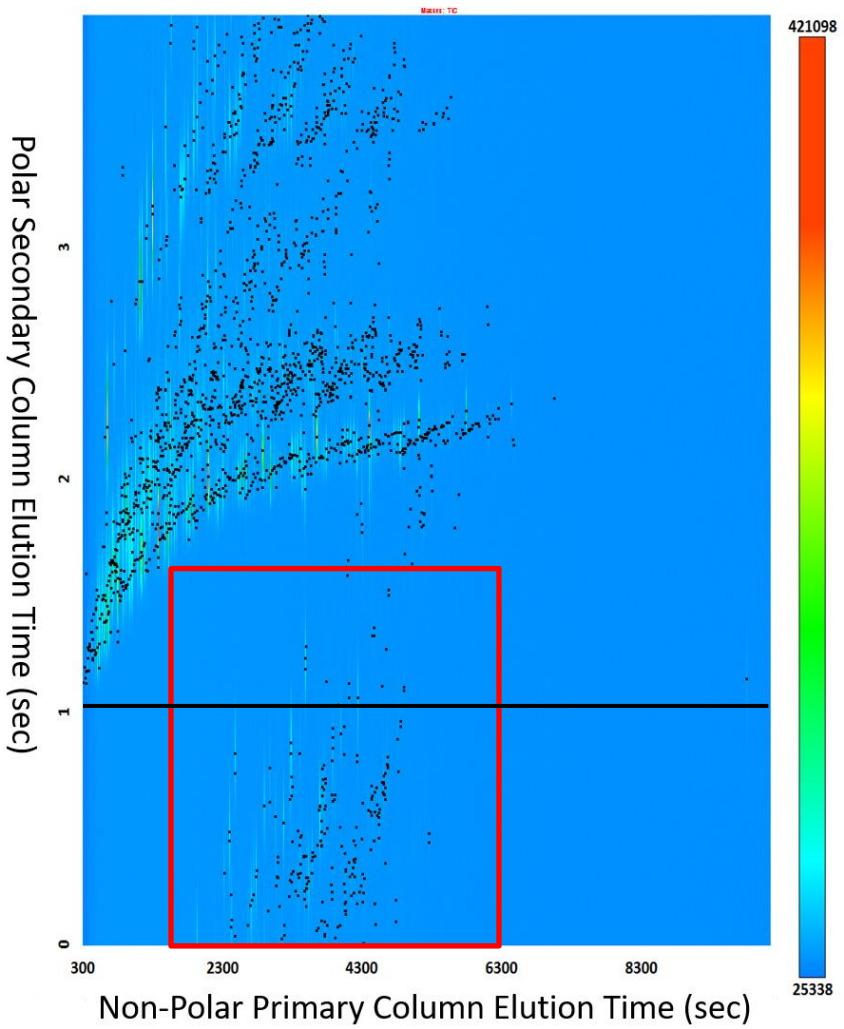

Figure 3.1. Jet-A sample analysis using normal-column configuration. The sample exhibits a phenomenon known as wrap-around, highlighted in the red box. Wrap-around is noted because the analytes appear to elute before the solvent line, marked with a black line for clarity. This phenomenon implies the method was unsuccessful.

The chromatogram for the analysis of Jet-A, using the normal-phase configuration (Figure 3.1), exhibited a phenomenon where some analytes (red box) appear to elute before the solvent (noted as a black line in Figure 3.1 for clarity), which is theoretically impossible as the solvent is chosen to have a boiling point significantly lower than analytes in the mixture. This observed elution indicates a phenomenon known as wrap-around occurred. This occurs when analytes do not have enough time to traverse the secondary column before the modulator sends a new analyte packet from the primary column to the secondary column.[18] Two methods are used to resolve this issue: 1) increase the secondary oven temperature-offset such that analytes move through this

column faster or 2) increase the modulation time to allow packets sufficient time to move through the secondary column before the next packet is released. The modulation time controls the size of the aliquot delivered onto the secondary column from the primary column. Therefore, it is desirable to keep the modulation time small to maintain the separation of compounds from the primary column and avoid overloading the secondary column. Keeping the modulation time small therefore improves separation and resolution.[18] As such, the modulation time was not changed; instead, the secondary oven offset was increased to + 35 °C, and the modulation temperature offset was increased to + 20 °C. These changes greatly improved the separation and eliminated the observed wrap-around (Figure 3.2).

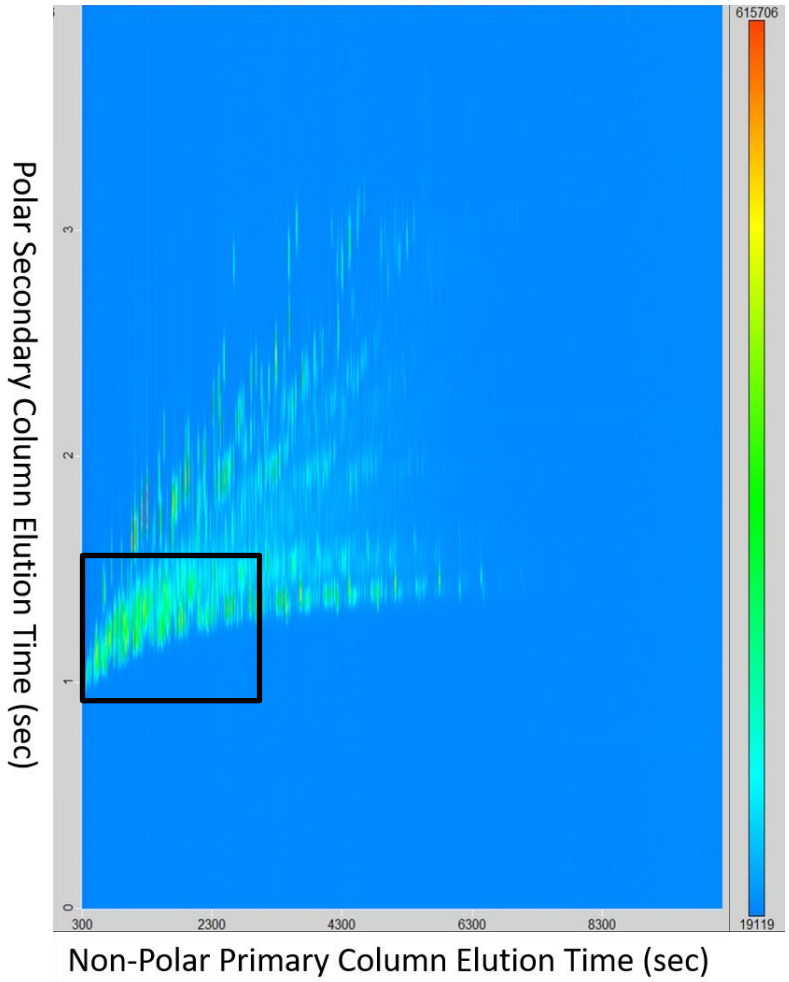

Figure 3.2. Chromatogram of normal-phase GC×GC separation of Jet-A. The lack of baseline separation of small alkane compounds is highlighted by the black box.

However, while this method sufficiently separated aromatic compounds, it does not sufficiently separate *n*-, *iso*-, and cycloalkanes, as shown in Figures 3.2 and 3.3. In these figures, many alkanes can be observed without baseline separation (Figure 3.2, black box) between peaks, which implies many compounds are eluting simultaneously. Additionally, compounds belonging to three different chemical classes (*n*-, *iso*-, and cycloalkanes), as identified by comparison of their EI mass spectra measured, to those available from NIST,[19] should not be eluting in the same area of a chromatogram (Figure 3.3). Furthermore, since the goal of this project was to investigate jet fuels from both petroleum and alternative sources, which are mainly composed of saturated hydrocarbons,[20] insufficient separation of *n*- and *iso*-alkanes will not allow proper characterization of these mixtures. Therefore, the column configuration was inverted to a reverse configuration to better separate alternative fuel and fuel blending components–reversing the column configuration should allow for better separation of the saturated analytes,[21] due to the difference in retention index between linear and branched isomers, which is greater when using a polar stationary phase as compared to a nonpolar one; therefore reversing the column configuration such that the longer primary column has a polar stationary phase, should allow for a better separation of the *n*- and *iso*-alkanes.[22]

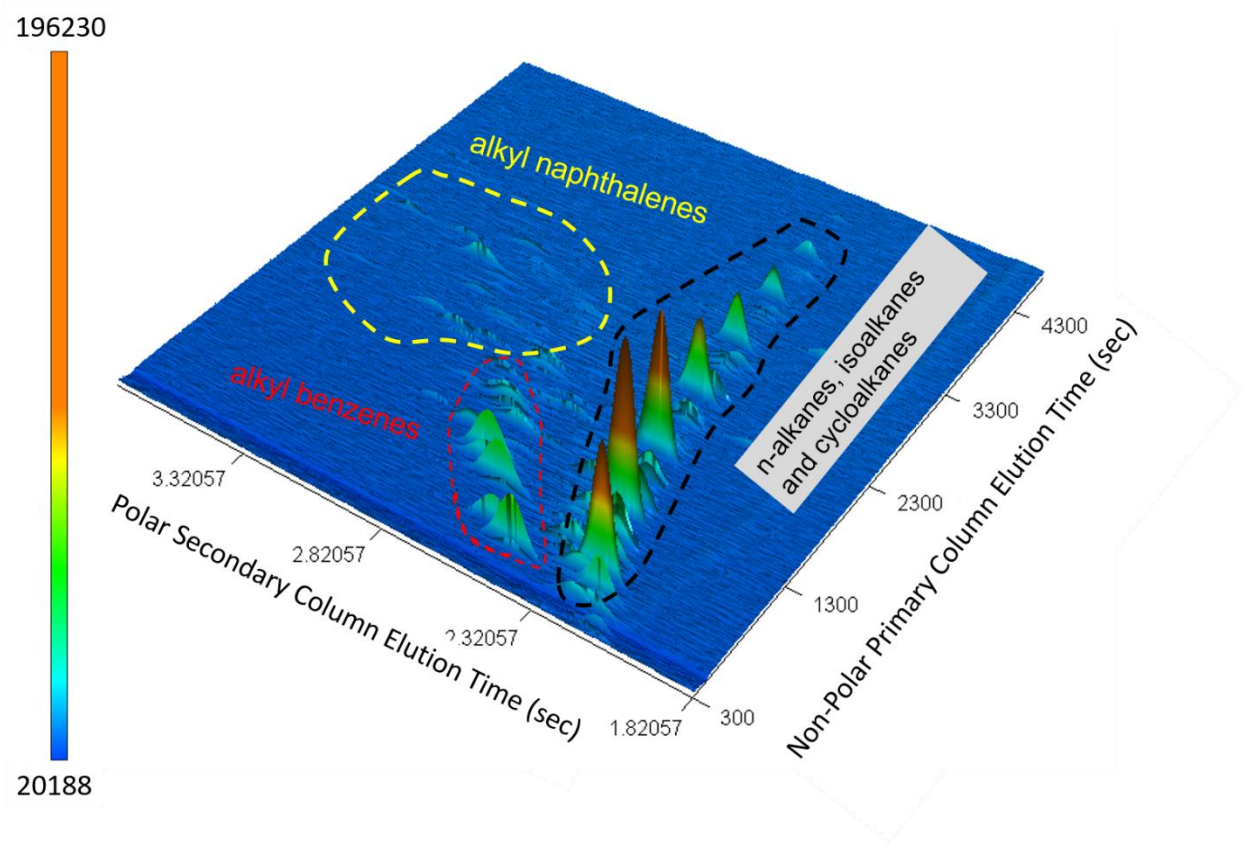

Figure 3.3. 3D GC×GC chromatogram of Jet-A fuel with three chemical classes outlined: 1) n-alkanes, iso-alkanes, and cycloalkane compounds, 2) alkyl benzene compounds, and 3) alkyl naphthalene compounds. Compounds were identified based on their EI MS match to the NIST library.

The columns were reversed and a 30 m primary column (Rxi-17Sil ms) with a polar proprietary stationary phase was used. Also, a slightly longer 2 m secondary, nonpolar column, (Rxi-1 ms) with a stationary phase composed of 100% dimethylpolysiloxane, was used. Note that the stationary phase is slightly different from the previously used columns; the percentage of dimethylpolysiloxane was increased in the secondary column in order to increase the difference in polarity between the stationary phases of the primary and secondary columns. The following method was then utilized to separate Jet-A. The oven was heated to 200 °C at the rate of 1 °C /min, then held at the maximum temperature of 200 °C for 4 minutes. Due to the increased separation, the modulation time previously utilized (4 s) was insufficient to prevent wrap-around from occurring and thus was increased to 8 s. The total modulation time of 8 s was split between the two stages (4 s each), 1.3 s of which was used for the hot jet pulse and 2.7 s for the cold jet pulse.

The modulator hot jet was offset by + 20 °C from the secondary oven containing the nonpolar column. The secondary oven was offset by + 35 °C from the primary oven and followed the same temperature program as the primary oven: heated to 75 °C and held there for 0.2 minutes after sample injection, heated to 235 °C at the rate of 1 °C /min where it was held for 4 minutes. Data were collected over a *m/z* range of 45-510 and the data analyzed as discussed in the experimental section above (Section 3.2).

The reverse-column configuration substantially improved separation of *n*- and *iso*-alkanes as well as cycloalkanes while maintaining the separation of aromatic compounds, Figure 3.4. Separation and identification of the aromatic compounds by using the normal-column configuration was maintained in the reverse-column configuration, and many more *n*-, *iso*-, and cycloalkanes were identified by using the reverse-column configuration. New compound class elution regions were determined by model compound studies on the reverse-column configuration. The determination of the elution boundaries was completed by using model compounds, conducted by Dr. Mark Romanczyk and were described in his graduate dissertation, Chapter 4.[23] In Figure 3.4, the orange line notes an example of the separation between compounds with the same carbon number, that formed a pattern of an elution line on the chromatogram. These carbon numbers were based on the chemical structures, which were determined by a comparison of the mass spectra of those compounds and the NIST EI MS library. Each elution line is the separation of a separate carbon number, and the area of elution is representative of the type of compound present, Figure 3.4.

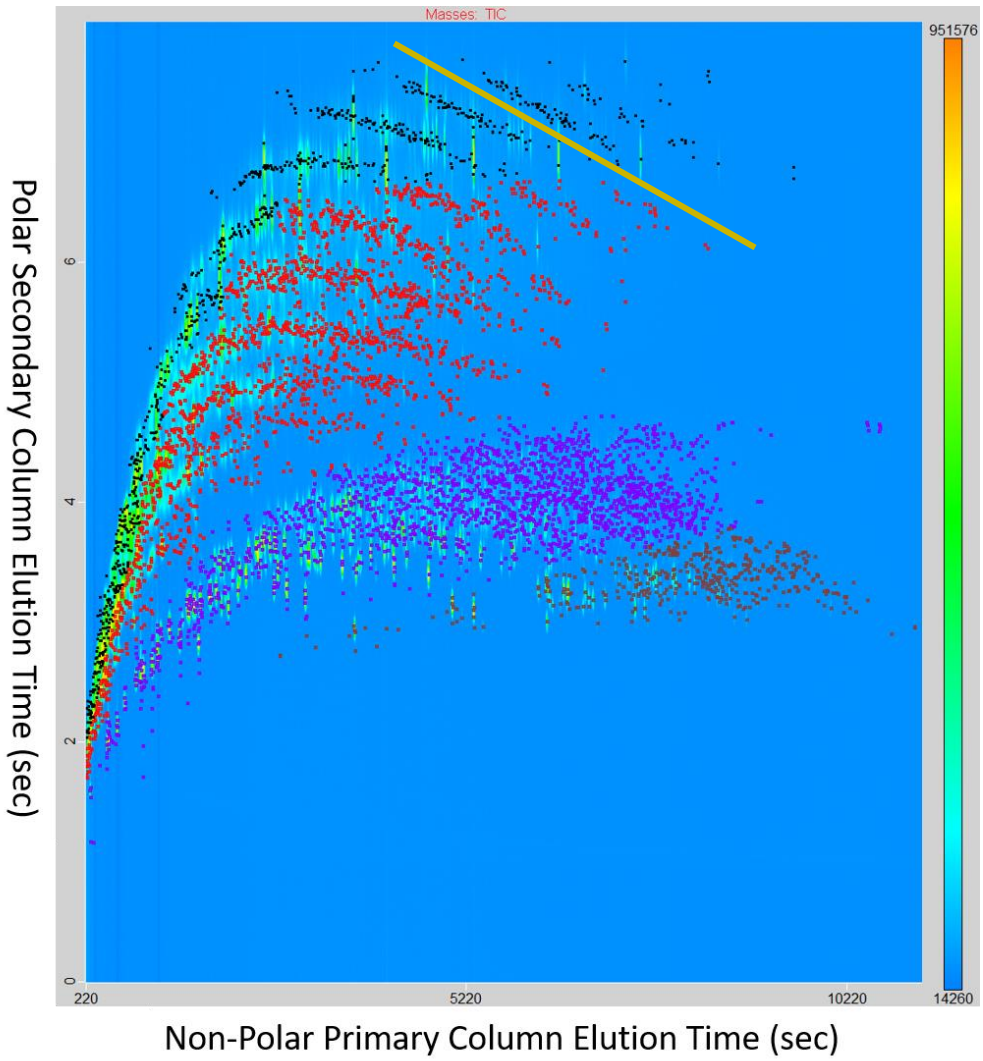

Figure 3.4. GC×GC chromatogram of Jet-A where each elution peak apex is labeled with a dot marker. The n- and iso-alkanes are marked in black, cycloalkanes are in red, alkyl benzenes are in purple, and alkyl naphthalenes are in brown. Compound class elution regions were determined by model compound studies. The orange line notes an elution trend line in which all the compounds are of a specific carbon number. This elution trend is present throughout the chromatogram of the saturated compounds.

Although this method efficiently separated the larger compounds, upon closer inspection of smaller compounds, coelution still occurred, Figure 3.5. Unfortunately, this method was already pushing the bounds of the maximum temperatures possible without dephasing the capillary columns. The solution then was to increase the length of the columns to improve separation. Thus, a longer primary column was tested: the polar primary column was increased from 30 m to 60 m in length.

Figure 3.5. A)GC×GC chromatogram of Jet-A zoomed in on the smaller analytes eluting before 2,000 seconds primary column elution time and 5.5 seconds secondary column elution time. B) The 3-D representation of the same GC×GC chromatogram shown in A. The z-axis represents intensity, and the color intensity scale, which represents counts, is noted on the left. C) A further zoomed-in GC×GC chromatogram of 720 ± 100 seconds primary column elution time and 3.5 ± 0.5 seconds secondary column elution time. The tooth-like mountains with multiple apexes (pink circle) are undesired co-elution of compounds while only one elution peak, with one apex (black circle), should ideally be observed for all compounds. D) A closer look at the undesired co-eluting compounds noted in the pink circle shown in C. It can be observed that no baseline separation is achieved for many compounds.

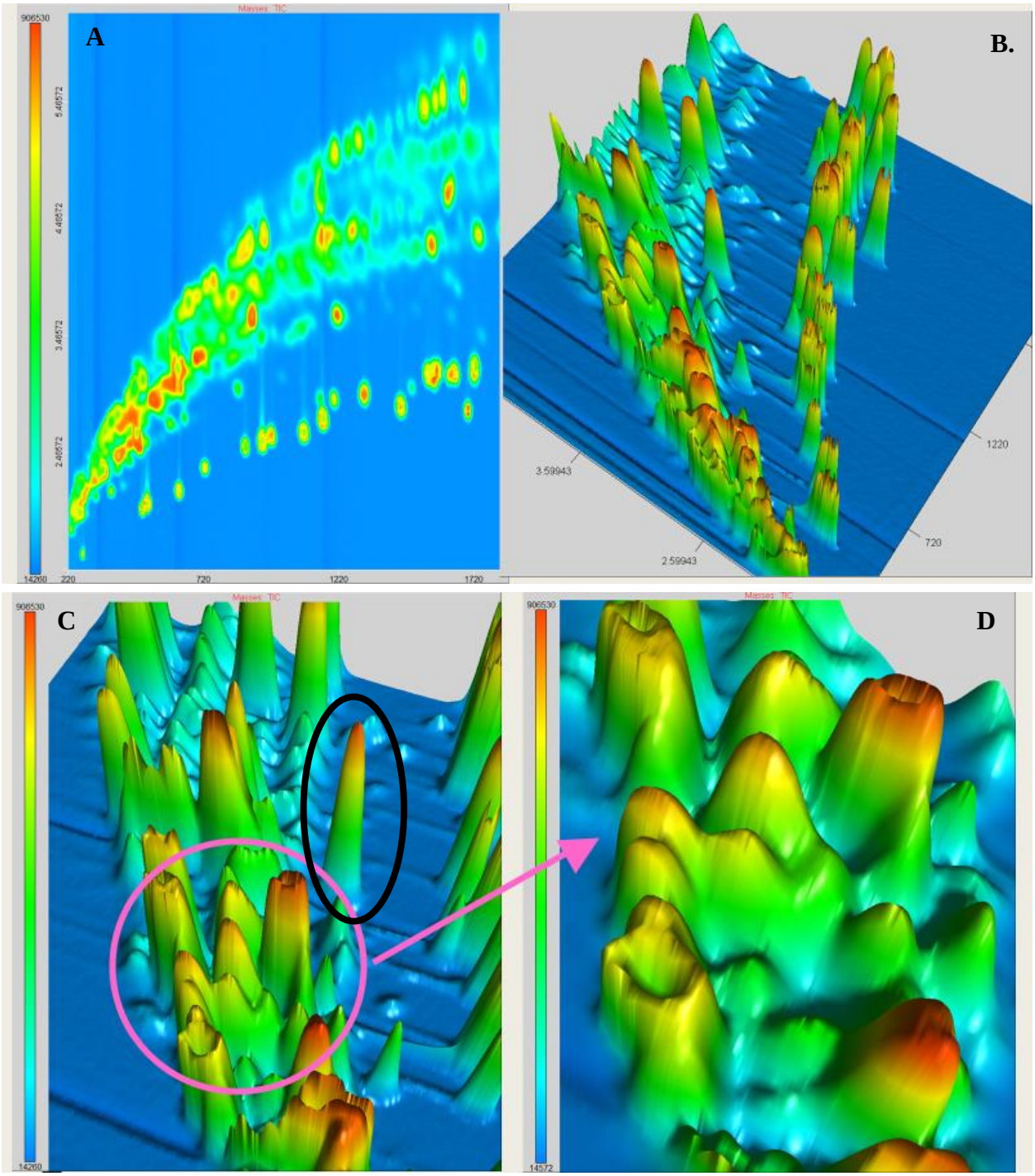
A
B.
C
D
906530
14260
220
720
1220
1720
3.59943
2.59943
1220
720

The new reverse-phase column configuration and the following method was used to analyze Jet-A. The primary oven was heated to a maximum temperature of 180 °C at a rate of 1 °C /min. The oven was then held at the maximum temperature for 6 minutes. The secondary oven was offset by + 10 °C from the primary oven and followed the same temperature program as the primary oven. The modulator hot jet was offset by + 80 °C from the secondary oven containing the nonpolar column. Data were collected over a *m/z* range of 45-510 and the data was analyzed as previously discussed in the experimental section (Section 3.2). The resulting chromatogram of Jet-A analyzed using this method is shown in Figure 3.6. Compounds belonging to four general chemical classes were observed: *n*- and *iso*-alkanes, cycloalkanes, aromatic compounds, and naphthenic compounds. Compared to the literature, more compounds were able to be separated and observed while maintaining a consistent elution pattern and elution boundaries for the chemical classes.[24-26]

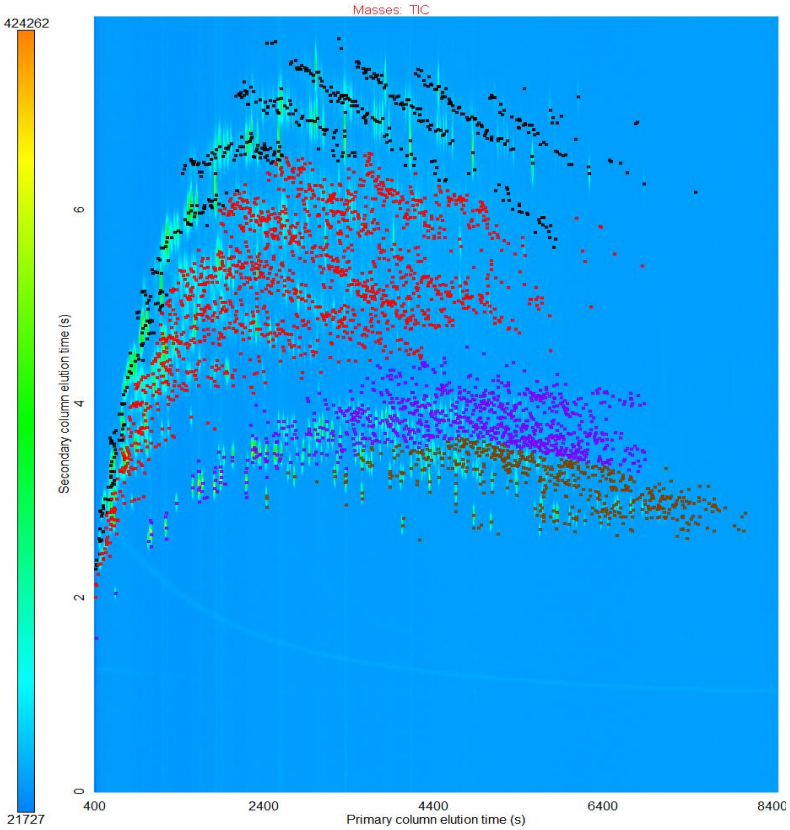

Figure 3.6. Jet-A GC×GC chromatogram obtained by using longer column sets. Each elution peak apex is labeled with a dot marker. The n- and iso-alkanes are marked in black, cycloalkanes are in red, alkyl benzenes are in purple, and alkyl naphthalenes are in brown.

The reverse configuration method using the longer columns generated the best separation of all compounds in Jet-A and was therefore used to analyze all other fuel and fuel additive samples. Samples of synthetic iso-paraffins (SIP), Fischer-Tropsch synthetic-8 (FT-S8), hydroprocessed esters and fatty acids (HEFA), and catalytic hydrothermal conversion jet (CHCJ) were analyzed using the reverse configuration method using the longer column setup, and the resulting chromatographs are shown in Figure 3.7A-D.

Figure 3.7. Compounds are classified in colors: black- *n*- and *iso*-alkane compounds, red- cycloalkane compounds, purple- aromatic compounds, and brown- naphthalene compounds. Each mark on the figure is a unique compound with a specific chemical structure assigned to it. The heat map of color indicates the intensity (counts) of the compound peak. All x-axis denotes elution time from the primary column (seconds) and y-axis denotes elution time from the secondary column (seconds). A) FT-S8 aviation fuel additive diluted 1:100 for analysis. B) 50/50 Jet-A/ HEFA aviation fuel diluted 1:100 for analysis. C) SIP alternative fuel additive diluted 1:500 for analysis, consisted of one analyte: 2, 6, 10-trimethyldodecane. D) CHCJ alternative pathway aviation fuel diluted 1:100 for analysis.

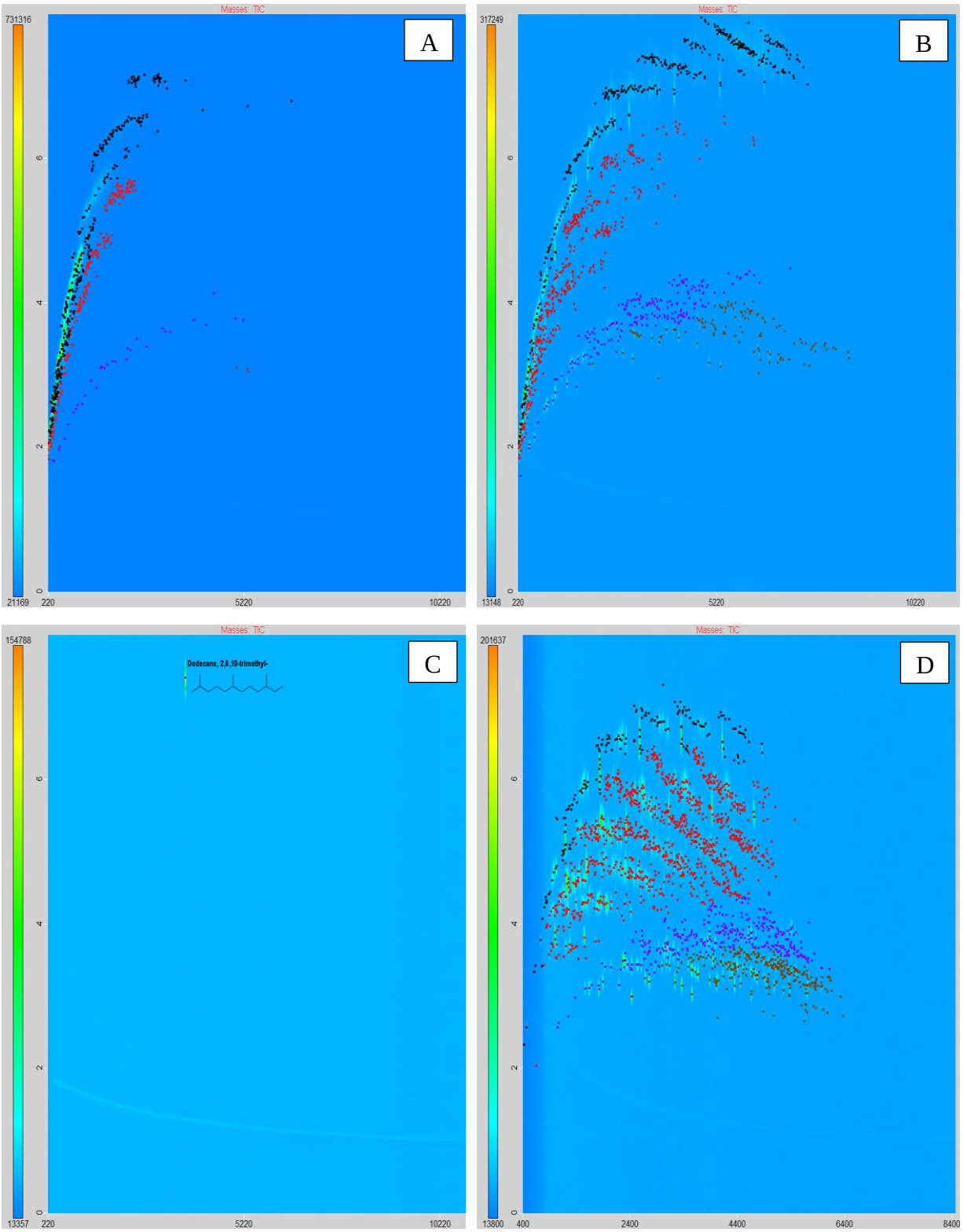
Masses: TIC
731316
21169
220
5220
10220
A
Masses: TIC
317249
13148
220
5220
10220
B
Masses: TIC
154788
13357
220
5220
10220
Dodecane, 2,6,10-trimethyl-
C
Masses: TIC
201637
13800
400
2400
4400
6400
8400
D

Comparing Figures 3.6 with 3.7 a and c, it becomes apparent why FT-S8 and SIP are used as fuel additives and not neat alternative fuels: they both lack aromatic and naphthalene compounds. Such compounds are vital for aviation fuels because their chemical structures allow them to penetrate and swell the nitrile rubber O-ring seals in aircrafts, preventing the fuel from leaking out of an aircraft's engine.[27,28] Therefore, lacking these compounds, FT-S8 and SIP cannot swell O-ring seals and function as neat alternative aviation fuels. Further, FT-S8 has been approved by the ASTM for use in aircrafts when blended up to 50 % with Jet-A.[28] In contrast, SIP is approved by the ASTM for use in aircrafts only up to a 10 % blend with Jet-A.[28] These blending limits can be explained by the data collected here. As seen in Figure 3.7a, FT-S8 contains some *n*-, *iso*-, and cycloalkanes along with a few aromatic and naphthalene compounds. By comparison, SIP (Figure 3.7c) is composed entirely of one C15 compound: 2,6,10-trimethyldodecane. Therefore, FT-S8 can be blended at a higher volume than SIP, as it contains more compounds similar to Jet-A. It is still desirable to blend these additives rather than using them neat, however, as emissions from blended fuels can be between 50 and 85 % of those of neat Jet-A.[29] Figure 3.7 b and d on the other hand, are approved for use as fuels and their chemical compositions are more comparable to the Jet-A chemical composition, Figure 3.6, with the exception of some larger molecule components. Now that appropriate separation and analysis methods were developed for these mixtures, the next step was to identify the compounds in each sample. This will be discussed in the next section.

3.3.2 Determination of the chemical composition of aviation fuels and fuel blending components

A three-step identification method was utilized to determine the chemical compositions of the aviation fuel (Jet-A) and the fuel blending components. First, the mass spectrum of each compound, collected at the apex of the GC×GC elution peak, was compared against standard libraries of EI mass spectra collected at 70 eV electron energy. This comparison identified possible compound formulations and structures which matched the observed fragmentation pattern and/or molecular ions present. A similarity score ranging from 0 to 999, representing how well the obtained spectrum matched the library spectrum (0 - 99.9%), was assigned to each library match. A higher similarity score is usually indicative of a suitable chemical and structural match. However, when there is no molecular ion, no molecular weight information can be used to predict the chemical formula and structure. This is especially problematic for linear saturated hydrocarbons, which

fragment very easily. For example, tetradecane (*n*-C14) was analyzed using GC×GC/(EI) TOF MS with 70 eV EI energy, and a spectrum was obtained. The computer proposed this species to be pentadecane (*n*-C15) with a 928-similarity score, Figure 3.8. Although this is a high matching score, the wrong compound was identified from the data, which is problematic for many of the linear saturated hydrocarbons. To circumvent this problem, a second level identification was used: comparison of the observed chromatographic retention times to the standard model compound mixtures.

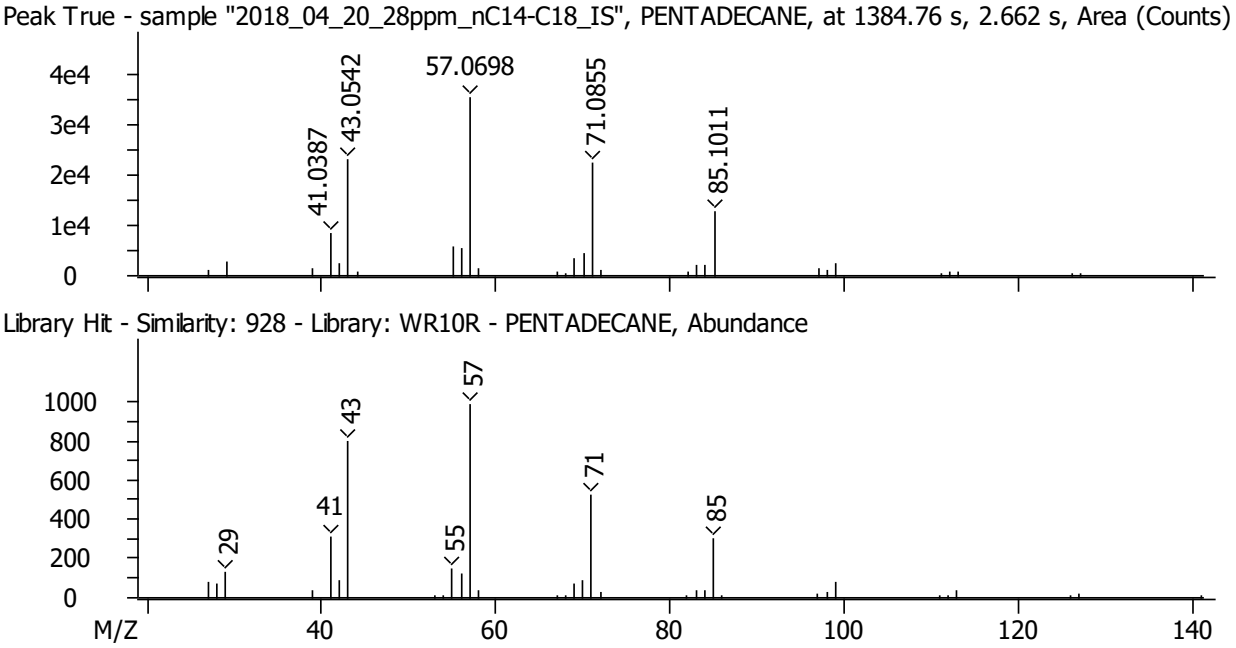

Figure 3.8. EI (70 eV) TOF mass spectrum from a GC×GC/(EI)TOF MS and NIST library mass spectrum for tetradecane (n-C14) (top) and pentadecane (n-C15) (bottom), similarity score 928.

First, a mixture of linear alkanes, ranging from *n*-C14 to *n*-C28, was analyzed, and retention times were determined and reported with Jeremy Manheim.[32] Another mixture used for compound identification based on chromatographic retention time was a model compound mixture composed of alkyl benzene isomers. These specific compounds were studied because their fragmentation patterns could not be used to identify them accurately. All of the compounds in the model mixture, but one, were determined to be in Jet-A (Table 3.1). In Table 3.1, slight retention time shifts were observed when comparing the model compound mixture to the Jet-A sample.

However, this is an innate obstacle of the GC×GC itself which has been noted to suffer from retention time-shifting.[30,31]

As a third-identification method, the elution boundaries of alkanes[33] were used in addition to the aromatic compound elution boundaries (determined here) to verify chemical identification and structural assignments. The elution boundaries were also used to determine if the computer matching of the EI MS to the NIST library was reasonable (e.g., it would be unreasonable for the library match to predict an *n*-alkane structure in an elution area characteristic of aromatic compounds).[23]

By using all three steps: EI library matching, model compound retention times, and elution boundaries for the major chemical classes, the chemical composition of each fuel was evaluated. Given the unique nature of some of the compounds in these fuels, some structural and chemical assignments were not possible. However, by using the chemical class elution boundaries, the type of compound could at least be determined.

Table 3.1. Model compound retention times for the polar (x) primary GC column and nonpolar (y) secondary GC column compared to retention times for compounds in Jet-A which were determined to be the same compounds.

MW	Compound	Known Compound Retention Time (x)	Known Compound Retention Time (y)	Jet-A Retention Time (x)	Jet-A Retention Time (y)
106	o-xylene	1240.24	2.515	1240.24	2.592
106	m-xylene	1064.19	2.463	1064.19	2.525
106	p-xylene	1056.19	2.479	Resolution	Resolution
106	ethylbenzene	1032.18	2.422	1032.18	2.479
120	propylbenzene	1552.23	2.983	1552.33	2.967
120	isopropylbenzene	1368.28	2.839	1368.28	2.818
120	2-ethyltoluene	1808.40	2.967	1808.4	2.942
120	3-ethyltoluene	1632.35	2.823	1632.35	2.947
120	4-ethyltoluene	1624.35	2.901	1624.35	2.967
120	1,3,5-trimethylbenzene	1664.36	3.034	1664.36	2.998
120	1,2,3-trimethylbenzene	2184.52	3.043	2184.51	2.993
120	1,2,4-trimethylbenzene	1880.42	2.895	1880.42	2.942

3.3.3 Determination of the chemical composition of light base oils

The developed fuel analysis method was also used to analyze light base oils by using the same reverse-column configuration with a polar 60 m capillary column (Rxi-17Sil ms, Restek; Bellefonte, PA) followed by a nonpolar 2 m capillary column (Rxi-1 ms. Restek; Bellefonte, PA). The primary oven housing the nonpolar column was set to an initial temperature of 65 °C and held there for a duration of 1 minute after sample injection. Then the oven was heated to 270 °C at the rate of 1 °C/min and held at the maximum temperature for 6 minutes. The total modulation time of 5 s was split between two stages (2.5 s each), 0.75 s of which was used for the hot jet pulse and 1.75 s for the cold jet pulse. The modulator hot jet was offset by + 80 °C from the secondary oven containing the nonpolar column. The secondary oven was offset by + 10 °C from the primary oven and followed the same temperature program as the primary oven.

This methodology was utilized to analyze the chemical composition of two light base oils. Each of the base oil samples, referred to as Base Oil A and Base Oil B, were analyzed as follows. Compounds eluting from the GC×GC entered the EI source region through the transfer line that was held at 300 °C. The compounds were ionized by EI at 70 eV electron energy. The detected mass spectral range was *m/z* 15-500, and the data were analyzed by the method previously described in the experimental section (Section 3.2).

The characteristic GC×GC elution boundaries for the different types of alkanes in the base oils, including linear, branched, and cyclic alkanes, have been previously determined with model compounds[34] as well as verified in this research using the model compounds as discussed previously. Based on these elution boundaries, the different classes of compounds were differentiated (Figure 3.9). To determine the exact linear alkane retention times with carbon numbers pertinent to this work, a model compound mixture was analyzed for linear alkanes with carbon atoms ranging from 14 to 28. The retention times for the model compounds were compared to the base oil samples, Table 3.2. The compounds in the base oil samples with the same retention times as the model compounds yielded EI mass spectra similar to those of the model compounds, implying that these species are present in the base oil samples. Intriguingly, linear alkanes with 19 to 28 carbon atoms were not detected in either sample. The base oil samples were analyzed at various mass fractions (ppm), by diluting the base oils in *n*-pentane, to ensure that linear alkanes present at low concentrations were detected. Based on the retention times, linear alkanes with 14 to 18 carbons were present in Base Oil A and linear alkanes with 15 to 18 carbons in Base Oil B,

Table 3.2. Overall, the compounds in Base Oil A ranged from carbon numbers 14 to 20 while those in Base Oil B ranged from carbon number 15 to 28.

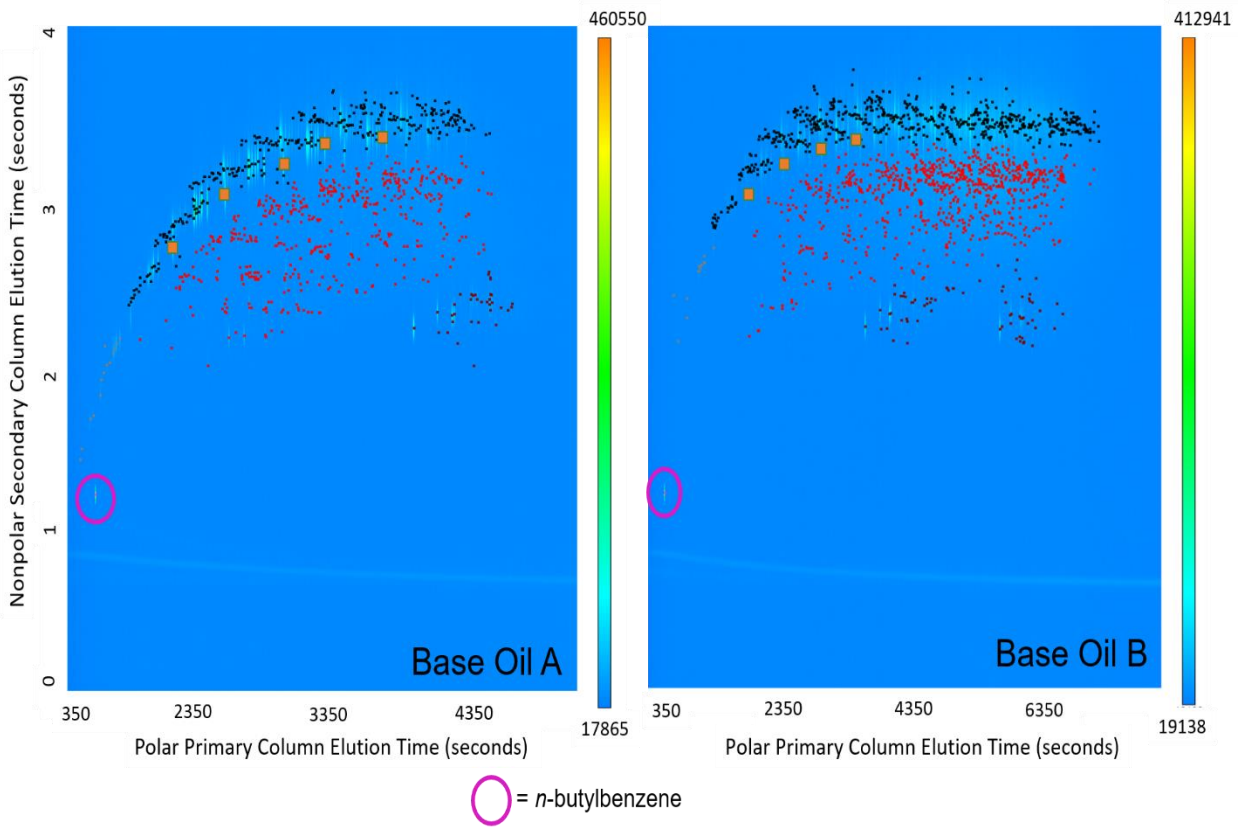

Figure 3.9. 2D-Gas chromatograms measured for Base Oil A (left) and Base Oil B (right) at mass fractions of 4550 ppm and 11400 pm in n-hexane, respectively, by using GC×GC/EI TOF MS. Each orange square represents a different linear alkane, each black dot represents a different iso-alkane, each red dot represents a different mono-, di-, or tricyclic alkane, and each brown dot represents a different tetra- or pentacyclic alkane. The internal standard, n-butylbenzene, that was spiked into each base oil is noted by the purple circle.

Table 3.2. Retention times in the primary (polar) column and the secondary (nonpolar) column for standard linear alkanes that have similar retention times as compounds in Base Oil A and Base Oil B. N/A denotes "not applicable" as a compound with this retention time was not found in the base oil samples.

	Polar Column Retention Time (s)			Nonpolar Column Retention Time (s)		
Linear Alkane[1]	**Standard**	**Base Oil A**	**Base Oil B**	**Standard**	**Base Oil A**	**Base Oil B**
C14	1384.76	1384.76	N/A	2.664	2.664	N/A
C15	1894.65	1894.65	1894.65	2.988	2.978	2.993
C16	2464.52	2464.52	2469.52	3.168	3.168	3.178
C17	3064.38	3064.38	3064.38	3.261	3.258	3.266
C18	3664.25	3664.25	3669.25	3.286	3.291	3.317
C19	4249.11	N/A	N/A	3.343	N/A	N/A

[1]Linear alkanes C20-C28 are not shown as they did not match any retention times in the base oils.

3.4 Conclusions and Future Directions

The primary aim of this study was to determine the best GC×GC/(EI) TOF MS column configuration and temperature program method for the analysis of fuel and oil samples, including petroleum-based aviation fuel, alternative aviation fuels, aviation fuel blending components, and light base oils. An additional aim was to determine the chemical compositions of the fuels and oil samples.

Overall, a reverse-column configuration was more beneficial for the efficient separation of the saturated hydrocarbons in the sample set while still providing sufficient separation of aromatic species. This setup allowed me to best assess the chemical composition of the aviation fuel and the fuel additives of interest. For instance, the chemical composition of Jet-A, a petroleum-based aviation fuel, was found to be more complex than the chemical compositions of alternative aviation fuels and fuel blending components. As would be expected since Jet-A can be used neat, whereas the blending components cannot. This complexity will likely influence the physical performance of alternative aviation fuel and fuel blending components. Modern fuel approval tests are based on measuring bulk physical properties, such as the density, energy content, flash point, and freezing point of the fuel.[3] However, it is largely unknown how the compounds in the fuel influence specific

desirable or undesirable physical properties. For instance, it is known that aromatic compounds negatively impact combustion efficiency and produce soot due to incomplete combustion in jet engines,[35-37] but the impact of other compounds on similar properties is largely unknown.

Knowledge of the composition of Jet-A gained here could facilitate future research into how the compounds present in a given fuel influence its physical properties. For example, the larger carbon number distribution of linear alkanes and aromatic compounds found in Jet-A, as compared to the alternative aviation fuel CHCJ, may influence CHCJ's freeing point, vaporization temperature, and its ability to swell nitrile O-rings. Further, as CHCJ fuel lacks small aromatic compounds, which have been shown to be critical for swelling O-rings,[38] it can now be hypothesized that the fuel may leak from the fuselage, resulting in a loss of fuel from the aircraft. Further, reviewing the chemical compositions of alternative fuel blending components SIP and FT-S8 showed that these mixtures are too simplistic to provide the physical properties necessary for proper aviation fuels, as they lack aromatic compounds, which is why these samples are categorized as aviation fuel blending components, rather than neat aviation fuels. Continuation of this work may include pairing chemical composition determined by using GC×GC/(EI) TOF MS with physical performance testing to correlate the chemical composition of a given fuel to the physical performance of the fuel and new fuel candidates. This may be accomplished by utilizing surrogate fuel mixtures similar to those used in fuel combustion modeling research.

This work also determined the chemical composition of two light base oil samples. It was found that the base oils both consisted of branched and linear alkanes as well as mono-, di-, tri-, tetra-, and penta-cyclic alkanes. Base Oil A had a lower average carbon number than Base Oil B. Base Oil A was found to be a simpler sample, as it was found to contain fewer types of chemical compounds than Base Oil B. Overall, the compounds in Base Oil A ranged from carbon numbers 14 to 20 while those in Base Oil B ranged from carbon number 15 to 28. Additionally, Base Oil A contained linear alkanes of sizes from C14 to C18 while Base Oil B contained linear alkanes of sizes from C15 to C18. The exact chemical composition of each compound class and their relative amounts in the base oil influence the physical and chemical performance of the final lubricant product. For the best performance, it is best that these processed base oils to contain no linear alkanes. This analysis method may be used to determine the linear alkane content of future base oil samples obtained from various processing techniques in order to improve refining methods. A manuscript was published on this work titled, Identification and Quantitation of Linear Saturated

Hydrocarbons in Lubricant Base Oils by Using APCI (O2, isooctane) LQIT and GC×GC/EI TOF Mass Spectrometry.

Future work may also investigate the thermal stability of the compounds in the mixtures to ensure no components are thermally labile such that they are altered or degraded during analysis. If compounds are heat-labile then the analyzed components are not true to the original mixture. This could create a false idea of what the mixture is composed of and false positive compound identifications.

3.5 References

(1) Wang, Z., Fang, W., Lin, R., Guo, Y., Zhou *Fuel*. **2006**, 85, 1794-1797.

(2) B.C., Bruno, T.J. *Energ Fuel.* **2011**, 25, 5200-5214.

(3) ASTM Standard D4054, "Standard Practice for Qualification and Approval of New Aviation Turbine Fuels and Fuel Additives", ASTM International, West Conshohocken, PA, **2010**, www.astm.org.

(4) ASTM Standard D975-19b, "Standard Specification for Diesel Fuel", ASTM International, West Conshohocken, PA, **2019**, www.astm.org.

(5) Rumizen, M. ASTM Users' Guide. *CAAFI*. **2013**.

(6) Cookson, D.J., Lloyd, C.P., Smith, B.E. *Energ. Fuel.* **1987**, 5, 438-447.

(7) Cookson, D.J., Smith, B.E. *Energ. Fuel.* **1990**, 4, 152-156.

(8) Cookson, D.J., Shawt, I.M., Smith, B.E. *Fuel*. **1985**, 64, 509-519.

(9) Cookson, D.J., Smith, B.E. *Fuel.* **1995**, 74, 70-78.

(10) Pasadakis, N., Sourligas, S., Foteinopoulos, C. *Fuel.* **2006**, 85, 1131-1137.

(11) Cramer, A., Hammond, M.H., Myers, K.M., Leska, I.A., Morris, R.E. Energ. Fuel. **2015**, 29, 7026-7035.

(12) Johnson, K.J., Rose-Pehrsson, S.L., Morris, R.E. *Petrol. Sci. Technol*. **2006**, 24, 1175-1186.

(13) Lai, W.C., Song, C. *Fuel*. **1995**, 10, 1436-1451.

(14) Islam, G., Granot, O., McIndoe, J.S. *Anal. Lett.* **2017**, 50, 1593-1601.

(15) Lovestead, T.M., Burger, J.L., Schneider, N., Bruno, T.J. *Energ. Fuel.* **2016**, 30, 10029-10044.

(16) Libardoni, M. "Comprehensive Two-Dimensional Gas Chromatography (GCxGC) – Exploring Effective Use as a Routine Analytical Technique." Life Science and Chemical Analysis Center, **2007**, St. Joseph, Michigan.

(17) Vendeuvre, C., Ruiz-Guerrero, R., Bertoncini, F., Duval, L., Thiébaut, D., Hennion, M.C. *J. Chromatogr. A.* **2016**, 1086, 21-28.

(18) Chow, H.Y.J., Górecki, T. *Anal. Chem.* **2017**, 89, 8207-8211.

(19) P.J. Linstrom and W.G. Mallard, Eds., NIST Chemistry WebBook, NIST Standard Reference Database Number 69, National Institute of Standards and Technology, Gaithersburg MD, 20899, https://doi.org/10.18434/T4D303

(20) Anamaria, P.P.P., Yinglei, H., Kramlich, J., Garcia-Perex, M. *Biorresources.* **2018**, 13, 2632-2657.

(21) Hu, S.Z., Li, S.F., Cao, J., Zhang, D.M., Ma, J., He, S., Wang, X.L., Wu, M. *Pet. Sci. Technol.* **2014**, 32, 565-574.

(22) Vendeuvre, C., Ruiz-Guerrero, R., Bertoncini, F., Duval, L., Thiébaut, D., Hennion, M.C. *J. Chromatogr. A.* **2016**, 1086, 21-28.

(23) Romanczyk, M. **2019**, 'Developing Mass Spectromic Methods for Distinguishing Isomers, Characterizing Complex Mixtures and Determining the Capability of Organic Compounds to Swell Aircraft O-ring Seals' PhD Thesis, Purdue University, West Lafayette.

(24) Striebich, R.C., Shafer, L.M., Adams, R.K., West, Z.J., DeWitt, M.J., Zabarnick, S. *Energ. Fuel.* **2014**, 28, 5696-5706.

(25) Jennerwein, M.K., Eschner, M., Gröger, T., Wilharm, T., Zimmermann, R. *Energ. Fuel.* **2014**, 28, 5670-5681.

(26) Van der Westhuizen, R., Ajam, M., De Coning, P., Beens, J., de Villiers, A., Sandra, P. *J. Chromatogr. A.* **2011**, 1218, 4478-4486.

(27) Link, D., Gormley, R. J., Baltrus, J.P., *Energ. Fuel.* **2008**, 22, 1115-1120.

(28) Wilson, G.R., Edwards, T., Corporan, E., Freerks, R.L. *Energ. Fuel.* **2013**, 27, 962-966.

(29) Blakey, S., Rye, L., Wilson, C. W. *Proc. Combust. Inst*. **2011**, 33, 2863-2885.

(30) Pinkerton, D.K., Parsons, B.A., Anderson, T.J., Synovec, R.E. *Anal. Chim. Acta.* **2015**, 871, 66-76.

(31) Prebihalo, S.E., Berrier, K.L., Freye, C.E., Bahaghighat, H.D., Moore, N.R., Pinkerton, D.K., Synovec, R.E. *Anal. Chem.* **2018**, 90, 505-532.

(32) Manheim, J., Wehde, K.E., Zhang, W.T.J., Vozka, P., Romanczyk, M., Kilaz, G., Kenttämaa, H.I. *J. Am. Soc. Mass Spectrom*. **2019**, (in review).

(33) Graham, J. L., Striebich, R., Myers, K. J., Minus, D. K., Harrison, W. E. *Energ. Fuel*. **2006**, 20, 759-765.

(34) Liang, Z., Chen, L., Alam, M.S., Zeraati Rezaei, S., Stark, C., Xu, H., Harrison, R.M. *Fuel*. **2018**, 220, 792-799.

(35) Corporan, E., Edwards, T., Shafer, L., DeWitt, M.J., Klingshirn, C., Zarbarnick, S., West, Z., Striebich, R., Graham, J., Klein, C. *Energ. Fuel*. **2011**, 25, 955-966.

(36) Beyersdorf, A.J., Timko, M.T., Ziemba, L.D., Bulzan, D., Corporan, E., Herndon, S.C., Howard, R., Miake-Lye, R., Thornhill, K.L., Winstead, C., Yu, Z., Anderson, B.E. *Amos. Chem. Phys*. **2014**, 14, 11-23.

(37) Timko, M.T., Yu, Z., Onasch, T.B., Wong, H.W., Miake-Lye, R.C., Beyersdorf A.J., Anderson, B.E., Thornhill, K.L., Winstead, E.L., Corporan, E., Dewitt, M.J., Klingshirn, C.D., Wey, C., Tacina, K., Liscinsky, D.S., Howard, R., Bhargava, A. *Energ. Fuel.* **2010**, 24, 5883 – 5896.

(38) Romanczyk, M., Velasco, J.R., Xu, L., Vozka, P., Dissanayake, P., Wehde, K.E., Roe, N., Keating, E., Kilaz, G., Trice, R., Kenttämaa, H.I. *Fuel.* **2019**, 238, 483-492.

CHAPTER 4. ASTM D2425 METHOD VERIFICATION: A FIRST LOOK AT BIAS, LIMIT OF DETECTION, AND LIMIT OF QUANTITATION FOR ASTM D2425 2019 UPDATED INSTRUMENTATION AND SAMPLE TYPE

4.1 Introduction

An update for ASTM D2425, "Standard Test Method for Hydrocarbon Types in Middle Distillates by Mass Spectrometry," was released in January 2019 to add modern mass spectrometric instrumentation and synthesized hydrocarbons to its scope.[1] This update was necessary because the previous standard was based on the use of an obsolete Consolidated Electrodynamics Corporation Type 103 mass spectrometer, last manufactured in 1970. Furthermore, this standard has been a mandatory test for synthesized renewable jet fuels (RJF) by ASTM D7566,[2] but RJF were not previously included in the scope of ASTM D2425. ASTM defines synthesized hydrocarbons as hydrocarbons derived from alternative sources, such as coal, natural gas, biomass, and hydrogenated fats or oils, by processes such as gasification, Fischer-Tropsch synthesis, and hydroprocessing. While conventional hydrocarbons are hydrocarbons derived from the following sources: crude oil, natural gas liquid condensates, heavy oil, shale oil, and oil sands. It is unknown if the new method is appropriate for synthesized hydrocarbons as the method was initially created and validated for conventional hydrocarbons.

The D2425-2019 standard method workflow is presented in Figure 4.1. Briefly, the analysis begins with separating a sample into saturated and aromatic hydrocarbons by one of three accepted liquid chromatography separation procedures dictated by ASTM methods D2549, D1319 and D6379.[3-5] The resulting fractions are analyzed by either an electron ionization magnetic sector mass spectrometer ((EI) B-MS) or a gas chromatography electron ionization quadrupole mass spectrometer (GC/(EI) Q-MS) (referred to as Procedure A and Procedure B, respectively). The produced mass spectra, one for each fraction, includes all of the analyte molecular ions and their fragment ions. These ions are assigned to fourteen predefined hydrocarbon types based on their mass-to-charge ratios (*m/z*). ASTM defines the fourteen hydrocarbons types as: cycloparaffins, aromatic compounds, saturated compounds, paraffins, mononaphthenes, dinaphthenes, trinaphthenes, alkylbenzenes, indane and tetralin, indene (C_nH_{2n-10}), naphthalene, acetylnaphthene

(C_nH_{2n-14}), acetylnaphthylene (C_nH_{2n-16}), and tricyclic aromatic compounds (where n is any whole number). These compound classifications will be used throughout this chapter.

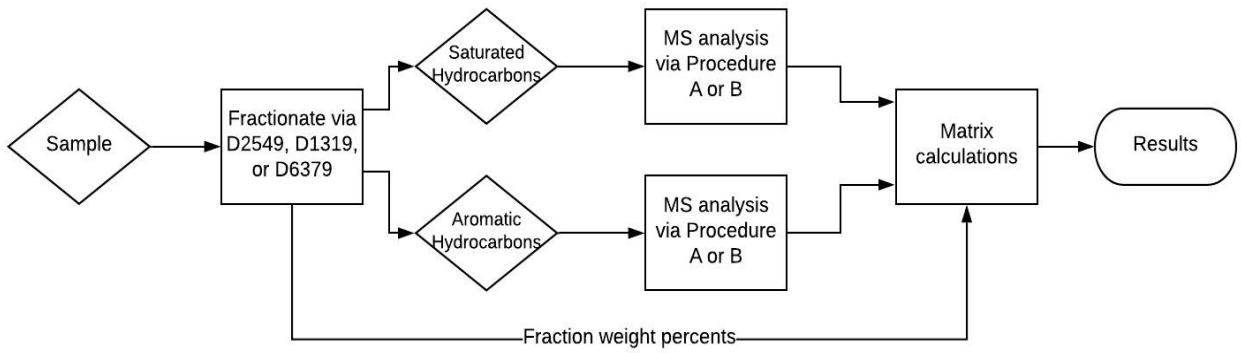

Figure 4.1. ASTM D2425-2019 analysis workflow

The categorization of ions in the MS is based on the assumption that certain *m/z*-ratios are the most characteristic for a particular hydrocarbon type. The combined abundances of all ions assigned to each type are then used to determine the weight percentage (wt %) of different hydrocarbon types in a sample by using the calibration data given in Table 3 in the 2019 update of ASTM D2425. The table provides the theoretical abundance proportions of the ions in the spectrum of each hydrocarbon type to generate the weight percentage for each hydrocarbon type by utilizing ion abundances (obtained from measured peak heights) determined by a MS.[1] To determine the weight percentages of different hydrocarbon types for the whole sample, the results obtained for each fraction are normalized to the gravimetric weight percent of the saturate and aromatic fractions. However, the updated D2425 method does not provide new calibration data necessary for the analysis of the new sample type, synthesized hydrocarbons, such as RJFs, or the new instrument type utilized in Procedure B. Therefore, it is unknown whether the calibration data given in the 2019 method, Table 3, can be used to appropriately determine the content of different hydrocarbon types in the new sample type or any sample when using the new instrument.

While the January 2019 method update is a step towards modernization, it still lacks validation parameters. First, the updated method does not present all the essential performance characteristics to ensure the validity of the method. For example, knowing the magnitude of total error is essential for result interpretation and use but is not included in the 2019 method update. The updated standard method contains precision estimations, but not bias values, meaning the

method does not comment on accuracy. It is also essential to know the lowest concentration of an analyte that can be detected and quantitatively determined by the method at a specified level of confidence, 'limit of detection' (LOD) and the 'limit of quantification' (LOQ). Unfortunately, the 2019 D2425 method update does not provide either of these limits nor any guideline for the lowest concentration that may be determined by the method.

Given that D2425 is a required method to verify that cycloparaffins and aromatic compounds are present below the maximum allowed limits in RJFs, bias determination is imperative. For example, the maximum allowed level for aromatics is only 0.5 wt % for most synthetized RJF sample types,[2] making the LOQ an essential figure to be determined. To improve the 2019 ASTM method D2425, this study evaluated the LOD and LOQ, as well as estimated the method bias for Procedure B (GC/(EI) Q-MS) with both conventional and synthesized hydrocarbons as defined by ASTM. The LOD, LOQ, and bias were evaluated as an intra-laboratory study following the Eurachem guide.[6]

4.2 Experimental section

4.2.1 Instrumentation hardware

Experiments were performed following Procedure B, which is based on the use of a gas chromatograph/(electron ionization) quadrupole mass spectrometer (GC/(EI) Q MS). An Agilent 7890B GC was utilized with helium (>99.996% pure) as the carrier gas and liquid carbon dioxide (>99.7% pure) for cryogenic oven cooling. Samples were injected via an Agilent 7693A automatic liquid sampler with a 10 µL Agilent ALS Syringe (5181-3354) by using dichloromethane as a syringe cleaning solvent. The GC contained two parallel GC columns, each with an individual inlet. These experiments only utilized one of the columns with a split/spitless inlet. The column used in this research had no active phase (10 m x 100 µm x 0 µm; Agilent Part No: 160-2635-10). A variable carrier gas flow was utilized as discussed below in the methods section (Section 4.2.2). The second column (not used in this research) was a ZB-1ms column (60 m x 250 µm x 1 µm) and had a constant 0.4 mL/min carrier gas flow. The second column is only discussed here because both columns were connected into a tee-connection that was attached to the EI source of the MS. Thus, though the second column was not used, the flow of the second column did affect the flow of analytes into the EI source. The GC was coupled with an Agilent 5977B single quadrupole MS

with an inert plus extractor EI source and triple-axis electron multiplier detector. Specific GC parameters are discussed below as the parameters were adjusted for each sample that was analyzed (Section 4.2.2.1).

4.2.2 Methods

Elias Ikonen developed all GC/(EI) Q MS methods used in this research in Porvoo, Finland at the Neste Corporation Research and Development Center. Two different sets of GC conditions were utilized in this investigation, but the same MS and data analysis method were used for all samples, as discussed below.

4.2.2.1 *GC method conditions*

The conditions of the GC methods are discussed below separately for each sample type, the aromatic compounds (Section 4.2.2.1.1) derived from RJF and the saturated compounds (Section 4.2.2.1.2) derived from the RJF and both the aromatic and saturated compounds derived from GO.

4.2.2.1.1 Aromatic compound fraction of RJF

An inlet split ratio of 50:1 was utilized. The concentrations of each sample solution was 10 mg/mL. A 1 μL volume of each sample was injected into the inlet and held at a temperature of 280 °C. The GC oven temperature was set to -30 °C and was held there for 7 minutes, after which it was ramped at a rate of 50 °C/min until a temperature of 250 °C was reached, which was maintained for 0.5 minutes. The initial helium carrier gas flow was set to 0.06 mL/min and held there for 7 minutes, after which it was quickly ramped at a rate of 20 mL/min until a flow rate of 0.7 mL/min was achieved. This flow rate was maintained until the end of the program.

4.2.2.1.2 Saturated compound fraction of RJF and both saturated and aromatic compound fractions of GO

An inlet split ratio of 140:1 was utilized. The concentration of each sample solution was 100 mg/mL. A 1 μL volume of each sample was injected into the inlet and held at a temperature of 280 °C. The GC oven temperature was set to -30 °C and held there for 2 minutes, after which it was ramped at a rate of 50 °C/min until a temperature of 250 °C was reached. This temperature was held for 0.5 minutes. The initial helium carrier gas flow was set to 0.2 mL/min and held there

for 2 minutes, after which it was quickly ramped at a rate of 20 mL/min until a flow rate of 0.7 mL/min was achieved. This flow rate was maintained until the end of the program.

4.2.2.2 *MS conditions*

The MS was operated as outlined in the 2019 version of ASTM D2425[1]: positive electron ionization mode using 70 eV electron kinetic energy, 230 °C ion source temperature, 300 °C transfer line temperature, and 150 °C quadrupole temperature. Mass spectra were collected at a scan speed of 9.8 scans/s over the *m/z* range of 40 – 292. The instrument was autotuned using the standard spectrum tune program (Stune), which monitors the relative abundance (%) of target ions compared to an internal calibration mixture of perfluorotributylamine (PFTBA).

4.2.2.3 *Data analysis*

The mass spectra, one measured for each fraction, show analyte molecular ions and their fragment ions. These ions were assigned to fourteen predefined hydrocarbon types based on their characteristic *m/z*-ratios as described in the 2019 update of ASTM D2425.[1] The summed abundances of the ions (determined from the relevant peak heights) assigned to each hydrocarbon type, together with the calibration data given in the 2019 ASTM D2425, were mathematically processed to produce the mass percent of each hydrocarbon type as described below.

After summing the characteristic ion abundances for each hydrocarbon type. The average number of carbons for the alkylbenzenes and naphthalenes in the aromatic hydrocarbon fraction were also determined. The average number of carbons determines what calibration matrices and sensitivities should be used in further calculations for the aromatic and saturated hydrocarbon fractions. The matrix calculations consisted of solving a set of simultaneous linear equations. These calculations were performed separately for the aromatic and saturated hydrocarbon fractions. Each linear equation illustrated the distribution of the summed abundances of the characteristic ions for each specific hydrocarbon type compared to all hydrocarbon types. The linear equation coefficients are given in D2425-2019 as matrices.[1] The coefficients were the sums of the abundances of the characteristic ions for each hydrocarbon type. The variables were the unknowns to be solved, and they reflected the mass fractions of the hydrocarbon types in the sample. The unknowns (variables) were solved by multiplying the inverse of the square matrix (5x5 for the saturated compound fraction, 10x10 for the aromatic compound fraction) of the linear equation

coefficients by constants (the sum intensities of the hydrocarbon types) that were tabulated as a column matrix (5x1 for the saturated compound fraction, 10x1 for the aromatic compound fraction). The results were outputted as column matrices (5x1 for the saturated compound fraction, 10x1 for the aromatic compound fraction). The results were then converted to hydrocarbon type mass fractions by dividing each value by the corresponding sensitivity (response factor) given in D2425-2019.[1] To obtain the final result; the mass fractions were normalized to the gravimetric weight percentages of the fractions. The most convenient way to conduct these calculations is by automated calculation software. An in-house macro-based Microsoft Excel calculation sheet, developed by Neste, was used to generate the hydrocarbon type contents (wt %) of the samples.

4.2.3 Samples

Neat model compounds were used to evaluate the performance of the analytical method. Subsequently, a real RJF and GO were fractionated and utilized to evaluate the 2019 updated ASTM D2425 method.

4.2.3.1 *Sample sets for evaluation of instrument performance*

Three types of instrumental performance were evaluated, the accuracy of MS tuning, instrument signal as a function of the amount of the analyte, and instrument ruggedness. Each required a unique sample set. They are discussed below in this order.

Validation of MS tuning: The MS instrument was automatically tuned using the factory Stune function as part of the instrument's software. The 2019 version of ASTM D2425 dictates that MS tuning completed this way must be validated using n-hexadecane. A solution of 0.6 mg/mL n-hexadecane (Acros Organics, 99%) in dichloromethane (DCM) (Merck Millipore Dichloromethane, purity >99.8%) was used for tuning.

Investigation of the linearity of the instrument signal with respect to the amount of the analytes: Instrument signal linearity as a function of analyte mass percent was investigated by spiking a GO sample and a RJF sample with n-hexadecane-d_{34} (CDN Isotopes, Quebec, Canada, 98.6% enrichment), by increasing the weight percent from 0 to 10 w/w %. The spiked fuel samples, RJF and GO, were analyzed in duplicate, in the order of increasing n-hexadecane-d_{34} mass percent, with a blank of DCM between each sample.

Investigation of instrument ruggedness: Two test samples were prepared by fractionating a GO sample into saturated and aromatic hydrocarbon compound types (according to ASTM D2549M as described in Section 4.2.4), and then diluting the fractions

with DCM to a concentration of 100 mg/mL. Each sample was then divided into five sub-aliquots, one for each of the tune tests. For each tune test, both saturated and aromatic hydrocarbon fractions were injected a total of eight times, with a DCM solvent blank between each set, such that the analysis order for each MS tune was: solvent, saturated hydrocarbons, aromatic hydrocarbons, solvent, saturated hydrocarbons, aromatic hydrocarbons, solvent, …, saturated hydrocarbons, aromatic hydrocarbons. This led to a total of 24 acquisitions per tune file and 120 acquisitions in total for all five tune files.

4.2.3.2 *Sample fractionation*

The separation of the samples into saturated and aromatic hydrocarbon fractions prior to GC/(EI) Q MS analysis was completed according to a modified version of the D2549 method. The method was modified to make it suitable for the samples studied here that mostly contained compounds with low boiling points. The modifications are specified in Section 4.2.4. The main modification was the way the solvent was removed, which was performed via distillation rather than evaporation. The modified method will be referred to as D2549M throughout this chapter. n-Pentane (VWR Chemicals, Analar, purity >99%), diethyl ether (VWR chemicals, emsure® for analysis, purity >99%), chloroform (VWR chemicals, Analar, purity >99%), ethanol (ETAX A, Altia, purity >94%) and n-hexane (VWR chemicals, HiPer Solv, purity >97%) were used in the fractionation procedure.

4.2.3.3 *Sample sets for evaluation of the 2019 updated ASTM D2425 method*

The complex mixtures investigated in this study were a synthesized hydrocarbon sample of renewable jet fuel (RJF) and a conventional hydrocarbon sample of gas oil (GO). The RJF sample was a synthesized paraffinic kerosene obtained via hydroprocessing of esters and fatty acids at Neste refinery, with a boiling point range of 172.6 - 287.9 °C. This sample type would be included in D7566-19 standard specification for aviation turbine fuels containing synthesized hydrocarbons. All RJF samples were prepared and analyzed by Katherine Wehde. The GO sample was a virgin middle distillate of a crude oil sample with a boiling point range of 197.6 - 304.7 °C obtained from a refinery crude oil distillation unit utilizing mostly Russian sour heavy crude oil (Urals oil). All GO samples were prepared and analyzed by Khalida Habebe. Data analysis for all samples, RJF and GO, was completed by Katherine Wehde.

Replicate samples of RJF and GO were used to determine the limit of detection (LOD), the limit of quantitation (LOQ), and bias. The sample-set for RJF was prepared as shown in Figure 4.2. Alkylcyclohexane and alkylbenzene model compounds: n-hexylcyclohexane, n-heptylcyclohexane, n-octylcyclohexane, n-nonylcyclohexane, n-decylcyclohexane, n-

undecylcyclohexane, n-dodecylcyclohexane, n-hexylbenzene, n-heptylbenzene, n-octylbenzene, n-nonylbenzene, n-decylbenzene, and n-undecylbenzene, were all purchased from abcr (Karlsruhe, Germany; purity >98%) and used as received. The sample set of RJF (RJF_S_1-8) was spiked with the model compounds in such a manner that the mass fraction of each alkylcyclohexane model compound was 0.75 w/w% in solution and the mass fraction of each alkylbenzene model compound was 0.23 w/w% in solution. The mass fractions of the spiked samples were corrected based on the purities of the model compounds. Additionally, a set of eight neat RJF fuel samples (RJF_0_1-8), with no model compound spiking, was also tested. The sample sets were fractionated into saturated and aromatic hydrocarbons according to ASTM D2549M (Section 4.2.4). After fractionation, the aromatic hydrocarbons were diluted with DCM to yield a 10 mg/mL solution (with a minimum of 100 µL DCM added), and the saturated hydrocarbons were diluted in DCM to yield a 100 mg/mL solution. The neat RJF_0_1-8 saturated hydrocarbon sample set and the RJF_0_1-8 aromatic hydrocarbon sample set were analyzed in one day. The spiked RJF_S_1-8 saturated hydrocarbon sample set and the RJF_S_1-8 aromatic hydrocarbon sample set were analyzed the following day. Analysis order was set to be the same as described above for the investigation of the instrument ruggedness (Section 4.2.3.1), with DCM solvent blanks between the sample sets.

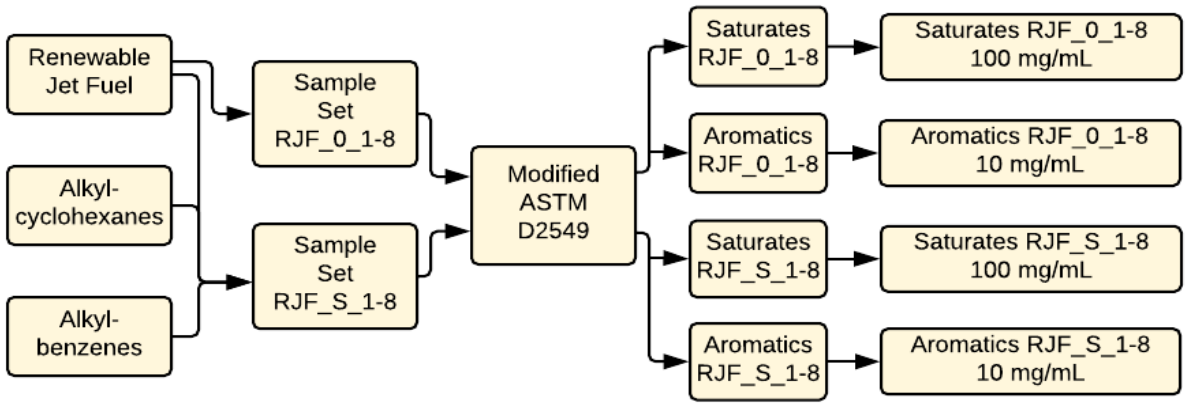

Figure 4.2. Scheme for the preparation of renewable jet fuel (RJF) sample for LOD, LOQ, and bias investigation. Samples are named as fuel type, spiked (S) or neat (0), sample number.

The sample-set for GO was prepared by Khalida Habebe similarly to that for RJF. However, for GO, the alkane and alkylbenzene model compounds used were: n-undecane (purity 99.3%), n-

tridecane (purity 99.7%), n-pentadecane (purity 99%), n-octadecane (purity 99.3%), 1,2,4,5-tetramethylbenzene (purity 98%), 1,4-diethylbenzene (purity 95%), pentamethylbenzene (purity 98%), 1-phenyloctane (purity 98%), 1-phenyldecane (purity 98%), and 1-phenylpentane (purity 99%), all purchased from Sigma Aldrich Chemistry with the following exceptions. n-Dodecane was purchased from Merk Millipore (purity 99%). n-Tetradecane (purity 99.4%), n-hexadecane (purity 99.1%), and n-heptadecane (purity 99.1%) were purchased from Acros Organics and used as received. The samples GO_S_1-8 were spiked with the model compounds in such a manner that the mass fraction of each alkane model compound was 2 w/w% in solution and the mass fraction of each alkylbenzene model compound was 1 w/w% in solution. The mass percentages of the spiked samples were corrected based on the purities of the model compounds. Additionally, a set of eight neat samples (GO_0_1-8), with no model compound spiking, were also tested. After fractionation, the samples were diluted with DCM in such a manner that both aromatic and saturated hydrocarbon fractions had a concentration of 100 mg/mL. The GO_0_1-8 saturated hydrocarbon sample set and the GO_0_1-8 aromatic hydrocarbon sample set were analyzed in one day. The GO_S_1-8 saturated hydrocarbon sample set and the GO_S_1-8 aromatic hydrocarbon sample set were analyzed the following day. Analysis order was performed as described above (Section 4.2.3.1), with DCM solvent blanks between the sample sets.

4.2.4 Modifications to ASTM D2549-17

Various modifications were made to the original ASTM D2549-17.[3] Outlined below are the section numbers from the original ASTM D2549 method, followed by the modification applied in this research. This modification was developed by the Neste Corporation.

1.1: Boiling point range was 125–538 °C.

8.1*:* Cleaning solvent was 50:50 solution of distilled water: hydrochloric acid 37%.

8.4.1: Sample was aspirated into a 2 mL disposable syringe. The syringe filled with sample was weighed.

8.4.2: 10 mL of n-pentane was added onto the top of the column to pre-wet the adsorbent. When the liquid level reached the top of the bauxite bed, the sample was transferred from the syringe onto the adsorbent. Walls of the column solvent reservoir bulb were rinsed with 20 mL of n-pentane, in small portions, allowing the liquid level to reach the top of the

bauxite bed before adding the next portion. Finally, 80 mL of n-pentane was added onto the column solvent reservoir bulb. The syringe was weighed before and after the additions to determine the weight of the added sample.

8.4.4: Pressuring gas was connected to the top of the column after 80 mL of n-pentane elute had been collected.

8.4.5-8.4.7: The ether-eluted fraction and chloroform-ethanol-eluted fraction were collected into the same 250 mL graduated flask to obtain the aromatic fraction.

8.4.8-8.4.11: A 100 mL distillation flask with boiling chips was weighted within an accuracy of 1 mg. The saturated compound fraction was transferred into the flask with the aid of n-pentane. n-Pentane was removed from the solution by using a distillation apparatus equipped with a Vigreux column at a distillate temperature of 37 °C. The temperature of Radleys temperature-controlled bath was set to 80 °C. After the distillate temperature, as measured by the distillation apparatus thermometer, started to decline, the flask containing the saturated compound fraction was removed from the bath and cooled to room temperature. The adapter, Vigreux column, and neck of the flask were flushed with n-pentane into the flask. The n-pentane was removed from the flask by a rotary evaporator equipped with nitrogen flushing. The weight of the saturated compound fraction was determined by weighting the flask in the beginning and intermittently during rotary evaporation until the difference of two successive measurements was under 20 mg. The contents of the 250 mL graduated flask containing the aromatic compound fraction was transferred with the aid of n-hexane into a 250 mL distillation flask containing boiling chips. The solvent was removed from the fraction by using a distillation apparatus equipped with a Vigreux column at a distillate temperature of 78 °C. The distillation flask and the Vigreux column were wrapped with aluminum foil. The temperature of Radleys temperature-controlled bath was set to 140 °C. After distillate temperature, as measured by the thermometer of the distillation apparatus, started to decline, the flask containing the aromatic compound fraction was removed from the bath and cooled to room temperature. The adapter, Vigreux column, and neck of the flask were flushed with n-hexane into the 250 mL flask. The 50 mL distillation flask with boiling chips was weighted within an accuracy of 1 mg. The aromatic compound fraction was transferred into the 50 mL flask with n-hexane. The solvent was removed from the fraction by using a distillation apparatus equipped with a Vigreux column at a distillate temperature of 60 °C. The temperature of Radleys temperature-controlled bath was set to 140 °C. When the distillate temperature, as measured by the thermometer of the distillation apparatus, started to decline, the flask containing the aromatic compound fraction was removed from the bath and cooled to room temperature. The adapter, Vigreux column, and neck of the flask were flushed with n-pentane into the 50 mL flask. The solvent was removed from the flask by a rotary evaporator equipped with nitrogen flush. The weight of the aromatic compound fraction was determined by weighing the flask intermittently during rotary evaporation until the difference of two successive weight measurements was under 20 mg. The recovery was evaluated by comparing the summed weights of the aromatic and saturated compound fractions and the sample weight. Recovery should reach at least 95% according to ASTM D2549-02. If recovery was under 95%, the analysis was considered a failure and a new

sample was used and the measurement repeated. If the recovery was over 100%, the reason was most likely inadequate removal of solvents. In this case, the residual solvents were removed by gently heating the flask with a fan heater while keeping the flask under nitrogen flow.

4.3 Results and Discussion

All instrument evaluations (Section 4.3.1) and all RJF results were determined by Katherine Wehde, including sample preparation, instrument measurements, and data interpretation. All GO samples were prepared and measured by Khalida Habebe. Data interpretation of GO samples, including LOD, LOQ, and bias were determined by Katherine Wehde. First, the MS instrument was evaluated in order to determine whether it satisfied the ASTM standards. After this, it was utilized to evaluate the updated 2019 ASTM D2425 method by determining the LOD, LOQ, and bias for several samples.

4.3.1 Instrument evaluation

The accuracy of MS tuning with respect to the relative abundances of the ions was first evaluated as dictated by the 2019 updated ASTM D2425 method. Then the linearity of the magnitude of the MS signal, as a function of the amount of the analyte, was examined using n-hexadecane-d_{34} dopant at different mass percentages. Finally, the instrument's ruggedness for tuning was assessed. They are discussed below in this order.

4.3.1.1 *MS tuning validation*

The MS instrument was automatically tuned using the Stune function on the instrument's software. A sample of n-hexadecane was used to determine whether the tuning of the relative abundances of ions measured using the MS instrument was within ASTM specifications. The sum of the heights of the peaks corresponding to ions of *m/z* 67, 68, 69, 81, 82, 83, 96, 97 (noted as Σ67) and ions of *m/z* 71 and 85 (noted as Σ71) were used to verify the tuning of the MS instrument. As outlined in the 2019 version of ASTM D2425,[1] an acceptable range for the Σ67/Σ71 is between 0.2 and 0.3. The test was performed in triplicate, the average was determined to be 0.23, which falls within the acceptable range. Therefore, the developed GC/(EI) Q MS method met the requirements of the 2019 ASTM D2425 tuning validation test, confirming that the instrument performed comparably with the instrument used to generate the calibration data given in the ASTM method. Appropriate

tuning of the MS is imperative because the magnitude of the signal will be used to derive the weight percentages of the various hydrocarbon types, and no external calibration method was offered in the 2019 updated ASTM D2425.

4.3.1.2 *Magnitude of the instrument signal as a function of the wt % of analyte*

The 2019 version of ASTM D2425 does not specify the type of the GC/(EI) Q MS instrument to be used. Therefore, the linearity of the magnitude of the signal of the instrument chosen, for this research, as a function of analyte concentration was evaluated. This was performed for samples of RJF and GO by spiking them with different amounts of n-hexadecane-d_{34} (0 - 10 w/w%; typical amounts of n-hexadecane for these sample types). Mass spectra were collected over the entire GC method run time of 8 minutes (Section 2.2.1.2). The recorded data were represented as a total ion chromatogram (TIC) which shows the sum of all ion abundances as a function of retention time. An extracted ion chromatograph (XIC) was then constructed that showed the abundance of fragment ions of m/z-value 66.10 + 0.5 of the dopant as a function of time. Next, the XIC peak area was normalized to the peak area of the TIC to obtain XIC/TIC. The XIC/TIC was plotted as a function of the weight percent (w/w %) of n-hexadecane-d34 doped into each sample (Figure 4.3A and B).

The resulting unweighted, linear regression lines were not forced to zero. The plots obtained for both the RJF and GO samples showed strong linearity with R^2-values greater than 0.999. Linearity was further evaluated using the residuals (ε), which are the differences between the experimental XIC/TIC peak height ratios (y_i) and the XIC/TIC peak height ratios obtained from the linear regression curves (v_i) (Equation 4.1). In Equation 1, the residuals (ε) are the difference between the experimental XIC/TIC peak height ratios (y_i) and the XIC/TIC peak height ratios obtained from the linear regression curve (v_i). Equations from the regression fit line (Equations 4.2 and 4.3) were used to solve for v_i, where x is the n-hexadecane-d_{34} mass percent and y is v_i. The residual was determined for each sample and the residuals were plotted as a function of mass percent of n-hexadecane-d_{34} (Figure 4.4).

Based on these plots, the linear regression model was considered valid for both sample matrices, on the instrument used, as no correlation was observed between the residuals and the n-hexadecane-d_{34} mass percent for either RJF or GO. Since no systematic errors were found, the

magnitude of the MS signal should correctly reflect the weight percent of the different hydrocarbon types.

Equation 4.1. Residual calculation

$$\varepsilon = y_i - v_i$$

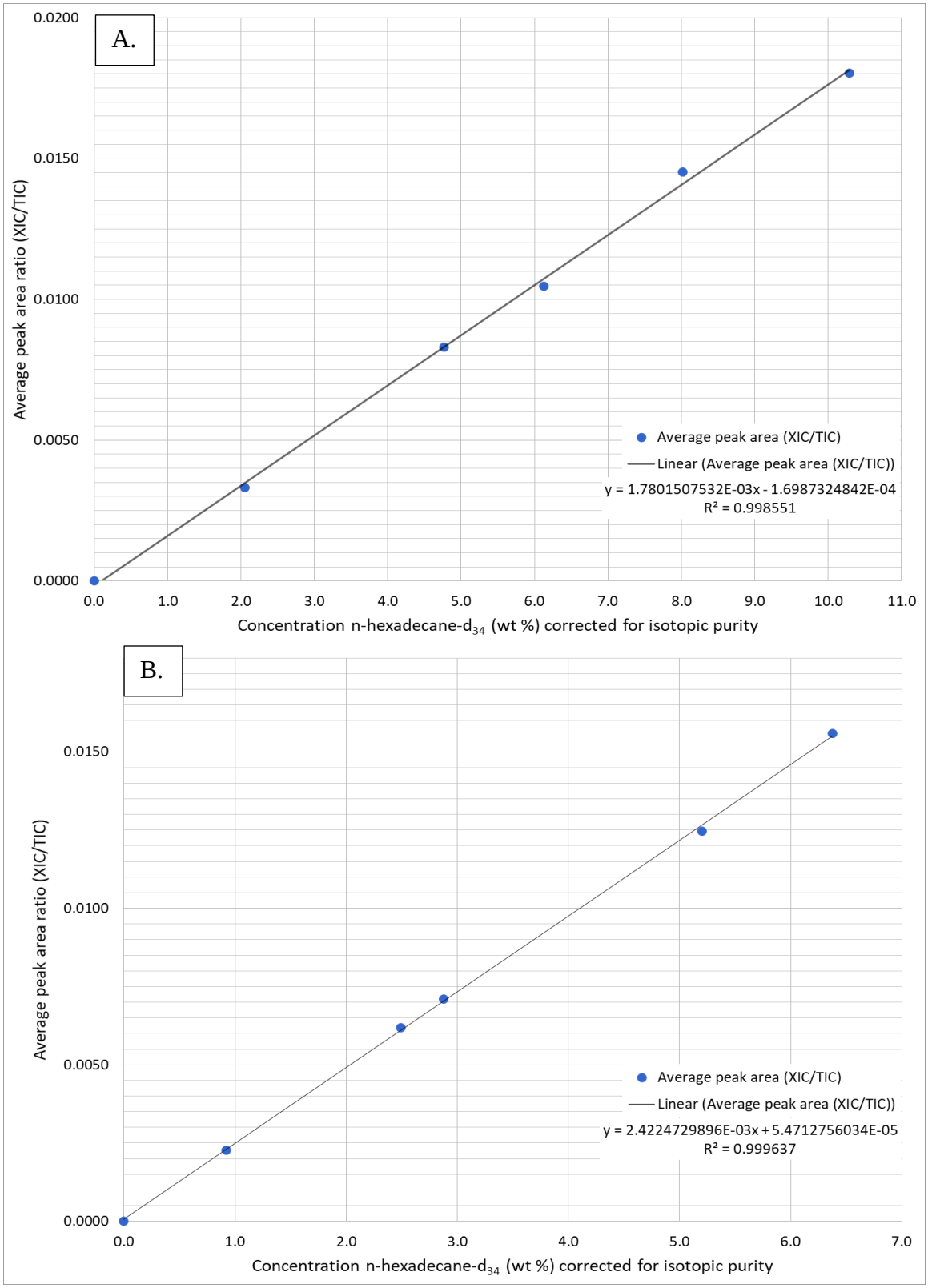

Figure 4.3. A) The average response for RJF linearity samples. B) The average response for gas oil linearity samples.

Equation 4.2. RJF linear regression fit line equation used to solve for y which is equal to v_i

Y=1.7801507532*10-3X- 1.6987324842*10-4

Equation 4.3. Gas oil linear regression fit line equation used to solve for y which is equal to v_i

Y=2.4224729896*10-3X+ 5.4712756034*10-5

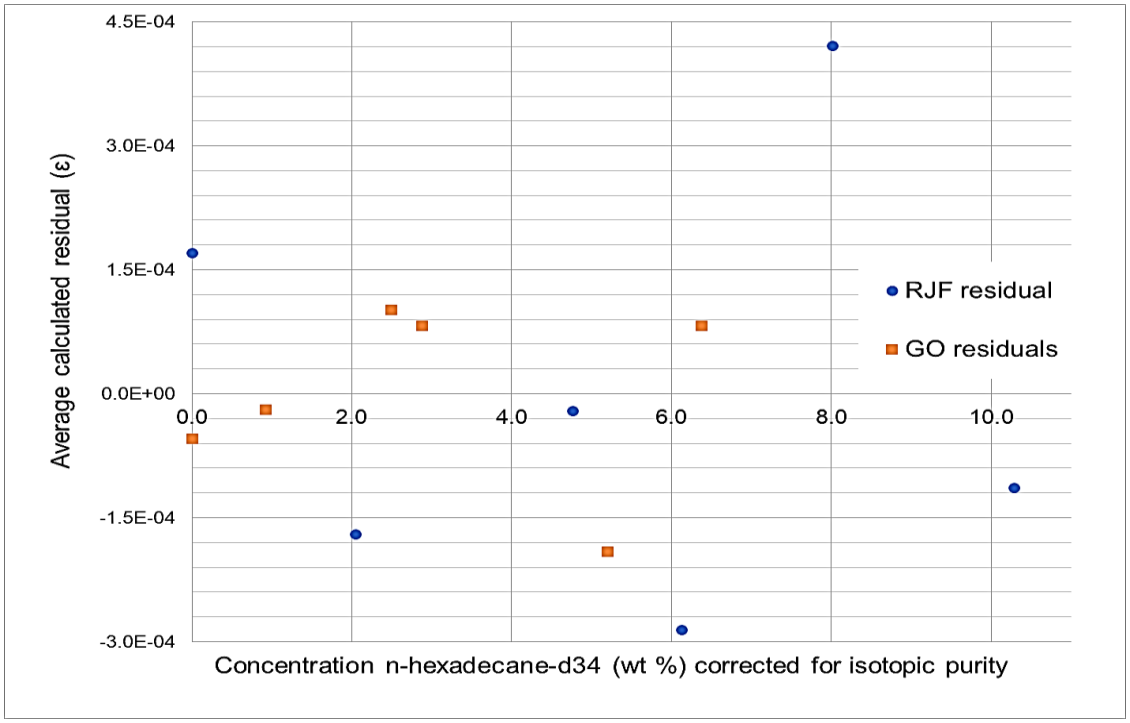

Figure 4.4. Renewable jet fuel (RJF) and gas oil (GO) samples residual plots. There is no observable correlation between the average residuals and the analyte concentration.

4.3.1.3 *Instrument ruggedness*

The ruggedness (or robustness) of a procedure is a "measure of its capacity to remain unaffected by small, but deliberate variations in method parameters. Ruggedness provides an indication of the method´s reliability during normal usage"(pg. 38).[6] Tuning the mass spectrometer was predicted to be the major parameter affecting intra-laboratory method performance. Tuning is typically conducted on a regular basis, as is standard with all mass spectrometers, and creates small but deliberate variations in the MS instrument parameters. An internal standard of PFTBA is used for automatically tuning the MS, which adjusts internal MS voltage settings to reach targeted ion ratios, for each fragment ion resulting from the internal standard (PFTBA). The target ion abundance is rarely reached for all six ions, and some may vary by over 25% when automatically

tuned (Table 4.1). Thus, a range of ion abundances were tested to evaluate ruggedness of this method.

Table 4.1. An internal standard, PFTBA, was used as the calibrant for targeted automatic tuning. The MS was tuned automatically five times and each time reached the ion abundances in the ranges specified below.

m/z	**Ion ratio target abundance (%)**	**Actual ion ratio abundance (%) range tested**
50	1.0	0.9 - 1.2
69	100.0	100.0
131	55.0	55.7 - 69.1
219	45.0	44.5 - 49.8
414	3.5	3.2 - 3.8
502	2.5	2.5 - 3.1

The mass spectrometer was automatically tuned five times consecutively, and the resulting tune files were then used to set instrument parameters, for each tuning test. Five identical saturated hydrocarbon samples and five identical aromatic compound samples were created and analyzed with the GC/(EI) Q-MS method, as described in the methods and materials Section 4.2.3.1. The measured ion abundance ratios were then utilized in the ASTM D2425 method,[1] for which the output is a weight percent for the following hydrocarbon types: cycloparaffins, aromatics, saturates, paraffins, mononaphthenes, dinaphthenes, trinaphthenes, alkylbenzenes, indane and tetralin, indene (C_nH_{2n-10}), naphthalene, acetylnaphthene (C_nH_{2n-14}), acetylnaphthylene (C_nH_{2n-16}), and tricyclic aromatic compounds (where n is any whole number).

The Dixon Q-test was used for the identification and removal of any outliers in the data sets. All data points within a single tune and between the five different tunes passed the Dixon Q-test, meaning there were no outliers identified for removal. Homogeneity of variance (HOV) was tested to determine whether any specific tune file resulted in a deviating data set. The Brown-Forsythe (BF) HOV test was chosen, because this data set is small and non-normal (moderately skewed and platykurtic overall) as identified by the specific kurtosis and skewness values (Tables 4.2 and 4.3).[8-11] The BF test uses the median of a data set to test whether samples have equal variances. If the calculated *p*-value is greater than α then the variances in the different groups are the same. For each sample, the calculated *p*-value for every hydrocarbon type was found to be greater than α, for an α equal to 0.01 (Table 4.4). Therefore, the data sets were all homogeneous in variance, at an α of 0.01, and the developed method and chosen instrument type were concluded

to provide robust results and repeatable data. All tune files resulted in data sets that were regularly varied, and no tune file resulted in a deviating data set. Therefore, the instrument type chosen is considered rugged with respect to tuning of the MS.

Table 4.2. Kurtosis values

Hydrocarbon Type	Tune 1	Tune 2	Tune 3	Tune 4	Tune 5	Whole Data Set
cycloparaffins	0.9808	-1.429	0.020	-1.031	-1.437	0.937
aromatics	0.727	-1.456	-0.237	-0.612	-0.560	0.996
saturates	0.727	-1.456	-0.237	-0.612	-0.560	0.996
paraffins	-0.993	-1.063	-1.083	-1.200	-1.169	0.887
mononaphthenes	0.094	-0.549	-0.125	-1.185	-1.600	0.946
dinaphthenes	2.460	-0.006	0.048	-0.816	-0.528	0.970
trinaphthenes	2.644	-0.463	0.790	-1.419	-0.197	0.987
alkylbenzenes	-1.139	-1.206	0.322	-0.128	-0.568	1.533
indane and tetralins	0.280	-0.696	-1.132	-1.450	0.554	1.206
indenes	1.003	-0.942	0.552	-1.069	-0.960	0.722
naphalenes	-1.092	-1.647	-0.557	-1.106	-0.751	0.980
acetylnaphthenes	-1.371	-1.094	-1.164	-1.051	0.403	2.230
acetylnaphthylenes	-1.096	-0.860	-0.175	-0.736	-0.583	0.809
tri-aromatics	-1.523	-1.445	-0.705	-0.775	-0.052	1.734

Table 4.3. Skewness. Highly skewed: x < -1 or x > 1, Moderately skewed: x < -0.5 or x > 0.5, Approximately normal: -0.5 < x < 0.5

Hydrocarbon Type	Tune 1	Tune 2	Tune 3	Tune 4	Tune 5	Whole Data Set
cycloparaffins	-1.153	-0.186	-0.994	-0.077	-0.319	0.695
aromatics	1.398	-0.353	-1.200	0.196	0.285	0.544
saturates	-1.398	0.353	-0.200	-0.196	-0.285	-0.544
paraffins	0.300	0.680	0.519	0.368	0.187	-0838
mononaphthenes	0.630	-0.557	-0.567	-0.439	-0.325	-0.532
dinaphthenes	-1.967	0.858	0.825	0.521	0.759	0.650
trinaphthenes	-2.080	0.431	1.041	0.005	0.962	0.538
alkylbenzenes	0.015	0.087	-1.129	-0.828	0.604	0.415
indane and tetralin	-1.147	-0.620	0.480	-0.173	1.029	0.952
indene	-1.309	0.206	-0.328	-0.502	0.613	-0.814
naphalene	-0.285	0.113	0.863	0.364	0.407	0.856
acetylnaphthene	0.074	-0.188	-0313	-0.006	1.305	0.696
acetylnaphthylene	-0.262	0.111	-0.048	0.057	-0.123	-0.110
tri-aromatics	0.302	0.295	0.074	0.122	1.017	0.580

Table 4.4. HOV test. If *p*-value > alpha, then the variance in the different groups are the same, accept the null hypothesis. An alpha of 0.01 was chosen to reduce the chance of Type I errors (false positives).

Hydrocarbon Type	***p*-Value**
cycloparaffins	0.312847
aromatics	0.667914
saturates	0.667914
paraffins	0.037833
mononaphthenes	0.093442
dinaphthenes	0.90792
trinaphthenes	0.957799
alkylbenzenes	0.485943
indane and tetralin	0.401475
indene	0.01535
naphalene	0.298588
acetylnaphthene	0.247675
acetylnaphthylene	0.259542
tricyclic-aromatics	0.15406

4.3.2 Method evaluation

The updated 2019 ASTM D2425 method was evaluated for the limit of detection (LOD), limit of quantitation (LOQ), and bias. They are discussed below in this order.

4.3.2.1 *Limit of detection*

To establish the lowest concentration of an analyte that can be detected (LOD), eight samples of RJF and eight samples of GO were taken through the entire measurement procedure as dictated by ASTM D2425 and outlined in Figure 4.1. The MS instrument was automatically tuned for the ion ratio ranges listed in Table 4.1, and the same tune was used for all samples. After MS analysis, the hydrocarbon compositions were used to determine the adjusted standard deviation. The adjusted

standard deviation is tabulated by dividing the standard deviation for a hydrocarbon type by the number of replicate samples; in this case, eight. For validation purposes, it is normally sufficient to provide an approximation of the LOD, using the "3s" approach, in which the adjusted standard deviation is multiplied by three.[6] Due to the large number of hydrocarbon types included in ASTM D2425, no test samples or reference sample matrices are available that would contain all the hydrocarbon types at low concentrations. Low concentrations are necessary to determine the lowest quantity of a substance that can be distinguished from the absence of that substance. However, dilution is not possible in this case because the solvent used for dilution should be the matrix blank, which could not be purchased. For this reason, LOD/LOQ values were determined for the least abundant hydrocarbon types in the RJF and GO samples and assumed to be valid for all hydrocarbon types in the respective sample matrix. Because the LOD should be determined for the least abundant analyte, the acetylnaphthylene hydrocarbon type was used for determining the LOD of the RJF sample, and the tricyclic aromatic compound type was used determining the LOD of the GO sample. The adjusted standard deviation for acetylnaphthylenes in RJF was 0.001, and the LOD was 0.004 w/w%. The adjusted standard deviation for tricyclic aromatic compounds in GO was found to be 0.002, and the LOD was found to be 0.01 w/w%.

4.3.2.2 *Limit of quantitation*

To establish the lowest concentration of an analyte at which quantitation is acceptable (LOQ), eight samples of RJF and GO were taken through the entire measurement procedure dictated by the updated 2019 ASTM D2425 (outlined in Figure 4.1). The instrument was tuned, and the same tune file was used for all samples. After MS analysis, the hydrocarbon type compositions were used to determine the adjusted standard deviation. The LOQ was calculated by multiplying the adjusted standard deviation by a factor, k_Q, which IUPAC defines as 10 in this case.[7] Because the LOQ should be calculated for the least abundant analyte, the acetylnaphthylene hydrocarbon type was used for RJF while the tricyclic aromatic compound type was used for GO. The adjusted standard deviation for acetylnaphthylenes in RJF was found to be 0.001, and the LOQ was found to be 0.01 w/w%. The adjusted standard deviation for tricyclic aromatic compounds in GO was found to be 0.002, and the LOQ was found to be 0.02 w/w%. While the 2019 version of ASTM D2425 offers no specific LOD or LOQ values for comparison, the reporting accuracy of the 2019 ASTM D2425 is listed as 0.1 w/w%, which is much higher than the LOD and LOQ values obtained

in this study. Therefore, the chosen instrumentation type and sample types in this study surpass the 2019 reported ASTM D2425 limits.

4.3.2.3 *Bias*

Because the real expression of trueness requires an infinite number of measurements, the trueness of this method is only a qualitative description of the quantitative measure of bias. There are three general approaches for determining bias: analysis of reference materials, recovery experiments using spiked samples, and comparison with results obtained via another method.[6] As stated in ASTM D2425-19, "there is no acceptable reference material suitable for determining the bias for this test method"(pg. 9, Section 16.3).[1] However, an estimation of the bias of hydrocarbon types can be determined using recovery experiments with spiked sample sets.

The bias of hydrocarbon type measurements were determined for the two hydrocarbon groups that were spiked into the sample sets: monocycloparaffins and alkylbenzenes for RJF and paraffins and alkylbenzenes for GO. Bias was calculated using the measured and actual summed content (wt %), of the average of the spiked analyte sample sets to determine a recovery percentage. The relative spiked recovery percentage was calculated with Equation 4.4. The RJF cycloparaffin content was calculated at 140% recovery, and the alkylbenzene content had a 63% recovery. The GO paraffin content was calculated at 117% recovery while alkylbenzene content had a 90% recovery. Both sample sets are positively biased for paraffin content (recovery percentage over 100% recovery) and negatively biased for alkylbenzene content (recovery percentage less than 100% recovery).

Equation 4.4. Relative spiked recovery percentage calculation

$$R'(\%) = \frac{\bar{x}' - \bar{x}}{x_{spiked}} * 100$$

In Equation 4.4: $\bar{x}'$ = average weight percent (monocycloparaffins and alkylbenzenes for RJF and paraffins and alkylbenzenes for GO) measured using the 2019 ASTM D2425 method; $\bar{x}$ = average weight (monocycloparaffins and alkylbenzenes for RJF and paraffins and alkylbenzenes for GO) for neat (non-spiked) RJF and GO samples measured using the 2019 ASTM D2425 method, and

x_{spiked} = the actual weight percent of monocycloparaffins and alkylbenzenes added into RJF and paraffins and alkylbenzenes added into GO.

The 2019 version of ASTM D2425 updated the sample types covered by this standard test method to include RJF samples. However, the bias estimation performed here for RJF suggests that this test method may not be appropriate for RJF samples. The cycloparaffin content in RJF was determined to have 140% recovery while the alkylbenzene content had only 63% recovery. This deviates from trueness (100% recovery) quite significantly when compared to the traditional sample type (GO), where the paraffin content was determined to have 117% recovery and alkylbenzene content 90% recovery. Spiking RJF with monocycloparaffins and alkylbenzenes and GO with paraffins and alkylbenzenes was an attempt to mimic natural compounds; however, in reality, there is no acceptable reference material for determining the bias for the test method as a whole. Instead, the spiking method used in this study provides an estimation of the bias for the specific hydrocarbons added into the sample matrices. However, without a valid reference material to evaluate the whole method, this cannot be fully confirmed. For future D2425 standard versions, the bias should be assessed using reference material, if possible. If a suitable reference material is found, the following actions should be considered: the bias should be eliminated/corrected, or the bias should be reported. If the latter approach is chosen, it should be acknowledged that the method is empirical rather than truly quantitative.[12]

4.4 Conclusions and Future Directions

The limit of detection (LOD), the limit of quantitation (LOQ), and bias were evaluated for Procedure B of the ASTM D2425 updated in 2019 for both sample matrices covered by this method: conventional (GO) and synthesized (RJF) hydrocarbons. First, the gas chromatograph/electron ionization quadrupole mass spectrometer (GC/(EI) Q MS) chosen for use in the procedure was evaluated. The MS tuning met the requirements given in the updated 2019 ASTM D2425. Further, the magnitude of the instrument signal as a function of analyte concentrations was linear within the relevant mass percent range. The chosen MS was also shown to be rugged for tuning; regular tuning of the instrument, which is commonly performed on all MS instruments, resulted in data sets that were regularly varied, and no deviating data sets were found. Therefore, since the instrument chosen, satisfied all the test parameters given in the updated 2019 version of ASTM

D2425, the GC/(EI) Q MS instrument used in this study has been proven suitable for use in Procedure B.

The measured LOD and LOQ values were 0.01 and 0.02 w/w% for GO and 0.004 and 0.01 w/w% for RJF, respectively. For RJF, bias values determined by recovery experiments were 140% and 63% for monocycloparaffins and alkylbenzenes, respectively. The GO recovery values were 117% and 90% for paraffins and alkylbenzenes, respectively. Based on these results, this method may not work well for RJF samples.

For future D2425 updates, bias should be evaluated using suitable reference materials, and significant measures should be made to eliminate or correct the bias for RJF. Alternatively, the bias should be reported. In general, to ensure the validity of a standard method for the intended use, it is advisable that the organization responsible of the method carefully assess and publish all relevant quantitative measures for all relevant method performance characteristics, particularly if used as a mandatory test in product certification. A manuscript was published on this work titled, Bias, Limit of Detection, and Limit of Quantitation for the ASTM D2425 Method Update in 2019.

A future direction may include use of other modern MS methods such as comprehensive two-dimensional gas chromatography paired with a high-resolution time-of-flight mass spectrometer with an electron ionization (EI) source. This would eliminate the need for chromatographic separation into saturated and aromatic compounds before analysis saving valuable time and resources. Additionally, the use of EI would allow many compounds to be identified and classified into hydrocarbon types based on their EI fragmentation pattern which may be compared to libraries for determination of the analyte's structure. This would eliminate the use of "typical *m/z*-ratios" to determine which hydrocarbon type the MS signal belonged to and remove the need to include in the calibration data set. This would remove the need to determine which calibration data would be necessary for conventional and synthesized hydrocarbons. If paired with a flame ionization detector (FID), the need for any calibration data would be eliminated as direct quantification of each signal would be possible for direct determination of the mass percent of each compound in the sample. I proposed this future work to the Neste Corporation and the company has agreed to fund this new research project during a new 2019-2020 collaboration with the Kenttämaa research group.

4.5 References

(1) ASTM Standard D2425, **2019**, "Standard Test Method for Hydrocarbon Types in middle Distillates by Mass Spectrometry", ASTM International, West Conshohocken, PA, 2019, www.astm.org.

(2) ASTM Standard D7566, **2018**, "Standard Specification for Aviation Turbine Fuel Containing Synthesized Hydrocarbons", ASTM International, West Conshohocken, PA, 2018, www.astm.org.

(3) ASTM Standard D2549, **2017**, "Standard Test Method for Separation of Representative Aromatics and Nonaromatics Fractions of High-Boiling Oils by Elution Chromatography", ASTM International, West Conshohocken, PA, 2017, www.astm.org.

(4) ASTM Standard D1319, **2018**, "Standard Test Method for Hydrocarbon Types in Liquid Petroleum Products by Fluorescent Indicator Adsorption", ASTM International, West Conshohocken, PA, 2018, www.astm.org.

(5) ASTM Standard D6379, **2011**, "Standard Test Method for Determination of Aromatic Hydrocarbon Types in Aviation Fuels and Petroleum Distillates- High Performance Liquid Chromatography Method with Refractive Index Detection", ASTM International, West Conshohocken, PA, 2011, www.astm.org.

(6) Magnusson, B. and Örnemark,U. (eds.) *Eurachem Guide: The Fitness for Purpose of Analytical Methods – A Laboratory Guide to Method Validation and Related Topics*, (2nd ed. b). Available from www.eurachem.org.

(7) International union of pure and applied chemistry (IUPAC) prepared by: Currie, Lloyd A. *Pure and Appl. Chem.* **1995,** 67, 1699-1723.

(8) Wang, Y., Rodriguez de Gil, P., Chen, Y.H., Kromrey, J.D., Kim, E.S., Pham, T., Nguyen, D., Romano, J.L., *Educational and Psychological Measurement.* **2017**, 77, 305-329.

(9) Zhang, S. (**1998**, April) *Fourteen Homogeneity of Variance Tests: When and How To Use Them.* Annual Meeting of the American Educational Research Association. San Diego, CA.

(10) Lee, H.B., Katz, G.S., Restori, A.F. *Journal of Mathematics and Statistics.***2010**, 6, 359-366.

(11) Wright, Craig S. (Nov. **2009**) Testing Homogeneity of Variance. Master's thesis, University of Newcastle, Australia, (Published April 2017). Available at: https://papers.ssrn.com/sol3/papers.cfm?abstract_id=2953900

(12) EURACHEM/CITAC Guide, *Quantifying Uncertainty in Analytical Measurement*, (3rd ed. **2012**). Laboratory of the Government Chemist, London (2012). Available from http://www.eurachem.org.

CHAPTER 5. CREATION AND VALIDATION OF A TRANSPARENT MINIATURE COREFLOOD DEVICE FOR CHEMICALLY ENHANCED OIL RECOVERY (CEOR) FORMULATION TESTING

5.1 Introduction

The high consumption rate of oil in the United States (US) demands greater crude oil production from an ever-dwindling supply — for instance, an average of 20.35 million barrels of oil were consumed every day in the US in 2018.[1] Traditionally, crude oil has been recovered by either using the natural pressure of the reservoir, referred to as primary flooding, and/or by injecting water or gas to displace more oil, referred to as secondary flooding.[2] However, primary and secondary flooding only yield an average recovery of 20-40% of the reservoir's oil, leaving 60-80% of the oil trapped underground.[2] Thus, enhanced oil recovery (EOR) approaches, or tertiary recovery methods, have been developed in an effort to recover the remaining trapped oil. One tertiary approach is chemically enhanced oil recovery (cEOR), which uses a mixture of chemicals to improve crude oil recovery volume.[3-8] It has been previously reported that most of the world's oil production wells are now mature, which means they contain a high percentage of residual, difficult to recover oil.[9] Thus, employing cEOR approaches to target the remaining oil in these more challenging reservoirs is a critical task.

For cEOR, selection of an appropriate brine, surfactant(s), and polymer(s) for formulation testing is the first — and one of the most important — steps. Currently, cEOR formulations are primarily evaluated based on the volume of crude oil recovered from rockcores in laboratory coreflood (CF) tests.[10] The purpose of laboratory CF tests is to mimic the oil reservoir conditions in which the cEOR formulation will be deployed and to determine if the formulation will perform in the oil reservoir and mobilize more crude oil for recovery. In these tests, a sample of reservoir rock or a representative rock, such as Berea rock, is saturated with reservoir oil. Next, a secondary recovery technique is performed where the rockcore is flushed with water/brine. Then, the rockcore is flushed with the potential cEOR formulation, and the volume of the oil recovered using the formulation is determined. These tests are all completed under pressure, called overburden pressure, that mimics the pressure in the oil reservoir of interest. The overburden pressure used in various CF tests is determined by geological information and the content of the rock morphology of the oil well of interest.[11] Depending on procedural choices, such as the aging period used for

saturation of the rock with crude oil prior to testing, the rate of pumping of the recovery solutions, and the time needed to set up and take down the equipment, CF tests can take 3-6 weeks for a single cEOR formulation. Additionally, traditional CF tests need a specialist to perform them, require bulky and costly machinery, and cost thousands of dollars for each tested cEOR formulation.

To combat the costs of traditional CF tests, miniature and micro model columns have been employed in the past to screen formulations. For example, a miniature sand-packed column (0.7" diameter and 3.3" length) filled with heavy oil and water has been utilized to test the efficiency of microbial feeding formulations, designed for microbially enhanced oil recovery (mEOR).[12] However, the column used in the mEOR test did not mimic the oil reservoir conditions as no overburden pressure was applied to the sand-packed column, failing to imitate operating conditions. Another study used a small sand-packed column (2" diameter and 6" length), filled with sand of 60-100 mesh size, to test alkaline formulations for EOR.[13] However, the sand-packed column did not model the reservoir of interest because the sand did not imitate the porosity and permeability of an oil well — the sand-packed column had a porosity of 35% and permeability of 3,000-3,800 mD, while most reservoir rocks have a porosity between 20-22% and permeability between 300-350 mD.[2] Finally, a nanofluid enhanced oil recovery formulation has been tested using small rockcores (1.5" diameter and 5" length).[14] The rockcores were cleaned by toluene and methanol, and then soaked in crude oil for 4 weeks. This approach may alter the rockcore's surface properties and do not mimic real oil reservoir conditions, as the cleaning procedure may change the wettability of the rockcore's surface or alter the natural minerals in the rockcore, such as halite.[15] Additionally, the timeline of oil soaking does not allow high throughput testing. Overall, none of the small-scale tests discussed above have mimicked the reservoir conditions appropriately, nor do they allow for high throughput data collection. Furthermore, no miniature CF tests for cEOR formulation screening have appeared in the literature that test surfactant and polymer mixtures on a small-scale with high throughput capabilities, while mimicking reservoir conditions.

To address the above issues, three transparent miniaturized coreflood (TMCF) devices were designed, built, and tested for being able to rapidly and economically prescreen of candidate cEOR formulations prior to traditional CF tests. The design, construction, and evaluation of the miniature coreflood prototypes, which lead to the final TMCF device creation, are discussed in in this Chapter.

5.2 Experimental

5.2.1 Materials

The brine was an aqueous solution containing sodium chloride (NaCl), potassium chloride (KCl), manganese chloride tetrahydrate ($MnCl_2 \bullet 4H_2O$), magnesium chloride hexahydrate ($MgCl_2 \bullet 6H_2O$), barium chloride dihydrate ($BaCl_2 \bullet 2H_2O$), sodium sulfate decahydrate ($Na_2SO_4 \bullet 10H_2O$), sodium bicarbonate ($NaHCO_3$), and calcium chloride dihydrate ($CaCl_2 \bullet 2H_2O$) (Fisher Scientific: Hampton, NH) at a total mass fraction of 9,400 ppm. This brine was created to mimic the brine used to complete secondary flooding on an oil well in the Illinois Basin. Given that most tertiary recovery techniques, cEOR, are performed after secondary flooding, the CF tests also mimicked this process by first conducting secondary brine flooding, followed by cEOR tertiary recovery. The chosen test rocks, Berea rock, were of varying sizes with a permeability between 300-350 mD and porosity between 20-22% (Cleveland Quarries; Vermilion, OH). The permeability and porosity were comparable to the typical oil reservoir characteristics where this cEOR formulation would be deployed.[2] Prototype 1.0 utilized rockcores of diameter of 0.75” and a length of 4”, while prototype 2.0, the TMCF device, used rockcores of diameter of 1” and a length of 6”. The traditional CF device utilized rockcores of diameter 1.5” and a length of 12”. The crude oil used in this investigation was collected, and provided, by Pioneer Oil from an active well in the Illinois Basin, and has been previously characterized — API gravity value of 32°, density of 0.87 g/mL and a viscosity of 12.28 cP (determined at 20 °C).[16] The oil was filtered after collection by using a 0.5 μm steel inline filter (Swagelok) before use in testing.

The cEOR formulation was a two-step process: first, a surfactant and polymer solution was injected, followed by a polymer solution injection. A solution of polymer 3230 (0.33 wt %) in brine was used, and surfactants S13D, A6, and L4-2 were added (0.64 g, 0.26 g, 0.15 g respectively) to a 100 mL portion of that polymer solution, to create the polymer/surfactant solution. An additional cEOR formulation was tested which was a solution of polymer 3330 (0.19 wt %) in brine. Surfactant S13D was added (0.99 g) to a 100 mL portion of that polymer solution to create the second polymer/surfactant solution.

5.2.2 Methods

The first step in a CF testing protocol is to calculate the pore volume of the rockcore. The pore volume must be determined to inform the volume of solution that must be pumped onto the rockcore in order to properly saturate all the pore space. To determine the pore volume, the rockcore was first dried in an oven (110 °C) for 2 days and then weighed to establish its dry weight. Then the rockcore was wetted with the brine (described in Section 5.2.1) under vacuum (Welch vacuum pump, Duo Seal 1402) for three hours, and then was weighed to determine the wet weight of the rock. By wetting the rockcore in brine solution under vacuum, the air can more readily be pumped out of the rockcore, allowing the brine to fill the pore spaces. It is assumed that all pores in the rockcore were saturated with brine. Therefore, the pore volume was calculated by converting the difference between the dry and wet weight to a volume by using the brine's density (1.0048 g/mL). Then the CF device was assembled, and the rockcore was re-saturated with brine to ensure wetting of the rock. The second step of the CF testing was to then saturate the rockcore with crude oil by injecting oil onto the brine-saturated rock. The oil injection occurred while the rockcore was housed in the CF device, which was under overburden pressure (manual pressure or hydro-fluidic overburden pressure depending on the prototype as discussed in section 5.3.1). This injection took place until recovery of the brine leaving the device ceased. The volume of brine displaced from the rockcore during this step was assumed to be equal to the volume of oil now inside the rockcore. The now oil-saturated rockcore was left under overburden pressure (manual pressure or hydro-fluidic overburden pressure depending on the prototype as discussed in section 5.3.1) to age, before CF testing continued. After aging, the oil-saturated rockcore was flushed with brine, to mimic the secondary recovery technique, followed by the two-step tertiary recovery technique using a cEOR formulation (step one: surfactant/polymer solution and step two: polymer solution in this case), followed by an ending brine flush. This concluded the CF test. All CF testing was conducted in this manner regardless of the device size.

To determine if the cEOR formulation performed well, where maximum oil recovery is desired, oil was collected for volume analysis at each stage of the CF testing process. The volume of oil was converted to a recovery percentage by normalizing the volume of oil recovered with the original volume of oil in the rockcore (equal to the volume of brine displaced during the oil saturation step of CF testing). Many cEOR formulations can then be compared to determine which formulation had the largest recovery percentage.

For this work, the cEOR testing protocol consisted of an initial brine flood of 2.5 pore volumes, followed by a surfactant-polymer mixture flood of 0.5 pore volumes, then a polymer flood of one 1 pore volume, and finally an ending brine flood of 1 pore volume. These volumes were chosen to mimic the traditional CF testing protocol and eventual oil field implementation volumes used by the funding agency, Pioneer Oil. The tertiary cEOR recovery process was performed under a controlled, constant fluid injection rate of 0.2 mL/min. This injection rate is consistent with previously published small CF device tests.[14,17]

Miniature CF Test Timeline: Day 1: The rockcore was cut, the rockcore pore volume was determined, and the core was saturated with brine. Then the core was saturated with filtered crude oil and allowed to age under overburden pressure for 5 days. Day 6: Fresh brine, polymer, and surfactant-polymer solutions were prepared. Day 7: Injection order: initial waterflood of brine solution of 2.5 pore volumes; surfactant/polymer mixture of 0.5 pore volume; polymer mixture of 1 pore volume; ending waterflood of brine solution of 1 pore volume. The recovered oil from each injection was collected into separate glass falcon tubes for later volume evaluation. In the final TMCF device set-up allowed for three rockcores to be aged at once following the same 6 day timeline. Then days 7-9 would be spent testing a cEOR formulation on each of the three TMCF apparatuses.

Traditional CF Test: The traditional CF tests followed the same protocol described above for establishing pore volumes of the larger rockcores used in these tests (1.5" diameter and 12" length). Once the CF device was assembled, the core was saturated with crude oil at an injection rate of 0.25 mL/min until two pore volumes of oil had been injected. The oil-soaked rockcore was then allowed to age for two weeks in the CF device under 400 psi hydrofludic overburden pressure. The test overburden pressure was determined to be 400 psi by the Pioneer Oil company for the oil reservoir of interest, by using geological survey information. Finally, the cEOR formulation was tested as described above but at an injection rate of 0.25 mL/min and by using the same pore volume ratios as outlined above for the miniature CF tests. The same rockcore with the crude oil, brine, and cEOR formulations were used in both the full-sized CF and miniature CF tests.

5.3 Results and Discussion

5.3.1 TMCF Device Design

The goal of this work was to produce a new, smaller CF device for increased ease of use and to make it faster and more economical to operate. Another goal was to enable a single operator, without expertise, to be able to utilize the miniature CF device. To achieve these goals, two prototypes were first built and evaluated. Prototype 1.0 was built using stainless steel as the outer chamber material and rubber tubing as the inner chamber material. These materials are consistent with commercial CF devices. The first-generation design for the miniature CF device, prototype 1.0 (Figure 5.1) was designed by Dr. Xueming Dong and manufactured by Randy Replogle and featured: 1) a metal core holder, 2) a manual overburden pressure on rockcore, and 3) 4” length x 0.75” diameter rockcore dimensions. For prototype 1.0, once inserted, the rockcore could not be removed intact from the inner rubber chamber. Therefore, the rockcore had to be broken to be removed from the apparatus.

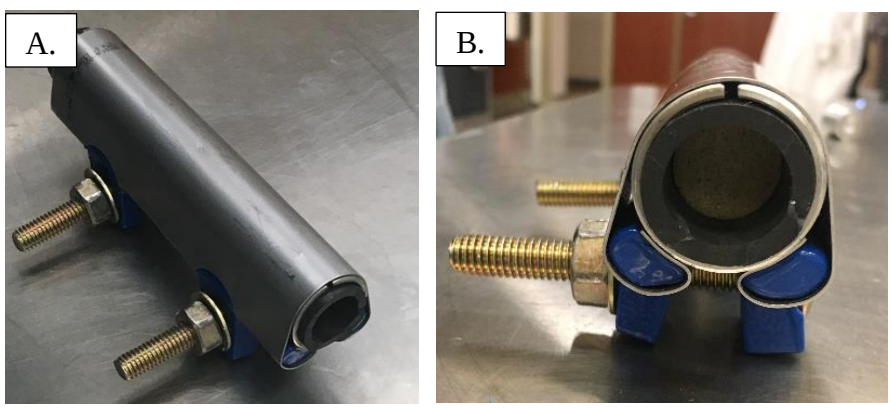

Figure 5.1. Miniature coreflood device prototype 1.0 from A) top view and B) side view.

The prototype 1.0 system, Figure 5.2, was designed for a rockcore with 1/30th the volume of the rockcore used in the traditional CF device. However, due to the small core size, the dead volume in the pumping lines lead to inconsistent data collection. Additionally, the overburden pressure used to mimic the pressure in the oil reservoir was applied manually; therefore, the actual pressure applied was unknown. Consequently, a second-generation (prototype 2.0) device was designed for a larger rockcore of 1/5th the volume used in the traditional CF device.

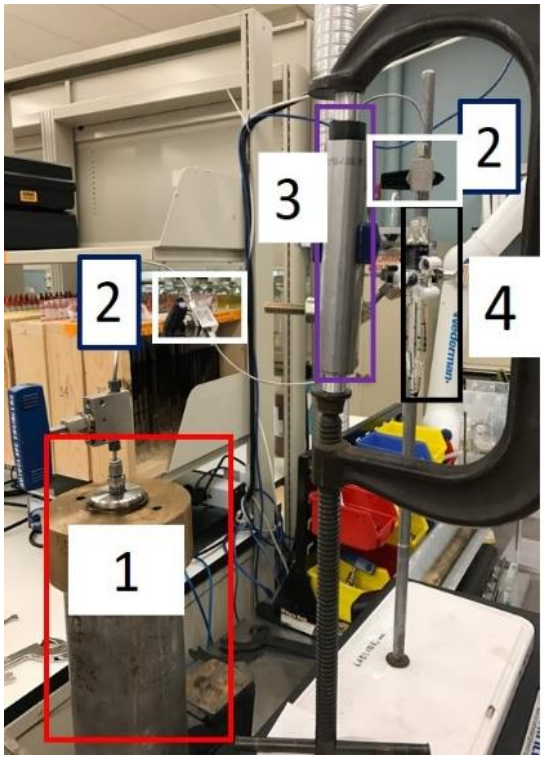

Figure 5.2. Miniature coreflood device prototype 1.0 system and its components assembled: 1) fluid accumulator, injection cylinder, 2) isolation valves, 3) core holder (core size: 4" length x 0.75" diameter), 4) collection tube

The design of the new prototype (prototype 2.0, TMCF) system is shown in Figure 5.3. To enable observation of oil migration during testing, polycarbonate, a transparent building material, was chosen for the outer chamber. For the inner chamber, flexible transparent PVC Tygon tubing was used, the flexible inner chamber tubing allowed the rockcores to be removed intact after CF testing. Allowing for further testing to be completed on the same rockcore after CF testing if desired. Additionally, the overburden pressure was applied via a hydrofludic pressure by a pump with a back-pressure transducer, which monitored the applied pressure to ensure consistency. The larger rockcore size also reduced the error introduced by the dead-volume of the pumping lines to a negligible amount. The resulting TMCF devices were lightweight (less than 3 pounds each), and the entire system contains three TMCF devices within two cubic feet of benchtop space (Figure 5.3). Due to its small size and lightweight building materials, the TMCF device is easy for a single operator to handle and has a timeline of 7 days for one coreflood test and 9 days for three coreflood tests. This design meets the goals for high throughput data collection (compared to a traditional

CF timeline of 3-6 weeks for a single coreflood test), small and lightweight machinery, and cost-effectiveness. The design of the new TMCF device will be discussed below.

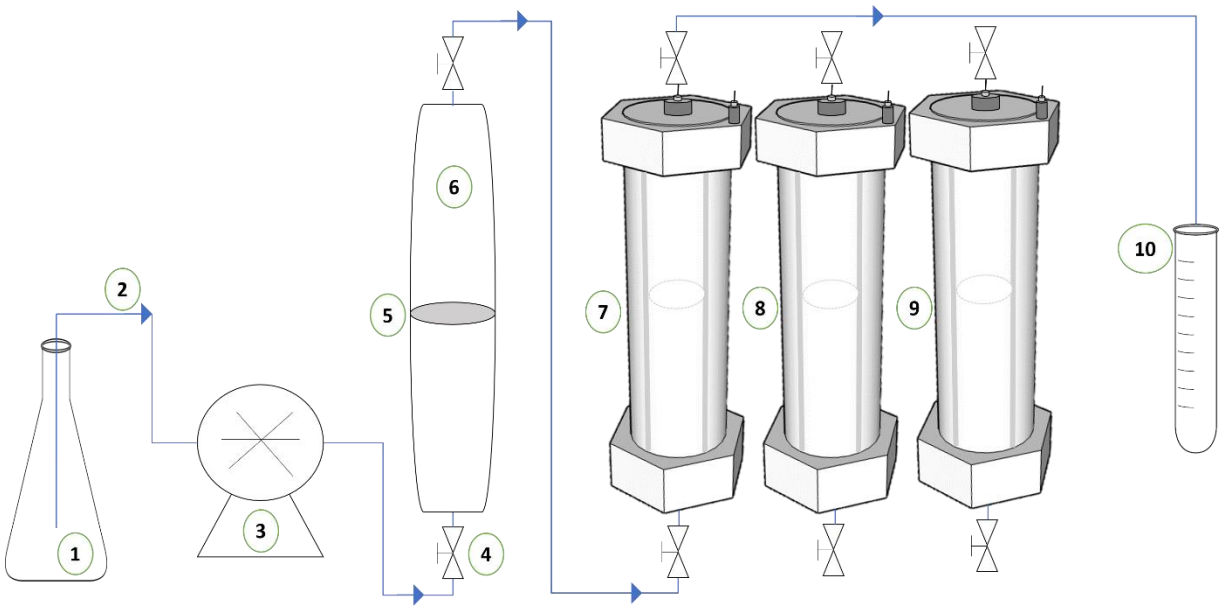

Figure 5.3. Second-generation TMCF device with three coreflood devices. 1) pump fluid; 2) pumping lines; 3) injection pump; 4) valve; 5) piston plate; 6) injection vessel where cEOR formulations are placed; 7-9) TMCF devices; 10) collection tube. Only one TMCF device can be used for cEOR formulation testing at a time. One TMCF device (7) is shown connected to the system in the figure. Flow direction is indicated by arrows on the pumping lines.

Each TMCF device is composed of two chambers. The inner chamber (D, Figure 5.4B) was used to house the rockcore and isolate it from the fluid used to create the surrounding hydrofluidic overburden pressure. This pressure was created by pumping deionized water between the inner chamber and the outer chamber (E, Figure 5.4B). A hydrofluidic overburden pressure of 80 psi was achieved through a port (B, Figure 5.4B), by using a pre-set isobaric pump which was monitored by a pressure transducer. This overburden pressure is 1/5th the overburden pressure used in traditional CF devices (400 psi, as determined by Pioneer Oil). O-rings (made of oil resistant Buna-N material) inside the endcaps of the device kept the inner and outer chamber liquids isolated (C, Figure 5.4B). Liquids were pumped onto the rockcore for testing by using port A in Figure 5.4B. An identical port was located on the bottom endcap used to recover brine and oil during cEOR formulation testing.

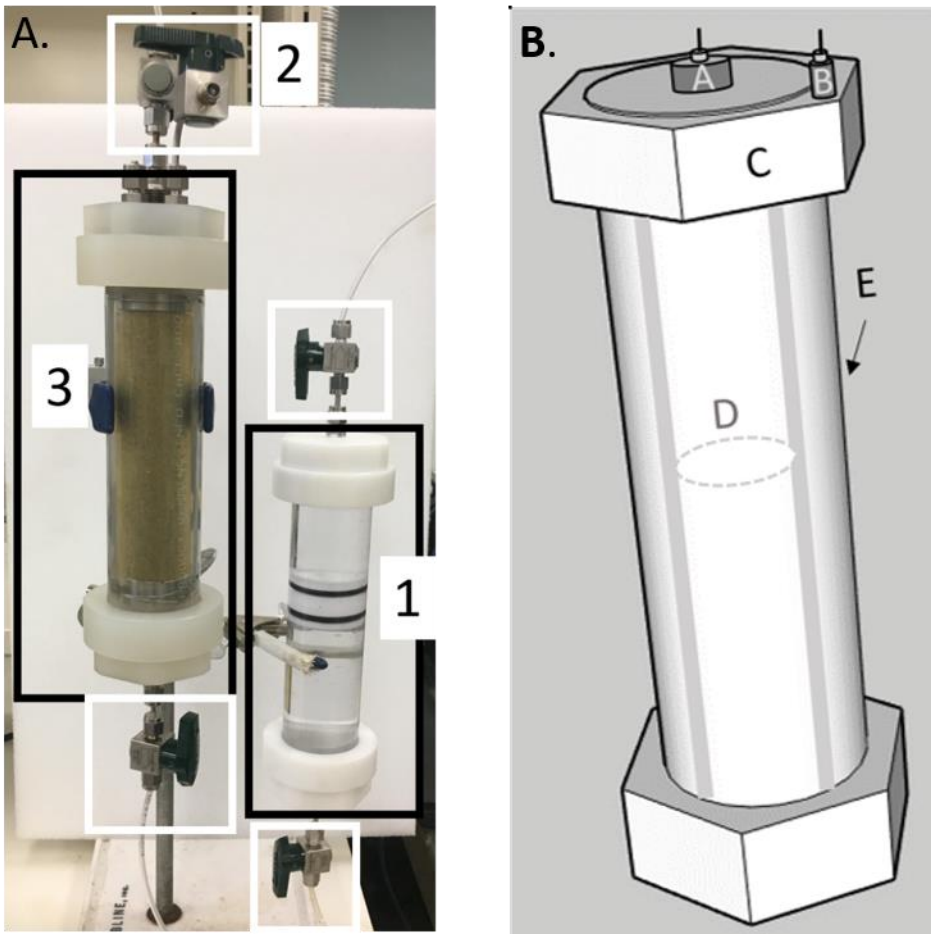

Figure 5.4. A. Miniature coreflood device prototype 2.0, TMCF, and its components in use with a rockcore inside the inner chamber: 1) fluid accumulator, injection cylinder 2) isolation valves, 3) core holder (core size: 6” length x 1” diameter) B. Miniature coreflood prototype 2.0, TMCF, schematic and its components: A) inner chamber injection port, B) outer chamber injection port, C) end cap, D) inner chamber tubing (PVC Tygon), and E) outer chamber transparent case (polycarbonate).

5.3.2 TMCF Device Performance

The performance of the three TMCF devices was tested by comparing the oil recovery percentage obtained using the same cEOR formulation, brine, crude oil, and rock type to that obtained with a full-scale CF device. The oil recovery percentage was used for comparison, instead of volume recovery, because the CF and TMCF devices used rockcores of different sizes. All tests were conducted at ambient temperature. The TMCF core size is 1/5th the volume used in the CF device but has the same permeability and porosity. The pore volume of each core was determined as described in the methods (Section 5.2.2). Even oil distribution in the TMCF device was ensured

by monitoring oil migration (Figure 5.5). The transparent design of the TMCF allows the operator to ensure even oil distribution, unlike the full-size CF, where visual core monitoring is impossible.

Figure 5.5. The new TMCF device design allows oil migration to be monitored during the initial oil saturation process to ensure an even and complete oil distribution.

To test the performance of the three TMCF devices as a prescreening approach for full-size CF testing, cEOR formulations that had already been examined in the large scale CF device were employed. One data set was obtained by using a solution of polymer 3230 in brine and a polymer/surfactant solution with the same polymer (3230) and surfactants S13D, A6, and L4-2. An additional cEOR formulation was tested which consisted of a solution of polymer 3330 in brine and a polymer/surfactant solution with the same polymer (3330) and surfactant S13D. Nine total cEOR formulation tests were carried out to evaluate and compare the performance of the TMCF devices to standard CF tests.

The following volumes were measured in each TMCF test: (1) the volume of brine displaced during initial oil saturation; (2) the volume of oil recovered during the initial waterflood (IWF); (3) the volume of oil recovered during each cEOR step: the surfactant and polymer (SP) flood and the polymer (P) flood; (4) the volume of oil recovered during the ending waterflood (EWF). These volumes were used to calculate the percentage of the rockcore that was saturated

with oil (Equation 5.1), the percentage of oil recovered from the initial waterflood (Equation 5.2), the percentage of oil recovered from cEOR (Equation 5.3), the overall oil recovery percentage (Equation 5.4), and the percentage of oil left in the rockcore (Equation 5.5).

Equation 5.1. Initial oil saturation

$$Initial\ Oil\ Saturation\ (\%) = \frac{Volume\ of\ original\ oil\ in\ place\ (Volume\ of\ brine\ displaced)\ (mL)}{Pore\ volume\ (mL)} * 100$$

Equation 5.2. Initial waterflood oil recovery

$$IWF\ Oil\ Recovery\ (\%) = \frac{Volume\ of\ oil\ recovered\ from\ waterflood\ (mL)}{Volume\ of\ oringinal\ oil\ in\ place\ (mL)} * 100$$

Equation 5.3. cEOR oil recovery

$$cEOR\ (\%) = \frac{Volume\ of\ oil\ recovered\ from\ SP +\ P + EWF\ (mL)}{Volume\ of\ oringinal\ oil\ in\ place\ (mL)} * 100$$

Equation 5.4. Overall oil recovery

$$Overall\ Oil\ Recovery\ (\%) = \frac{IWF + SP + P + EWF\ oil\ recovered\ (mL)}{Volume\ of\ oringinal\ oil\ in\ place\ (mL)} * 100$$

Equation 5.5. Oil left in place

$$Oil\ Left\ in\ Place(\%) = \frac{Volume\ of\ original\ oil\ in\ place\ (mL) - (Volume\ of\ oil\ recovered\ from\ IWF\ + SP\ + P\ + EWF\ (mL))}{Pore\ volume\ (mL)} * 100$$

One TMCF device was used to determine the oil recovery using the cEOR formulation of polymer 3230 and surfactants S13D, A6, and L4-2. The results obtained using the CF and one TMCF device are in excellent agreement for results obtained using this cEOR formulation on the commercial CF device, as shown in Table 5.1. In this case, the TMCF test results differed from the CF results by less than 5%.

Table 5.1. Compilation of results obtained for a formulation containing surfactants S13D, A6, and L4-2 and polymer 3330 by using a TMCF device and the CF device. Each result was determined in comparison to the original oil in place (OOIP), except the percentage of the rockcore that was saturated with oil (%OOIP) which was determined in comparison with the rockcore's pore volume. Therefore, the results are given as a percent opposed to a volume so that the test parameters from the differently sized rockcores can be compared.

Steps of the Test	TMCF Results	CF Results	Absolute Difference Between CF and TMCF Results
Percentage of the Rockcore that was Saturated with Oil (%OOIP)	62 %	67 %	5 %
Initial Waterflood Oil Recovery	30 %	33 %	3 %
Chemically Enhanced Oil Recovery (cEOR)	41 %	41 %	0 %
Overall Oil Recovery	71 %	73 %	2 %
Oil Left in Place	21 %	18 %	3 %

5.3.2.1 *TMCF Device Performance: Volume of Oil Recovered from Multiple Operators*

The next step was to test the same formulation (surfactant mixture S13D, A6, and L4-2 with polymer 3230) on three TMCF devices and determine the variance in data between different operators. Three different operators, with varying extents of laboratory experience — a senior graduate student (Dr. Xueming Dong), a graduate student (Katherine Wehde), and an undergraduate student (Tianru Jiang) — followed a written standard operating procedure to perform the 9-day TMCF test (Section 5.2.2). Testing on core 1 was completed by the senior graduate student (day 7), core 2 by the graduate student (day 8), and core 3 by the undergraduate student (day 9) (Figure 5.6). The average cEOR oil recovery for all three TMCF devices was 35% (standard deviation 4%), and the average total oil recovery (combined recovery from cEOR and primary waterflooding) was 76% (standard deviation 5%). The volume of oil recovered by the three different operators was not significantly different (student t-test at 95% confidence). The full-size CF device, operated by an expert using the same cEOR formulation, had an cEOR oil recovery of 41% and the overall oil recovery of 73%. The TMCF devices and CF device cEOR oil recovery differed by 6%, and overall oil recovery differed by 3%.

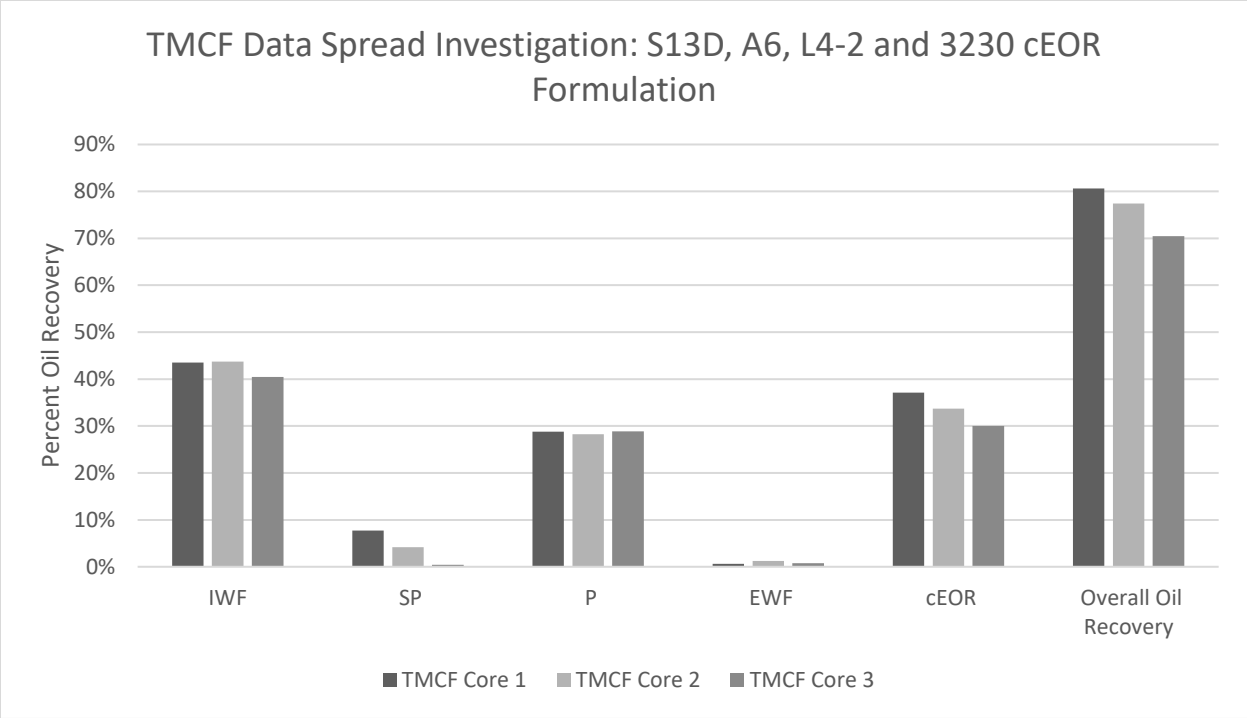

Figure 5.6. Percent oil recovery for each step of three TMCF tests carried out by three different operators. Core 1 was completed by the senior graduate student, core 2 by the graduate student, and core 3 by the undergraduate student over three days by using a cEOR formulation of three surfactants (S13D, A6, and L4-2) and a polymer (3230). Step 1 corresponds to the initial waterflood (IWF), followed by cEOR (a surfactant and polymer mixture flood (SP) followed by a polymer solution flood (P)), and finally an ending waterflood (EWF). The oil recovered from the cEOR process is shown, as well as the overall oil recovery, which includes the oil volume recovered upon both IWF and cEOR.

5.3.2.2 *TMCF Device Performance: Volume of Oil Recovered from Multiple Rockcores*

A second formulation, containing surfactant S13D and polymer 3330, was tested using five different Berea rockcores in the TMCF devices (Figure 5.7). Data from TMCF rockcore 1 were found to be outliers as the overall oil recovery was outside the statistical lower bound of the data set. The statistical lower bound of the data set was determined by subtracting one and a half times the interquartile range from quartile one (the lower quartile) of the data set. The statistical lower bound of the overall oil recovery is 46.5%, but the overall oil recovery from core 1 was less, at 40% recovery. Therefore, rockcore 1 was determined to be an outlier. This can partially be explained by the aberrant phase behavior this rockcore exhibited during testing. The most prominent behavior was formulation fingering, where the pumped solution breaks through at a given spot in the core (Figure 5.8). Proper oil migration is also shown for comparison in Figure

5.8, where the oil is being moved along the rockcore by the cEOR formulation in a single unit towards collection. Formulation fingering allows the pumped solution to break through the core and travel towards the collection port without mobilizing more oil within the core.[2] The reasons for this behavior for rockcore 1 are unknown but is likely due to a difference in rock morphology compared to the other test rockcores. However, this finding demonstrates that different rockcores may produce very different results. Furthermore, the transparent design of the device allowed for the recognition of the unexpected flow characteristics and a better understanding of the bad set of data. This would not be possible with a traditional CF device as such devices are not transparent. This issue is made more serious by the fact that replicate measurements are often not performed using CF devices as they are expensive and time-consuming, which increases the uncertainty of the results.

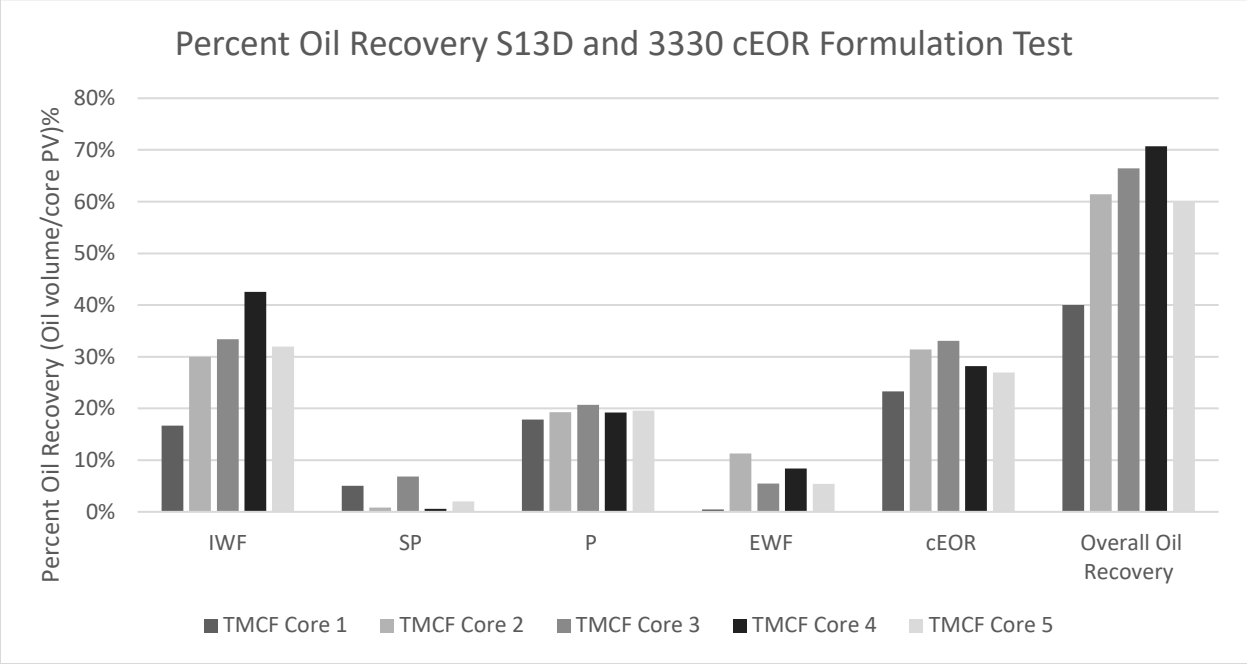

Figure 5.7. Percent oil recovery for each step of five TMCF tests using five different rockcores (1 – 5) flooded using a cEOR formulation containing one surfactant (S13D) and one polymer (3330). Step 1 corresponds to the initial waterflood (IWF), followed by cEOR (a surfactant and polymer mixture flood (SP) followed by a polymer solution flood (P)), and finally an ending waterflood (EWF). The oil recovered from the cEOR process is shown, as well as the overall oil recovery, which includes the oil volume recovered upon both IWF and cEOR.

Not including TMCF core 1, the overall average oil recovery obtained using the formulation containing S13D and polymer 3330 in the TMCF devices was 65% (standard deviation 5%) with a cEOR average recovery of 30% (standard deviation 3%). The total oil recovery obtained using the same formulation in the CF device was 60%, and the cEOR recovery was 29%. This cEOR formulation recovery data set (formulation S13D and polymer 3330) is within 5% variance for all repeated measurements. Although full-size CF tests are generally not repeated, 9% variability has been reported for triplicate analyses of a full-size CF test.[18] This value is in agreement with the overall variability of 6% or less observed here for the TMCF devices overall in all tests performed.

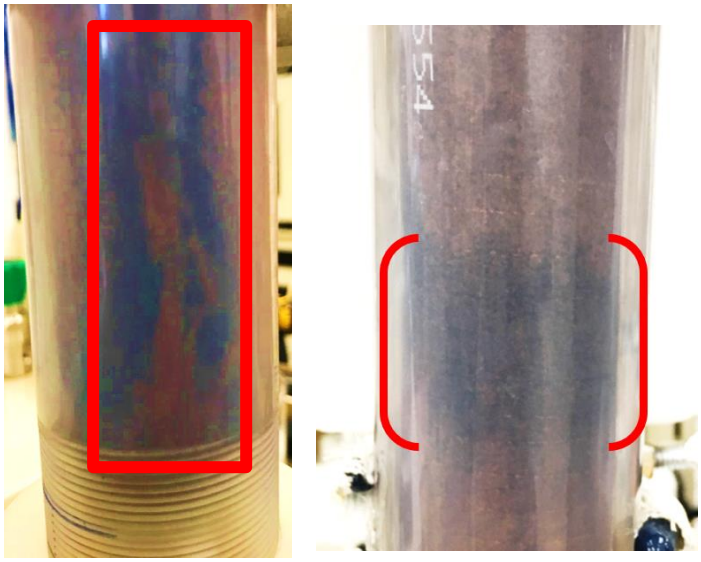

Figure 5.8. The core on the left exhibits formulation fingering, red box, seen during cEOR process on TMCF core 1. The proper oil migration is shown in red brackets on the rockcore on the right. No breakthrough of formulation fingering was observed. The color was augmented for ease of viewing in both pictures.

5.3.3 Semi-automated TMCF device

The initial TMCF device testing was considered a success as the oil recovery results were similar to the full-size CF testing results. To further the ease of use and high throughput of the device, a new device stand was constructed, as well as new operation pieces were added: backpressure transducer, electronic display, more fluid accumulators, and electric valves and controllers (Figure 5.9 A-C).

Figure 5.9. (A) Front view: 1. Formulation fluid accumulator holder; 2. Open space for future expansion to include more fluid accumulators or TMCF devices; 3. cEOR TMCF device holder; 4. Automatic valves; 5. Automatic valve controllers; 6. Backpressure transducer electronic reader, (B) Side view, and (C) Back view.

Figure 5.9 Continued

TMCF Device 2.0 Prototype Front View

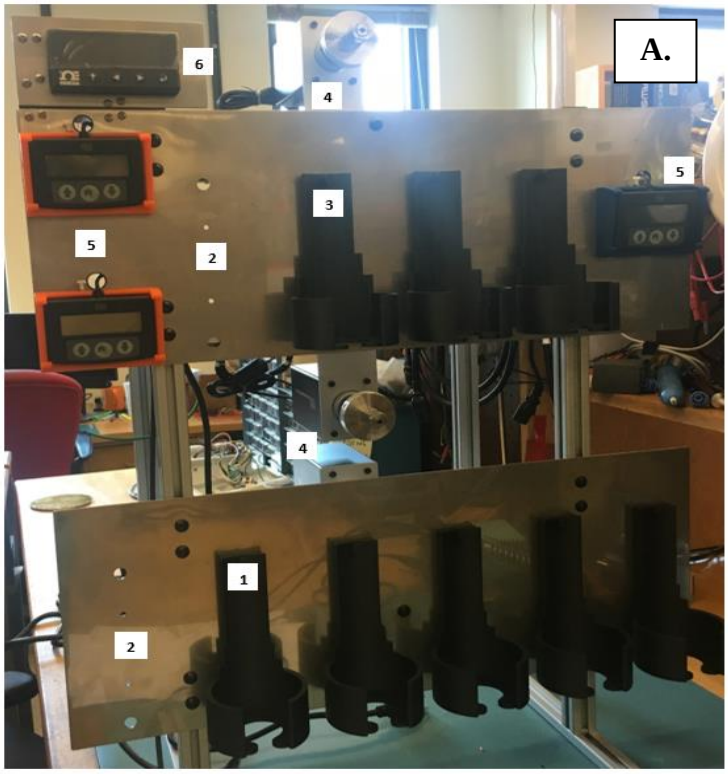

TMCF device 2.0 Prototype Side View

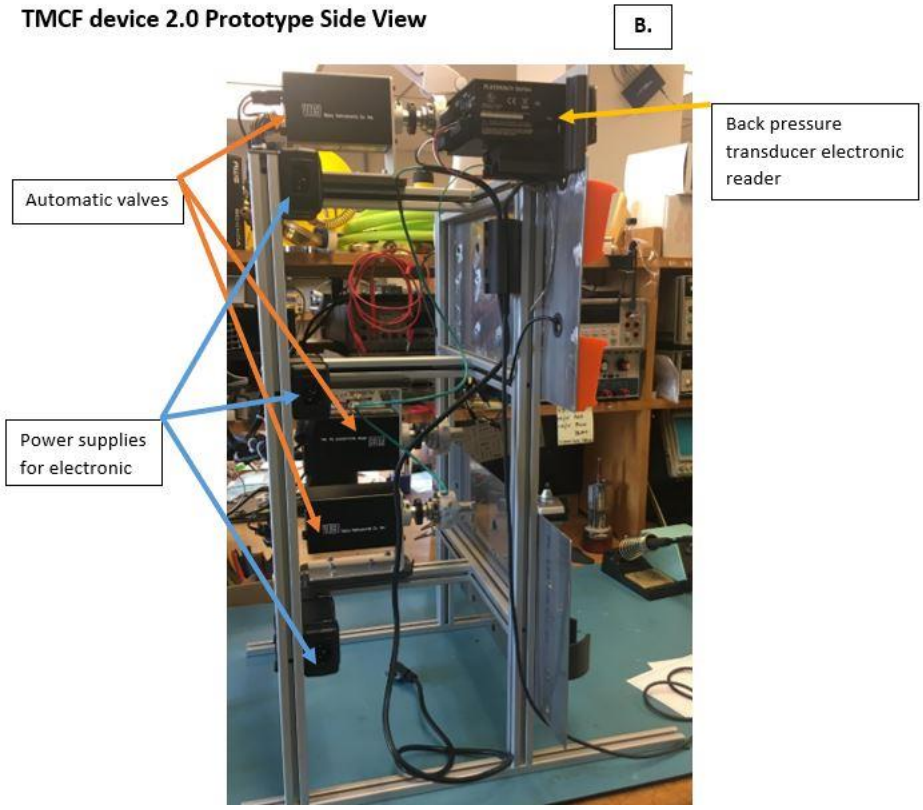

Figure 5.9 Continued

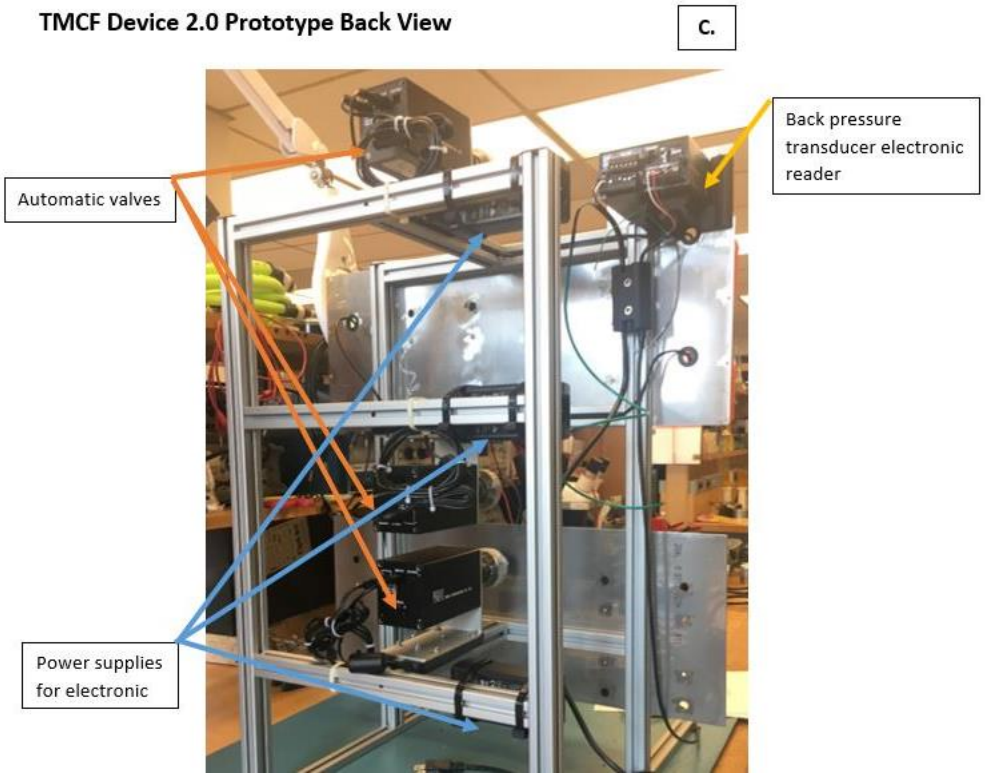

Testing of the new Tri-TMCF (prototype 2.0) has begun. All of the new fluid formulation accumulators (manufactured by Randy Replogle) have been pressure and stress tested. No leaking was observed at the end caps, nor between the chambers on either side of the pumping piston (up to 55 psi test range). The automatic valves have been programmed and connected to their controllers. The back-pressure transducer is programmed and is communicating with the digital display, which has also been programmed and calibrated for pressures between 0 and 50 psi. All parts have been connected (Figure 5.10).

The final steps of this project will be to test previously evaluated cEOR formulations on the new Tri-TMCF prototype device, test the reproducibility of those results, and compare test parameters between the old and new prototype to ensure suitable correlation with the expected performance.

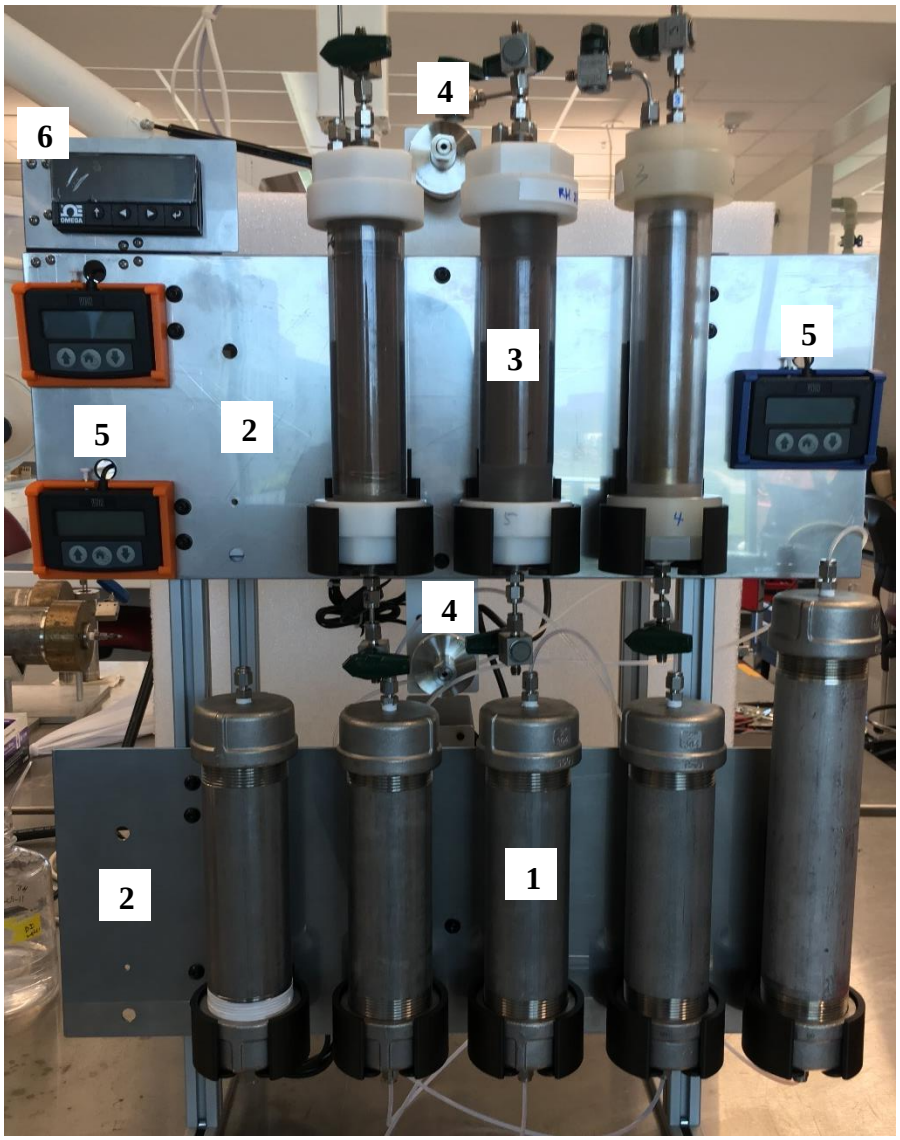

Figure 5.10. Front view of the Tri-TMCF device stand with all of its components: 1. Formulation fluid accumulator; 2. Open space for future expansion to include more fluid accumulators or TMCF devices; 3. cEOR TMCF device with rockcores inserted; 4. Automatic valves; 5. Automatic valve controllers; and 6. Backpressure transducer electronic reader.

5.4 Conclusions and Future Directions

I suggest that the TMCF device be used to prescreen candidate cEOR formulations before they progress to full-scale CF testing. If a formulation performs poorly in TMCF then it is predicted to perform poorly in CF as well. The low cost of the TMCF will allow multiple systems to be built and run in parallel, thereby simultaneously testing several formulations. I expect that TMCF will significantly decrease the time needed to optimize a cEOR formulation for a particular oil well. It

is important to note that TMCF should be considered as a support to traditional CF testing and should not be viewed as a replacement for CF devices, because CF tests are still likely the best prediction of cEOR formulation performance in oil fields.

The three TMCF devices enabled three different formulations to be tested, or one formulation to be tested three times, within a 9-day period, which is substantially shorter than the 3-6 weeks per formulation required for traditional CF devices. Therefore, these TMCF devices will allow numerous cEOR formulations to be quickly tested prior to traditional CF testing, which has not been previously possible. Furthermore, the TMCF devices allow the operator to observe oil migration through the transparent design, which enables rejection of questionable measurements from flawed rockcore phase behavior, such as formulation fingering. The TMCF devices are lightweight (less than 3 pounds each), small (the entire system requires less than two cubic feet of benchtop space), and easy to use. This allows a single operator to use the system efficiently without extensive training. The TMCF devices effectively address the three limiting factors of CF tests: time, cost, and training needed to operate the system. A manuscript on this work was submitted for publication titled Validation of Benchtop Miniaturized Coreflood Devices for Parallel Prescreening of Candidate Formulations for Chemically Enhanced Oil Recovery.

The final steps of this project will be to test previously evaluated cEOR formulations on the new semi-automated prototype system, test the reproducibility of those results, and compare test parameters between the manually tested TMCF prototype to ensure good correlation with the expected performance. Future directions should also include testing the injection flow rate of formulation to determine if the pumping rate effects the volume of oil recovered. The system can also move towards full automation for higher throughput and less hands-on time spent by an operator on the instrument and cEOR formulation testing. All new parts on the Tri-TMCF device (Figure 5.10) are able to be fully automated in the future with no future purchases necessary to complete this task other than a computer.

5.5 References

(1) Independent Statistics and Analysis. U.S. Energy Information Administration: Petroleum and Other Liquids. w.eia.gov/dnav/pet/pet_move_impcus_a2_nus_ep00_im0_mbbl_a.htm.

(2) Muggeridge, A., Cockin, A., Webb, K., Frampton, H., Collins, I., Moulds, T., Salino, P. Phil. *Trans. R. Soc. A.* **2014**, 372, 1-25.

(3) Green, D.W., Hirasaki, G., Pope, G.A., Willhite, G.P. Surfactant Flooding. Society of Petroleum Engineers Digital Edition: Tulsa, OK **2011**.

(4) Willhite, G.P., Seright, R.S. Polymer Flooding. Society of Petroleum Engineers Digital Edition: Tulsa, OK **2011**.

(5) Ambastha, A. Heavy Oil Recovery. Society of Petroleum Engineers Digital Edition: Tulsa, OK **2008**.

(6) Stoll, W.M., Shureqi, H., Finol, J., Oman, S.T. Oyemade, S., Kruijf, D., Wunnik, J., Oman, P.D. Arkesteijn, F. Bouwmeester, R. et al. *SPE Reserv. Eng*. **2011**, 14, 702–712.

(7) Denney, D.*J. Pet. Technol*. **2010**, 62, 42–43.

(8) Zhang, H., Dong, M., Zhao, S. *Energ. Fuel*. **2010**, 24, 1829-1836.

(9) Ahmadi, M.A., Shadizadeh, S.R. *J. Pet. Sci. Eng.* **2013**, 110, 66–73.

(10) Stoll, W.M., al Shureqi, H., Finol, J., et al. *Soc. Petrol. Eng. Reserv. Eval. Eng.* **2011**, 14, 702-712.

(11) Karimi, M., Adelzadeh, M.R., Mohammadypour, M. *Egypt. J. Petro.* **2014**, 23, 175-182.

(12) Kryachko, Y., Voordouw, G. *Int. Biodeterior Biodegradation*. **2014**, 96, 135-143.

(13) Khishvand, M., Akbarabadi, M., Piri, M., *Adv. Water Resour.* **2016**, 94, 379-399.

(14) Zhang, H., Dong, M., Zhao, S. *Energ. Fuel*. **2010**, 24, 1829-1836.

(15) McPhee, C., Reed, J., Zubizarreta, I. *Core analysis: a best practice guide*. Amsterdam: Elsevier. **2015**

(16) Yerabolu, R.; Kotha, R. R.; Niyonsaba, E.; Dong, X.; Manheim, J. M.; Kong, J.; Riedeman, J. S.; Romanczyk, M.; Johnston, T. *Fuel.* **2018**, *234*, 492–501.

(17) Hendraningrat, L., Torsæter, O. *Energ. Fuel*. **2014**, 28, 6228-6241.

(18) Akhlaghinia, M., Torabi, F., Chan, C.W. *Energ. Fuel.* **2013**, 27, 1185-1193.

CHAPTER 6. MONITORING OILS' VOLATILE COMPOUND COMPOSITIONS DURING CHEMICALLY ENHANCED OIL RECOVERY FORMULATION TESTING ON BEREA ROCKCORES BY USING TWO-DIMENSIONAL GAS-CHROMATOGRAPHY WITH FLAME IONIZATION DETECTION (GC×GC-FID)

6.1 Abstract

Due to growing energy demands and the unique oil characteristics in waterflooded oil wells, enhanced oil recovery (EOR) techniques are becoming a more viable option to recover more oil. One such EOR method is chemically enhanced oil recovery (cEOR), in which a chemical formulation is pumped into an oil well to increase recovery. To determine if a cEOR formulation will lead to greater oil recovery, laboratory coreflood (CF) tests are conducted to model recovery expected at an oil reservoir, by measuring the volume of oil recovered from CF tests. However, monitoring the difference in chemical compositions of oils recovered from CF devices could better our understanding of how a given cEOR formulation mobilizes different oil compounds from a rockcore. It is also unknown if the chemical composition of the recovered oil changes as the CF recovery continues. It is theorized that the smaller molecules will be recovered first followed by larger molecules as the cEOR formulation is employed. Thus, this study monitored the volume of an oil distillate (boiling point less than 300 °C) recovered throughout the CF testing process of two cEOR formulations, as well as the mass percentage (wt %) of molecules in the recovered oil distillate. The weight percentages of the molecules in the distillate were determined by using a comprehensive two-dimensional gas chromatograph for separation, followed by flame ionization detection (GC×GC-FID). Principal component analysis (PCA) was used to characterize possible differences between the recovered oil distillate samples in an unsupervised manner. It was determined that cEOR formulation one recovered less volume of the oil distillate overall, but the formulation mobilized larger molecules from the rockcore for collection and analysis. Intriguingly, the volume of oil recovered by using formulation two was larger than that recovered by using formulation one, and the chemical composition of the oil distillate contained more small molecules. These results imply that cEOR formulations affect not only the volume of oil recovered but also the chemical composition of the oil recovered from CF testing. Additionally, as the CF progressed, larger molecules were recovered from the rockcore. This work presents a new method for assessing

the effectiveness of a given cEOR formulation, leading to a greater ability to rationally design such formulations.

6.2 Introduction

Traditionally, crude oil has been recovered by using either the natural pressure of the reservoir (referred to as primary recovery) and by injecting water or gas to displace more oil (secondary recovery).[1] However, these methods are ill-suited to recover oil components that bind to rocks and stick in small pore throats: primary and secondary flooding generally result in an average recovery of only 20-40% of the original oil in place (OOIP).[1] Thus, enhanced oil recovery (EOR) approaches, or tertiary recovery methods, have been developed to better recover the remaining oil. One such tertiary approach is chemically enhanced oil recovery (cEOR), which uses a mixture of chemicals to improve the volume of recovered oil.[2-7] It has previously been reported that most of the world's oil production wells are mature,[8] meaning they contain a high percentage of residual, difficult to recover oil. Thus, it is imperative that rational methods for improving cEOR formulations are developed to better recover the remaining oil present in these wells.

At present, little is known about the chemical compositions of oils recovered using different cEOR formulations. One study related to this idea compared the chemical compositions of oil recovered from one well using a cEOR technique to oil recovered from a control well, not subjected to any EOR treatment. The oil wells were located in the Komi Republic, Russia, and contained high viscosity oils with a considerable amount of resins and asphaltenes.[9] It was determined that the oil recovered from the well subjected to the cEOR contained a higher concentration of cyclic compounds, aromatic compounds, resins, asphaltenes, and saturated hydrocarbons compared to the control well. The study, however, compared only the change in oil composition recovered by using cEOR to a control. Thus, it would be advantageous to monitor the differences in the oil recovered by different cEOR treatments containing different surfactant(s) and polymer(s). Additional research has also been reported that evaluated the microemulsion phase behavior of 685 microemulsion experiments with 24 different crude oils, 85 surfactants, and 18 co-solvents to develop and validate a model for predicting the optimal salinity and solubilization ratio to recover a specific API gravity oil using one of the surfactants studied.[10] This work provided a guide for identifying a microemulsion with the lowest interfacial tension for specific oil and well temperature. This is an impressive step towards better understanding how the structures of co-

solvents and surfactants affect phase behavior pertinent to cEOR, but Chang et al. (2019) did not investigate the chemical characteristics of the oil solubilized in their work nor any rock models. Monitoring the chemical composition of oil recovered by various cEOR techniques could help develop a better understanding of how different chemical classes in oils are mobilized, and lead to the design of better chemical formulations to use for cEOR, and thus enhance the volume of oil recovered.

Currently, developing a successful cEOR formulation takes a considerable amount of time and research. A potential cEOR formulation is evaluated in a laboratory first by microemulsion testing and then by monitoring the volume of oil recovered during coreflood (CF) tests.[5] In a CF test, a sample rockcore from a reservoir, or a representative model rockcore, is saturated with reservoir oil and flushed with a brine solution. This is followed by flushing with a potential cEOR formulation, which can consist of either a single solution injection, or multiple injections of various solutions containing any number or combination of surfactants, polymers, brines of various salinities, and pHs. The volume of oil recovered is then determined and used to evaluate the efficiency of oil recovery for that cEOR formulation. However, the recovered oil's chemical composition is not traditionally monitored during this process. As a result, little is known about how different cEOR formulations affect mobilization of different components of crude oil. Additionally, the oil's composition is not monitored during CF testing; thus, it is unknown whether the recovered oil's composition is different at different stages of CF testing. Because oil performance is related to its chemical composition, changes in oil composition during cEOR flooding could have a significant impact on both the performance and economic value of the recovered oil. Understanding which chemical classes of oil are either mobilized or remain in a rockcore during each step cEOR CF testing may help to develop a better understanding of how different cEOR formulations mobilize oil, and thus how to better recover residual crude oil from waterflooded reservoirs.

This research determined the mass percentage of volatile components ranging from C_6 to C_{31} present in a crude oil distillate (boiling point less than 300 °C). The oil distillate underwent CF testing and was subjected to two different cEOR formulations, and thus, comparison between the recovery capabilities of these two formulations were made. This carbon range was monitored as the most profitable fraction of crude oil contains hydrocarbons with approximately 6-28 carbon atoms. This fraction is most the most profitable as it is readily converted to finished fuel products.

For example, a carbon atom range of approximately C_6 to C_{12} is utilized in gasoline, a range of approximately C_8 to C_{18} is used for jet fuels, and diesel fuel is composed of a range of approximately C_{10} to C_{28}.[11] Recovered oil distillate was sampled throughout the two CF testing, and then the weight percentage of the volatile components in the recovered oil distillate samples was determined by two-dimensional gas chromatography with flame ionization detection (GC×GC-FID). It was determined that cEOR formulation two recovered a greater volume of oil and also recovered smaller hydrocarbons overall; however, both cEOR formulations released larger molecules as the CF experiments progressed.

6.3 Experimental

6.3.1 Materials

A brine solution was used in both cEOR CF tests to mimic secondary flooding. The brine solution was an aqueous solution containing sodium chloride (NaCl), potassium chloride (KCl), manganese chloride tetrahydrate ($MnCl_2 \bullet 4H_2O$), magnesium chloride hexahydrate ($MgCl_2 \bullet 6H_2O$), barium chloride dihydrate ($BaCl_2 \bullet 2H_2O$), sodium sulfate decahydrate ($Na_2SO_4 \bullet 10H_2O$), sodium bicarbonate ($NaHCO_3$), and calcium chloride dihydrate ($CaCl_2 \bullet 2H_2O$) (Fisher Scientific: Hampton, NH) at a total mass fraction of 9,400 ppm. This brine mimicked production water from an oil well in the Illinois basin where the crude oil used in this research was also recovered from.

The crude oil used in this investigation was previously characterized and had an API gravity of 32°, a density of 0.87 g/cm^3, and a viscosity of 12.28 cP (determined at 20 °C).[12] The crude oil was filtered through a 0.5 μm steel inline filter (Swagelok) before distillation. Distillation was performed to recover the light fraction of the crude oil, boiling point less than 300 °C. Distillation followed the American Standard Testing Method (ASTM) D86 standard for distillation.[13] A total of 300 mL of crude oil was distilled to recover approximately 200 mL of oil distillate to be utilized in the CF tests. The crude oil sample was prepared and distilled in this manner because the gas chromatography (GC) columns used for analyzing the oil composition during the CF tests was limited in temperature capacity (350 °C maximum temperature). Therefore, a distillation temperature of 300 °C was chosen to ensure all molecules would successfully elute from the GC columns for detection and quantification analysis. Specifics of the instrument and GC columns are listed in Section 6.3.2.1.

Both tests utilized a commercial test rockcore, Berea rockcore, which had a diameter of 1" and a cut length of 6" (Cleveland Quarries; Vermilion, OH). The received Berea rockcore was 12" in length, which was then cut in half, to the appropriate 6" length for each miniature CF device (Section 6.3.2), one-half for each cEOR formulation test. Table 6.1 lists the characteristics of the rockcore.

Table 6.1. Rockcore characteristics of the Berea rockcores used in this research.

Characteristic	Value
Diameter	1"
Length	Cut to 6"
Average dry mass	145.19 ± 2.28 g (measured)
Average nitrogen permeability	714.29 ± 7.67 mD (measured)
Porosity	20-22% (from manufacturer)
Average pore volume	16.75 ± 0.11 mL (measured)
Average volume of original oil in place (OOIP)	10.3 ± 0.3 mL (measured)

6.3.1.1 Test One: Testing of Formulation One, Polymer 3230 and Surfactants S13-D, A-6, and L4-2

cEOR formulation one involved a two-step process; first, a surfactant/polymer solution was injected followed by a polymer solution injection. For step one, the polymer/surfactant solution was created using surfactants Petrostep S13-D (Stepan Company), Petrostep A-6 (Stepan Company), and L4-2 (Huntsman Corporation) (0.63 g, 0.26 g, and 0.15 g respectively) added to a 100 mL volume of the polymer solution of FLOPAAM SNF-3230S (3230 for short) at 0.33 wt % in brine. For step two, a polymer solution composed of polymer 3230 (0.33 wt %, SNF Holding Company) in brine was used. Petrostep S13-D is an ether sulfate surfactant made by reacting tridecanol (13 carbons) with an average of 13 molar equivalents of propylene oxide followed by sulfating the resulting propoxylated alcohol.[14] This resulted in an average chemical formula of C_{13}-13PO-SO_4^- with a molecular weight of 1,056 daltons.[15] Petrostep A-6 is a 16-18 carbon branched alkyl xylene sulfonate.[16] Huntsman L4-2 is a nonionic co-surfactant that is a linear alcohol ethoxylate and acts to increase the salt and water hardness tolerance of the surfactants in the brine solution.[17] Lastly, the 3230 polymer is a copolymer and has an estimated molecular weight of 6-8 million daltons with a 30-mole percent degree of hydrolysis.[18] A copolymer is created when an acrylamide and acrylic acid are polymerized together to produce a polymer with a narrow

distribution of anionicity.[19] A miniature CF device was used to complete this CF test, which is described in the methods Section 6.3.2.

6.3.1.2 Test Two: Testing of Formulation Two, Polymer 3330 and Surfactant S13-C

cEOR formulation two was completed on the same miniature CF device as test one (Section 6.3.2). cEOR formulation two also used a two-step process: a surfactant/polymer solution was first injected followed by a polymer solution injection. Step one utilized a solution of Petrostep surfactant S13-C (0.97 g, Stepan Company) was added to a 100 mL volume of the polymer solution of FLOPAAM SNF-3330S (3330 for short) at 0.35 wt % in brine. This was followed by the second step which was a solution of brine with polymer 3330 (0.35 wt %). Petrostep S13-D is an ether sulfate surfactant made by reacting tridecanol (13 carbons) with an average of 9 molar equivalents of propylene oxide followed by sulfating the resulting propoxylated alcohol.[20] This resulted in an average chemical formula of C_{13}-9PO-SO_4^- with a molecular weight of 824 daltons.[15] The 3330 polymer is a copolymer and has an estimated molecular weight of 8-10 million daltons with a 30-mole percent degree of hydrolysis.[18]

6.3.2 Methods

The CF tests utilized a miniaturized CF device that has been previously described in detail in Chapter 5 of this dissertation. CF tests performed using this device have been reported to result in recovery data with less than 6% deviation.[21] Briefly, the dried rockcore was saturated with brine under vacuum. Then, the miniature CF device was assembled and the rockcore was re-saturated with brine to ensure complete wetting of the rockcore. The oil distillate was then injected into the brine-saturated rockcore, and this oil-saturated rockcore was left to age for five days. The core was then flushed with brine in a process called the initial waterflood. This was conducted to mimic secondary flooding, as most oil wells in which a cEOR formulation is deployed have already undergone secondary flooding. The waterflood was followed by the injection of the one of the cEOR formulations: first a surfactant/polymer solution, followed by a polymer solution, and then an ending brine flush. The identity and concentration of each cEOR formulation solution can be found in the materials section 6.3.1. The oil distillate was collected for analysis at each stage of the cEOR formulation testing process, resulting in a total of six samples (Figure 6.1): the original

oil distillate, oil distillate that flowed through the rockcore during oil saturation, oil distillate recovered from the initial brine flush (initial waterflood recovery), oil distillate recovered from the surfactant/polymer flush, oil distillate recovered from the polymer flush, and oil distillate recovered from the ending brine flush (ending waterflood recovery). The recovered samples were centrifuged at 1,800 rpm for 45 minutes to break any emulsions and efficiently separate the brine and oil distillate. The oil distillates recovered from CF testing were then analyzed on a GC×GC-FID instrument.

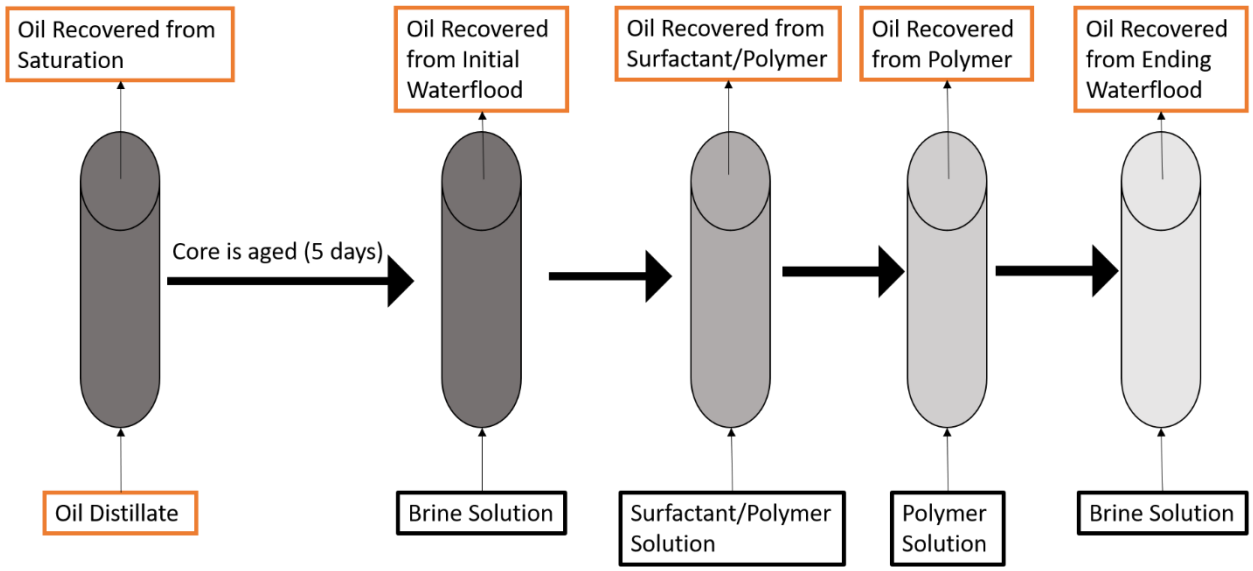

Figure 6.1. A graphic of the cEOR miniaturized-CF testing process. Each orange-highlighted box represents an oil distillate sample that was recovered for GC×GC-FID analysis, totaling six samples from each of the cEOR CF testing process.

6.3.2.1 Instrumentation Methods

The analysis of all oil distillate samples was performed by Dr. Petr Vozka using a comprehensive two-dimensional gas chromatograph with flame ionization detection (GC×GC-FID). The GC×GC-FID utilizes two orthogonal separation mechanisms to efficiently separate compounds with a wide range of boiling points and polarity, and is, therefore, a useful tool for analyzing complex mixtures such as oil.[22-27] An Agilent 7890B gas chromatograph was used with a non-moving quad-jet dual stage thermal modulator (LECO Corporation, Saint Joseph, MI). Cryo-cooled nitrogen gas was used for the cold jet modulation, heated nitrogen gas was used for the hot jet modulation, and

helium was used as the carrier gas during chromatographic separation. Relevant chromatographic conditions for the experiments performed on the GC×GC-FID are shown in Table 6.2. Data were processed by using ChromaTOF software version 4.71.0.0, which is optimized for GC×GC-FID. A 0.5 μL aliquot of neat sample was injected by using an Agilent 7683B series injector with an HP 7683 series autosampler.

The ChromaTOF software was also used for the classification of compounds eluting from the GC×GC. The classification used in this work was developed by following a previously published step-by-step procedure,[23] which involved the use of model compound mixtures to determine elution boundaries for each chemical class and carbon atom number. The classification considered in this research were the following hydrocarbon classes: *n*-alkane compounds, *iso*-alkane compounds, monocycloalkane compounds, dicycloalkane compounds, alkylbenzene compounds, cycloaromatic compounds (indans, tetralins, indenes, etc.), and alkylnaphthalene.

Quantitative analysis was completed in Excel, and the mass percentage of each group was determined by normalizing the peak area found from the integration of the GC×GC chromatogram peaks. Only peaks with a peak area percentage greater than 0.01 % were considered for further analysis. Peaks with lower peak area percentages were designated as noise and not considered for analysis. The response factors of all hydrocarbons are approximately the same (1.00 ± 0.05), meaning that the FID detector produces a signal proportional to an analyte's mass percent in that sample.[28] Therefore, based on the known hydrocarbon response factors, the response factor was set to one for data processing, and direct quantification of the mass percent (wt %) of all compounds in the distillate oil samples could be performed. This quantification was used to compare differences in each oil distillate sample and not as an absolute quantification, which would require the use of standards and a dopant.

Table 6.2. Experimental conditions of GC×GC-FID analysis.

Columns	Primary: DB-17MS (30 m × 0.25 mm × 0.25 µm) Secondary: DB-1MS (0.8 m × 0.25 mm × 0.25 µm)
Injection	0.5 µL split 30:1, inlet temperature 280 °C
Oven program	40-260 °C, rate 3 °C/min
Mobile gas	UHP Helium, 1.5 mL/min
Offsets	secondary oven 50 °C, modulator 15 °C
Modulation	2.5 s, hot pulse 0.42 s
Detector	FID, 300 °C, 200 Hz

6.3.2.2 Principal Component Analysis (PCA)

Principal component analysis (PCA) is a well-established method for data analysis.[29-33] PCA was applied to determine whether the chemical composition of molecules changed during CF testing. The analytes' weight percentages in the original oil distillate sample and the recovered oil distillate samples were input into the PCA software (Unscrambler multivariate analysis software by CAMO) in an unsupervised, simultaneous analysis of the data sets. PCA is a multivariable technique used to reduce the number of variables to a smaller set of orthogonal factors to display the correlation factors existing among the original variables. This allows the differences in large data sets to be more easily visualized. The first principal component (PC-1) describes the most dominant trend separating the data sets and the other principal components (PC-2, PC-3, PC-4, etc.) describe additional orthogonal trends in decreasing importance. Therefore, the sources of variation in the data sets are compressed down into a few PCs. The explained variance score of a PC shows how well that PC accounts for the differences in the data set, a large percentage indicated that PC accounts for a larger factor separating the data sets. Loading scores also indicate how much each of the original variables is influencing the direction of the PC. The loading score is determined by the cosine of the angle between the vector of the original variable and the PC vector, the closer the value is to one, the more that variable is influencing that PC. Each variable in this data set was given equal weight except for the molecular weight which was weighted to one divided by the standard deviation of that data set.

6.4 Results

6.4.1 CF Test: Oil Volume Recovery

Test one used cEOR formulation one: polymer 3230 with surfactants S13-D, A-6, and L4-2. Overall 92% of the oil distillate was recovered (including the volumes recovered from every step of the CF testing), while the cEOR formulation recovered 47% of the total volume (the volume of oil recovered by the surfactant/polymer flush, polymer flush, and the ending waterflood). Test two used cEOR formulation two: polymer 3330 with surfactant S13-C to complete a laboratory CF test. Overall 99% of the oil distillate was recovered (including the volumes recovered from every step of the CF testing), while the cEOR formulation recovered 58% of the total volume (the volume of oil recovered by the surfactant/polymer flush, polymer flush, and the ending waterflood). Table 6.3 includes the volume of oil distillate recovered during each step of the CF process. The volume of oil distillate was determined by visual measurements in a conical tube marked at every 0.1 mL. Therefore, an inherent error may occur across the measurements but there is no way to accurately quantify that error although it should be less than 0.1 mL for each measurement. Figure 6.2 displays the percentage of oil recovered as a percentage of the original oil in place (OOIP) for each formulation test. Given the data in Table 6.3 and Figure 6.2, formulation two was more successful at recovering a larger volume of the oil distillate from the rockcore.

Table 6.3. Oil distillate recovery volumes for each cEOR formulation CF test.

Step of CF test	**Oil distillation volume recovery (mL) for cEOR formulation 1: polymer 3230 and surfactant S13-D, A-6, and L4-2**	**Oil distillation volume recovery (mL) for cEOR formulation 2: polymer 3330 and surfactant S13-C**
Initial waterflood (IWF)	4.5	4.3
Surfactant and polymer flood (SP)	1.1	0.7
Polymer flood (P)	2.8	2.5
Ending waterflood (EWF)	0.9	2.9

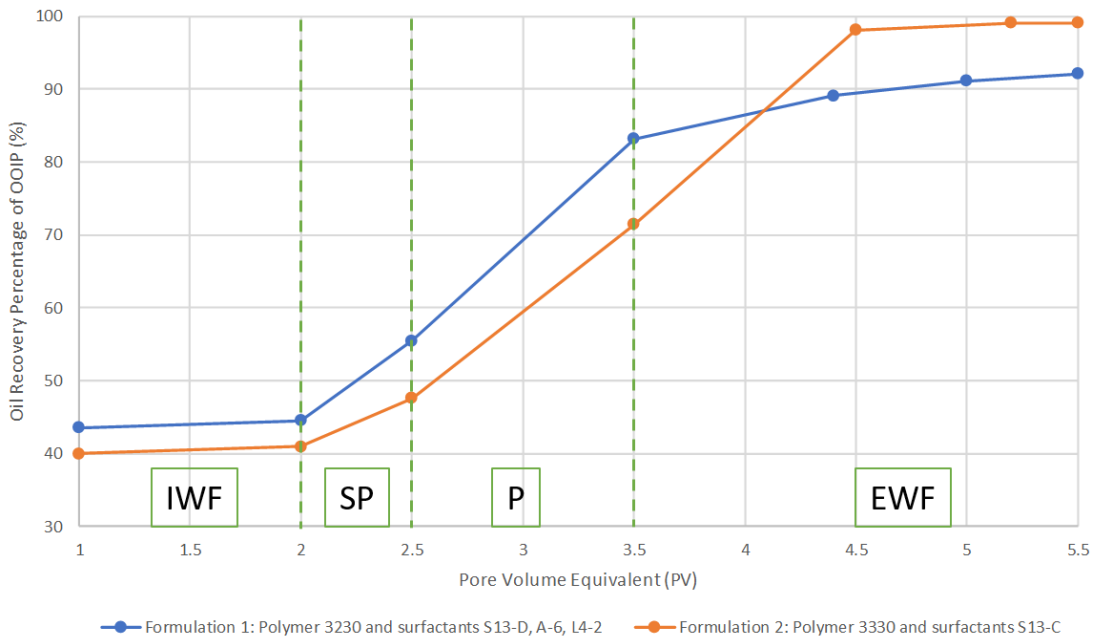

Figure 6.2. Oil recovered for each formulation as a function of the percentage of original oil in place (OOIP) and pore volume (PV) equivalents injected. Green dashed lines represent different CF steps: initial waterflood (IWF), surfactant and polymer flood (SP), polymer flood (P), and ending waterflood (EWF). Formulation two recovered more oil overall but does not surpass the oil volume recovered over formulation one until the EWF injection.

6.4.2 GC×GC-FID Analysis

Each oil distillate sample was measured twice on the GC×GC-FID to ensure reproducible data collection. These data were collected by Dr. Petr Vozka. A wide range of carbon numbers was monitored for each chemical class observed in the oil distillate samples. Table 6.4 lists the carbon number ranges monitored for each chemical class. Additionally, Figure 6.3 displays the resulting chromatogram from GC×GC-FID analysis of the original oil distillate. Each sample of recovered oil distillate was also measured in this manner, and the resulting chromatographic peaks were distributed into chemical classes as shown in Figure 6.3.

Table 6.4. The carbon atom range observed for each oil distillate sample in the GC×GC-FID.

Chemical class	**Carbon atom number range**
n-alkane compounds	7-30
iso-alkane compounds	7-31
monocycloalkane compounds	6-26
dicycloalkane compounds	8-25
tricycloalkane compounds	10-17
alkylbenzene compounds	6-24
cycloaromatic compounds (indans, tetralins, indenes, etc.)	9-21
alkylnaphthalene	10-20

The area of each chromatographic peak was then utilized to calculate the mass percentage of that given compound in the sample. This was completed by comparing the peak area of each compound to the total peak area of the entire sample. For example, in the original oil distillate, the *n*-alkane with seven carbons accounted for 4% of the peak area of the entire sample. This would then translate to *n*-alkane C7 being 4 wt% in the sample. The weight percentage of each compound in the sample was determined in this manner. This resulted in over 100 chemical composition data points for of each sample. Therefore, the resulting data set of all analyzed samples was too large to find meaningful differences using human lead analysis and statistics alone. Therefore, unsupervised PCA was completed on the entire data set for both cEOR formulations to determine statistically meaningful differences between the chemical compositions of the oil distillate samples. This will be discussed in the next section 6.4.3, PCA results.

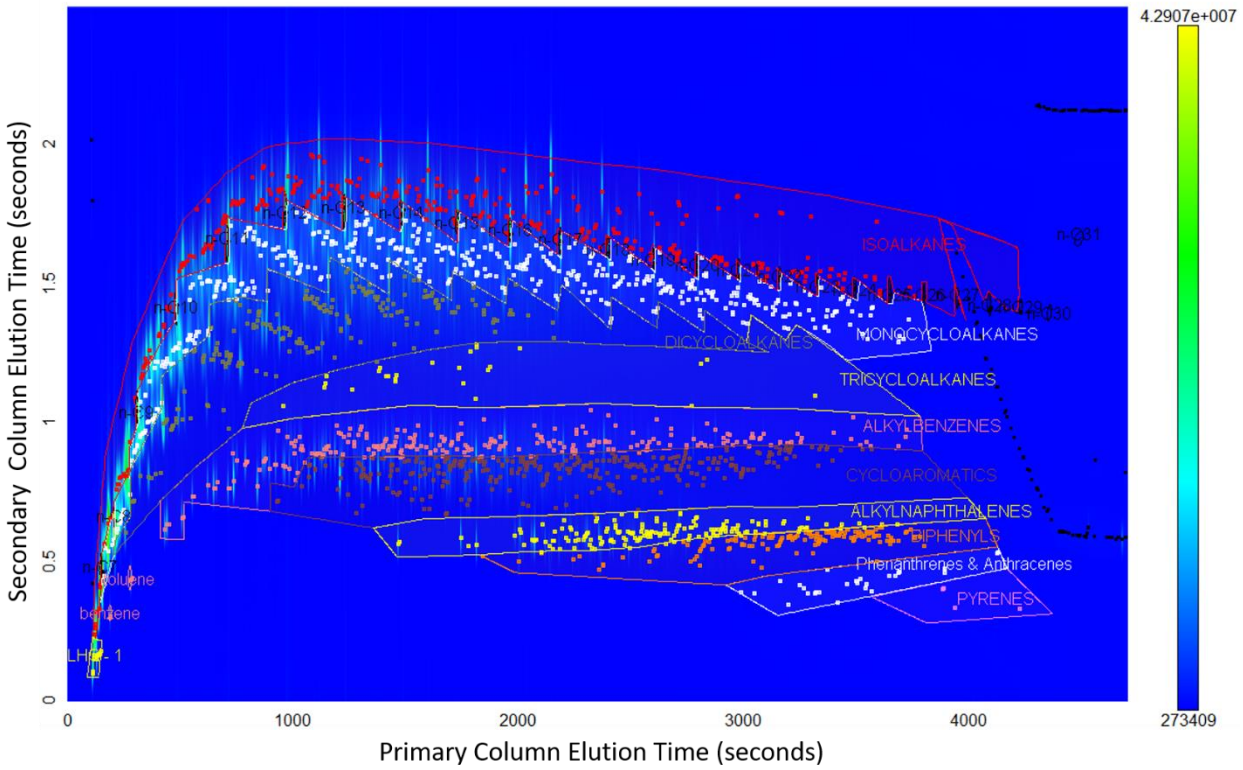

Figure 6.3. A chromatogram of the original oil distillate. The chromatogram has three dimensions of information: the elution times of the primary and secondary GC columns, as well as abundance or signal intensity (z-axis represented by heat mapping colors noted on the right-hand side scale). Each chemical class is marked and color-coded. The apex of each elution peak is marked with a colored dot. The *n*-alkanes are marked in black with the associated carbon numbers, *iso*-alkanes are red, monocycloalkanes are white, dicycloalkanes are green, tricycloalkanes are light green, alkylbenzenes are peach, cycloalkanes are maroon, alkylnaphthalenes are yellow, biphenyls are orange, phenanthrenes and anthracenes are off-white, and pyrenes are light purple.

6.4.3 PCA results

The duplicate GC×GC-FID analysis data of the determined weight percentages of each chemical compound in each of the samples was utilized to calibrate the PCA with cross-validation completed by the computer program via random data selection. Each sample was grouped according to the cEOR formulation as well as the step in the CF process in which the oil distillate was recovered, including the original oil distillate. Figure 6.4 shows the resulting PCA plot with principal component one (PC-1) accounting for 98% of the explained variance in the data set and PC-2 accounting for another 1% of data variance. The resulting PCA plot, therefore, explains 99% of the variance across the entire data set. This is a promising result as the less PCs that are needed

to differentiate most of the data set, the more robust the model is. In figure 6.4, as the coreflood collection timepoints progress, the data points trend from right to left on the PC-1 component with the exception of the surfactant/polymer recovery being to the left of the polymer recovery in each formulation test. Additionally, the ending waterflood recovery of formulation two is also to the right of the polymer flood recovery.

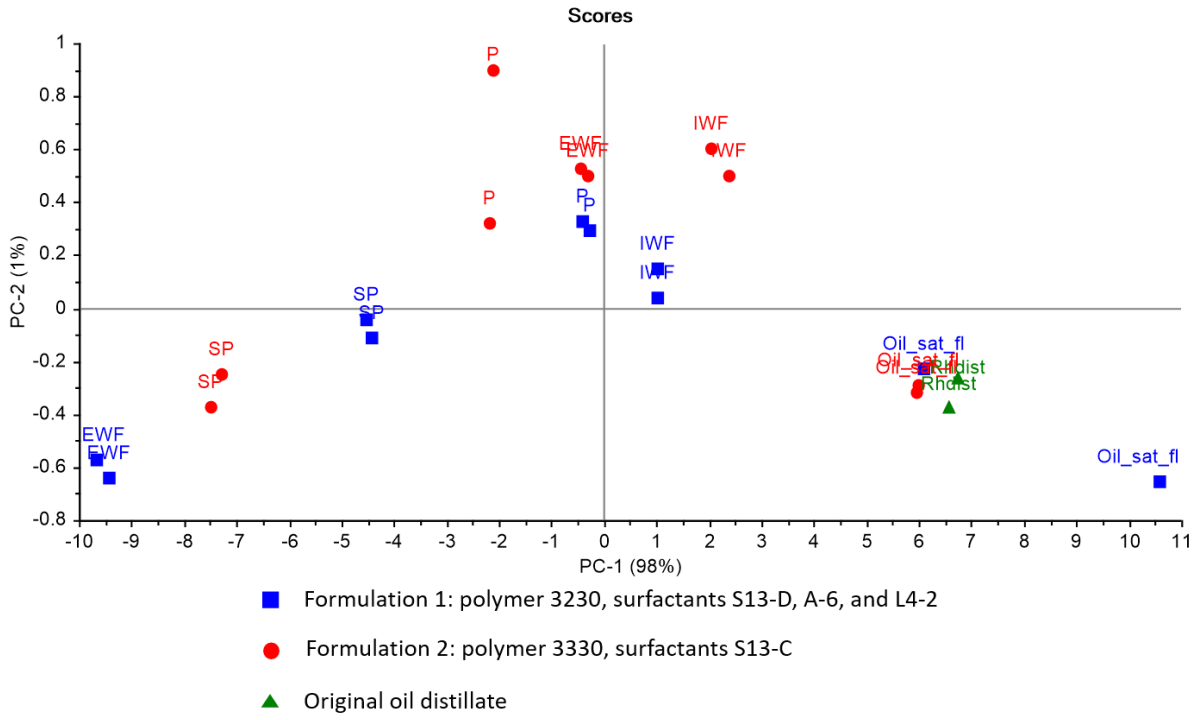

Figure 6.4. PCA plot of the entire oil distillate data set. Each sample was grouped according to the cEOR formulation as well as the step in the CF process in which the oil distillate was recovered, including the original oil distillate. PC-1 accounts for 98% of the explained variance in the data set and PC-2 accounts for another 1% of data variance.

The correlation loading for each data component (chemical class and carbon number) illustrates how much of an influence each data component has on that PC. The closer a data component's correlation loading value is to one, the more of an influence that value has on that component (Figure 6.5). Data components inside the 50% circle have little to no influence on that component and data components clustered together are highly correlated variables while data components on opposite sides of the correlations loadings plot are anti-correlated variables (Figure 6.5).

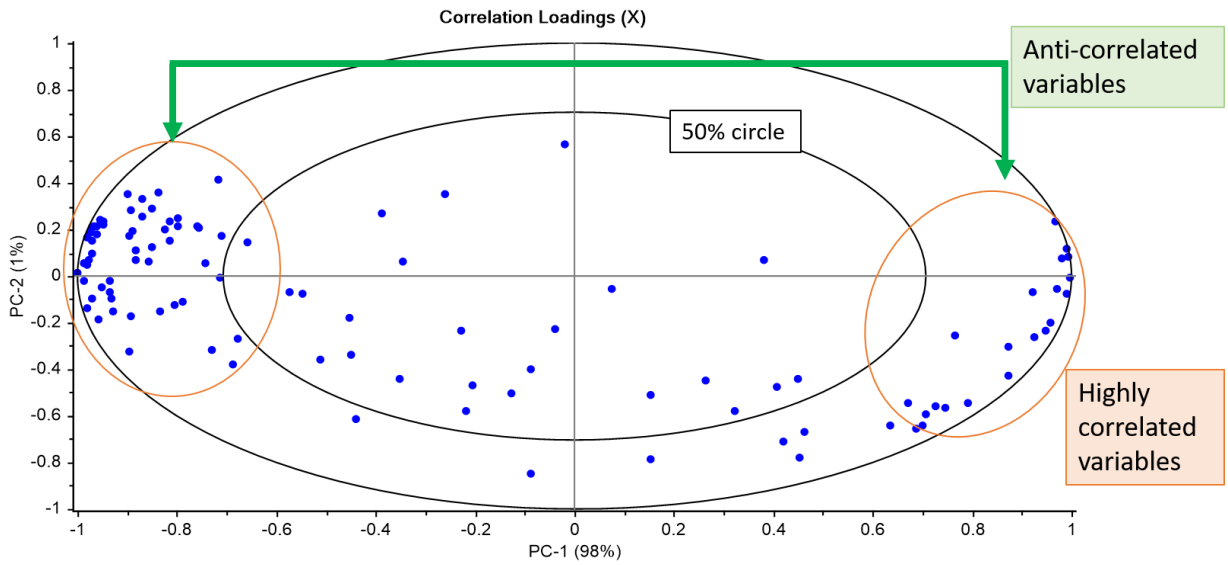

Figure 6.5. Correlation loadings plot of each data component (X) used to define each PC. The closer a data component's correlation loading value is to one, the more of an influence that value has on that component. There are two clusters of highly correlated variables that define the PC-1.

The data components in the correlation loadings plot can be broken down into categories to determine what is influencing PC-1, which accounts for the most significant variance between the datasets. The most significant factor influencing the data spread across PC-1 was the size of the molecules, with smaller molecules being in the far right quadrant and larger molecules being in the far left quadrant, and medium-sized molecules were somewhere in between (Figure 6.6). If a smaller subset of molecule sizes are focused on, carbons 6-10 and 15+ (Figure 6.7), one can see how the smallest molecules are furthest to the right of the loading plot and the largest are furthest to the left. As the carbon size increases, the data point in the loading plot moves from right to left. This is important to note because the characterization dictating the location (quadrant) of the loading plot is the same as the PCA plot quadrant characteristic. Such that a data point that lies to the right in the PCA plot would be a data point that has the most, small molecules in that sample; and as the data point in the PCA plot moves toward the left, the sample would then have more large molecules in it. Additionally, some molecules of intermediate size, carbon 16 (Figure 6.7) for example, extend to both sides of the correlations loadings plot. In this instance, molecular shape has an influence on where in the plot the different molecules are located, although no trend was determined overall for chemical class or shape because GC×GC-FID cannot determine chemical

structures. In the case of 16 carbon atom molecules, as the molecule has an increased collisional cross section it appears to shift on the loadings plot from right to left. General structures of carbon 16 atoms are shown in Figure 6.7 to demonstrate this relationship. Therefore, it appears molecules of both a smaller carbon number and smaller collisional cross section trend to the right on the PCA plot while larger carbon number and larger collisional cross section molecules trend to the left of the PCA plot.

As PC-2 only accounts for 1% spread in the data, defining a clear trend for the small data set is difficult. It appears to be somewhat connected to the shape of the molecule, with alkanes on the upper portion of the plot and cyclic and aromatic compounds in the lower portion of the plot. However, with the small sample set that trend is not clearly defined.

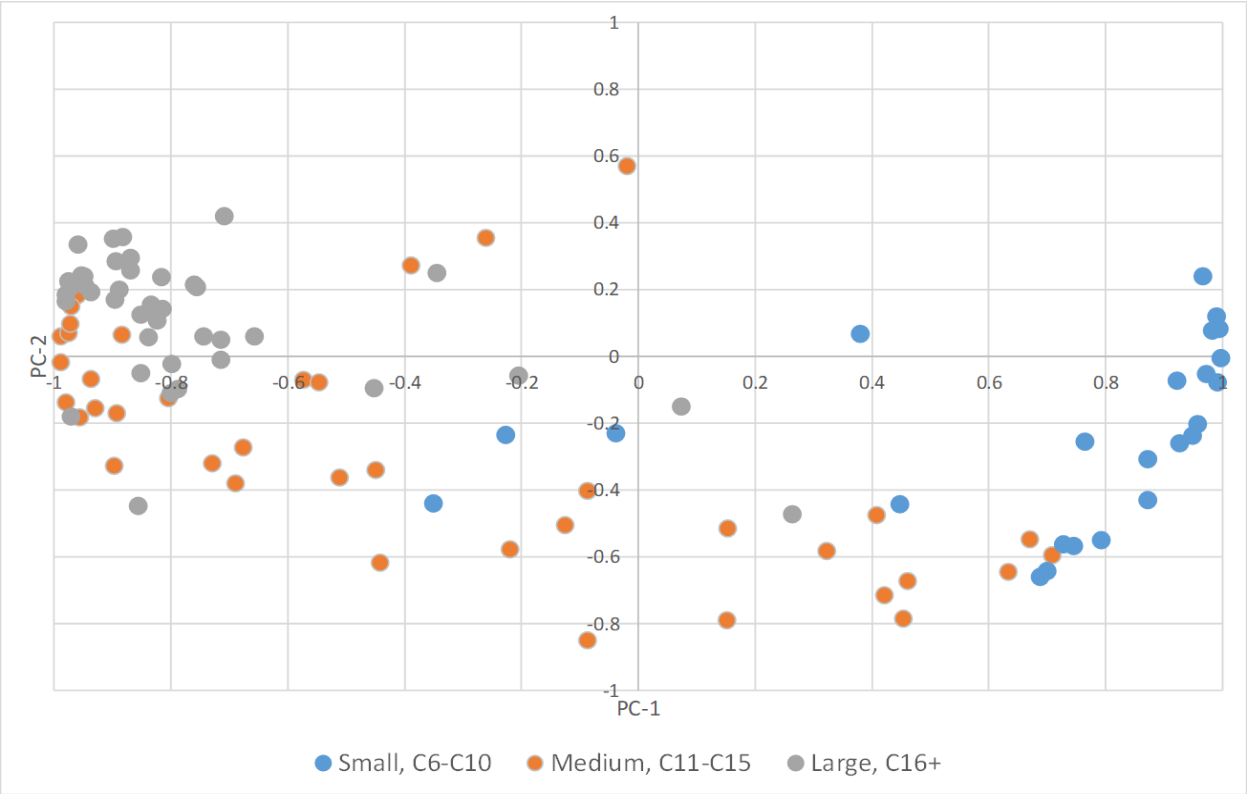

Figure 6.6. Correlation loading values categorized according to molecular size: small molecules have carbon numbers 6-10, medium molecules have carbon numbers 11-15, and large molecules have carbon numbers greater than 16.

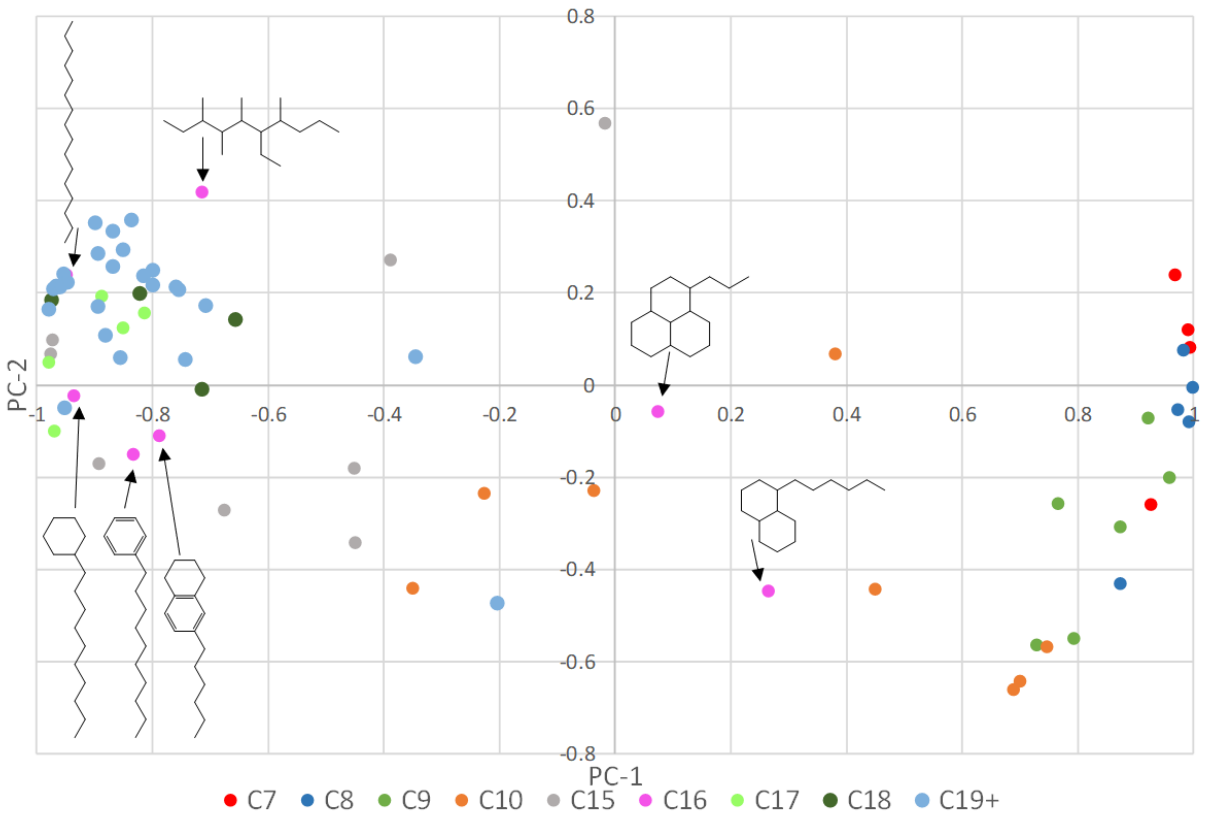

Figure 6.7. Correlation loading values categorized according to molecular size: small carbon numbers 6-9 can be seen to the right of the plotting area and large carbon numbers greater than 17 are on the left side. Note carbon numbers 11-14 are not shown here for simplicity but are included in Figure 6.6. General structures of carbon 16 molecules are displayed to expression how collisional cross section may also play a role in PC-1. GC×GC-FID is not capable of determining chemical structures, these are general, proposed structures based on the compound's determined chemical class.

By examining the PCA plot (Figure 6.4) with the new trend of the correlation loadings plot in mind, one can observe that as the CF test progressed, the oil distillate that was recovered contained more, larger molecules in the sample. Notably, cEOR formulation 1, polymer 3230 and surfactant S13-D, A-6, and L4-2, ending waterflood released more, larger molecules than cEOR formulation 2, polymer 3330 and surfactant S13-C. Additionally, both cEOR formulations released larger molecules compared to the original oil distillate, the oil distillate from saturating the rockcore, and the initial waterflood. This can be observed as oil distillate samples collected from each step of the cEOR process, SP, P, and EWF, contained larger molecules than the other oil distillate samples. It is also important to note that although the SP flood occurred prior to the P flood, the SP flood released larger molecules than the P flood in both cEOR formulation tests

(Figure 6.4). Therefore, the chemical composition of the flood influences the size of molecules eluting from the rockcore and it is not that the more pore volumes injected released larger carbon compounds. Formulation two, which contained the larger molecular weight polymer, released larger molecules during the SP and P flood compared to formulation one. Finally, there was no observable trend or significant contribution to the variance of the data set between the types of hydrocarbon classes monitored throughout this study.

6.5 Conclusions and Future Work

The chemical composition of an oil distillate sample was monitored during recovery from two different cEOR formulation tests using a miniature laboratory CF testing techniques. The oil distillate recovered by the two different cEOR formulations resulted in different compositions of larger or smaller compounds throughout the CF testing process. It was also noted for some chemical compounds, collisional cross section also contributed to when compounds were recovered during the CF experiment. From this research, it can be observed that different cEOR formulations not only recover different volumes of oil but also oil of different chemical compositions at different time points during a CF experiment. It would, therefore, be advantageous to monitor the chemical composition of oil during additional CF tests of various cEOR formulations as well as different oils. This could lead to a better understanding of how the chemical structure of surfactants and polymers facilitate the recovery of different chemical classes in crude oils from rockcore surfaces. A manuscript on this work is currently in preparation.

The miniature coreflood system paired with GC×GC-FID analysis could be used to develop a model to better understand how the chemical properties of surfactants and polymers influence the chemical composition of oil released from a rockcore. Using this system would allow high-throughput (three formulations can be tested in 9 days using the miniature device and provide comparable results to traditional CF testing), high-resolution data to be collected. This could then be paired with the chemical structure of surfactants and polymers, tested in a systematic fashion, to see if different carbon chain lengths or functional groups influenced the chemical composition of oil recovered from rockcores. Another variable to be considered could also be oil type and different crude oils, composed of various chemical compositions, could also be explored to better understand the role of surfactant and polymer structures in the success of cEOR. Additionally, to determine a stronger correlation between molecular structure and elution, mass spectrometry

experiments could also be paired with this experimental review to better determine the structure of different compounds eluting at different times during the CF instead of the overall larger chemical classes that were used in this experimental procedure. This would help elucidate the relationship between collisional cross section and time of elution in the CF experiment eluded to in this initial research.

6.6 References

(1) Muggeridge, A., Cockin, A., Webb, K., Frampton, H., Collins, I., Moulds, T., Salino, P. *Trans. R. Soc. A.* **2012**, 372, 1–25.

(2) Green, D.W., Hirasaki, G., Pope, G.A., Willhite, G.P. Surfactant Flooding. Society of Petroleum Engineers Digital Edition: Tulsa, OK **2011**.

(3) Willhite, G.P., Seright, R.S. Polymer Flooding. Society of Petroleum Engineers Digital Edition: Tulsa, OK **2011**.

(4) Ambastha, A. Heavy Oil Recovery. Society of Petroleum Engineers Digital Edition: Tulsa, OK **2008**.

(5) Stoll, W.M., Shureqi, H., Finol, J., Oman, S.T. Oyemade, S., Kruijf, D., Wunnik, J., Oman, P.D. Arkesteijn, F. Bouwmeester, R. et al. *SPE Reserv. Eng*. **2011**, 14, 702–712.

(6) Denney, D. *J. Pet. Technol*. **2010**, 62, 42–43.

(7) Zhang, H., Dong, M., Zhao, S. *Energ. Fuel*. **2010**, 24, 1829-1836.

(8) Ahmadi, M.A., Shadizadeh, S.R. *J. Pet. Sci. Eng.* **2013**, 110, 66–73.

(9) Sherstyuk, S.N., Serebrennikova, O.V., Stakhina, L.D., Kadichagov, P.B. *Journal of Siberian Federal University* **2010**, 3, 110-119.

(10) Chang, L., Pope, G.A., Jang, S.H., Tagavifar, M. *Fuel* **2019**, 237, 494-514.

(11) Caslab.com. Petroleum Hydrocarbon Ranges. [online] Available at: http://www.caslab.com/Petroleum-Hydrocarbon-Ranges/ (2019).

(12) Yerabolu, R., Kotha, R.R., Niyonsaba, E., Dong, X., Manheim, J.M., Kong, J., Riedeman, J.S., Romanczyk, M., Johnston, C.T., Kilaz, G., Kenttämaa, H.I. Fuel. 2018, 234, 492–501.

(13) ASTM Standard D86, “Standard Test Method for Distillation of Petroleum Products and Liquid Fuels at Atmospheric Pressure,” ASTM International, West Conshohocken, PA, 2018, www.astm.org.

(14) Stepan Company. Enhanced Oil Recovery Methods. WO 2017/176454 A1. World Intellectual Property Organization: International Bureau. October **2017**.

(15) Chang, L. Pope, G.A, Jang, S.H., Tagavifar, M. *Fuel.* **2019**, 237, 494-514.

(16) Gao, B. **2012** Development of a novel EOR surfactant and design of an alkaline/surfactant/polymer field pilot (PhD Thesis) The University of Texas at Austin. Austin, Tx USA.

(17) Huntsman Corporation. (**2010**). Technical Bulletin: Products for Enhanced Oil Recovery. Woodlands, USA. Huntsman Petrochemical LLC.

(18) Randall Scott Seright. (**2009***). First Annual Report: Use of Polymers to Recover Viscous Oil From Unconventional Reservoirs*. DOE Award No.:DE-NT0006555.

(19) SNF Floerger. (**2012**). *Enhancing Polymer Flooding Performance: 30 Years of Experience in EOR* [Brochure]. France: Altavia St. Etienne.

(20) Tipley, K.A. **2012** Development of ASP formulations for reactive crude oil in high clay, high temperature reservoirs (Master Thesis) The University of Texas at Austin. Austin, Tx USA.

(21) Wehde, K.E., Dong, X., Jiang, T., Hilger, R., Borgohain, R., Schultheiss, N.C., Kenttämaa, H.I. *J. Petrol. Sci. Eng.* **2019**. (Submitted).

(22) Vozka, P. Modereger, B.A., Park, A.C., Zhang, W.T.J., Trice, R.W., Kenttämaa, H. I., Kilaz, G. *Fuel*. **2019**, 235, 1052–1060.

(23) Vozka, P., Kilaz, G. *Fuel*. **2019**, 247, 368-377.

(24) Mao, D., Van De Weght, H., Diels, L., De Brucker, N., Lookman, R., Vanermen, G. *J. Chromatogr. A.* **2008**, 1179, 33-40.

(25) Kohl, A., Cochran, J., Cropek, D.M. *J. Chromatogr. A.* **2010**, 1217, 550-557.

(26) Chakravarthy, R., Acharya, C., Savalia, A., Naik, G. N., Das, A. K., Saravanan, C., Verma, A., Gudasi, K. B. *Energ. Fuel*. **2018**, 32, 3760–3774.

(27) Mao, D., Lookman, R., Weghe, H.V.D., Weltens, R., Vanermen, G., Brucker, N. D., Diels, L. *Chemosphere* **2009**, 77, 1508–1513.

(28) Gieleciak, R., Oro, N. A Study of FID Response Factor of GC×GC Systems for Hydrocarbon Compound Classes Existing in Diesel Fractions, CDEV-2013-1979-RT, CanmetENERGY: Devon, Alberta, Cananda, **2013**.

(29) Jolliffee, I.T. *Principal Component Analysis*, 2nd ed.; Springer-Verlag: New York, **2002**.

(30) Christensen, J.H., Hansen, A.B., Tomasi, G., Mortensen, J., Andersen, O. *Environ. Sci. Technol.* **2004**, 38, 2912-2918.

(31) Simpson, C.D., Mosi, A.A., Cullen, W.R., Reimer, K. *Sci. Total. Environ.* **1996**, 181, 265-278.

(32) Doong, R., Lin, Y. *Water Res.* **2004**, 38, 1733-1744.

(33) Aske, N., Kallevik, H., Sjöblom, J. *Energ Fuel.* **2001**, 15, 1304-1312.

VITA

Katherine Elisabeth Wehde was born in Illinois in October 1992. She naturally gravitated towards math and science with the support of her parents. Her father often included all the children in building projects, including designing and constructing a massive wooden fort in their backyard. Her mother allowed her to help at the dentistry office where she was able to develop oral x-rays by hand in a dark room. This, paired with the gift of travel, lead to her undying interest to learn how and why things worked. After taking her first chemistry class in high school, she knew that this was the subject she wanted to be her career. In the Fall of 2011, she started her college education at The Ohio State University (OSU) in Columbus, OH. She quickly joined Dr. J. Clay Harris's research group after telling him an awful dinosaur joke in class and was later co-mentored by Dr. Noel Paul who also put up with her humour. The pair mentored her through two projects at OSU including a gold reclamation project, in which gold was recovered and purified from old electronic parts, using more eco-friendly techniques than traditional industrial processes; as well as, the quantitation of drugs in animal tissue samples by HPLC/(ESI)TOF MS. The defence of the drug quantification by MS project lead to her graduation with research distinction and began her interest in MS and continuing her education. Additionally, her natural knack for organization and outgoing personality lead to her rise to managing director of the undergraduate analytical labs at OSU. In May 2015 she graduated with a Bachelor of Science in Chemistry, with Research Distinction in Analytical Chemistry, from OSU.

She then applied to the number one school for analytical chemistry, Purdue University. When making her decision about which graduate school to attend, Katherine was accepted to both the Chemistry Department at Purdue and the Purdue University Interdisciplinary Life Science (PULSe) Program, in which only 28 other people were accepted to that year. After careful consideration, she came to Purdue in the Fall of 2015 through the PULSe program where she then began laboratory rotations for her first year at graduate school. After rotating with four amazing professors, she decided to formally join Prof. Hilkka Kenttämaa´s group in Spring 2016. During her time in the research group, Katherine also taught a range of chemistry classes from general chemistry to first semester freshmen undergraduates to a graduate level MS course. For her exceptional teaching in the undergraduate general chemistry courses, Katherine was awarded the Arthur Kelly Teaching Award in Spring 2017. Katherine also completed an internship at Neste

Corporation in Porvoo, Finland during the Fall of 2018. Katherine began a promising career at Covance Clinical Laboratory Services in October 2019 as a study design lead. In December 2019, she was awarded a Doctor of Philosophy degree in Analytical Chemistry after four years as a graduate student and three years of successful analytical chemistry research at Purdue University.

PUBLICATIONS

1. Wehde, K.E.; Vozka, P.; Modereger, B.; Kilaz, G. ; Kenttämaa, H.I. Monitoring Crude Oil's Volatile Compound Composition during Chemically Enhanced Oil Recovery Formulation Testing on Berea Rockcores by using Two-Dimensional Gas Chromatography with Flame Ionization Detection (GC×GC-FID) *Fuel* (In preparation).

2. Ikonen, E. K.*; Wehde, K.E.*; Habeb, K.; Kenttämaa, H.I. Bias, Limit of Detection, and Limit of Quantitation for the ASTM D2425 Method Update in 2019. *Fuel*. **2019** (Accepted). (*Elias Ikonen and Katherine Wehde were co-authors and contributed equally to the research and writing)

3. Wehde, K.E.; Dong, X.; Jiang, T.; Hilgard, R.; Borgohain, R.; Kenttämaa, H.I. Validation of Benchtop Miniaturized Coreflood Devices for Parallel Prescreening of Candidate Formulations for Chemically Enhanced Oil Recovery. *J. Petrol. Sci. Eng.* **2019** (Submitted).

4. Niyonsaba, E.*; Wehde, K.E.*; Yerabolu, R.; Kilaz, G.; Kenttämaa, H.I. Characterization of Heavy, Medium, and Light API Gravity Crude Oils by Using the Distillation, Precipitation, Fractionation Mass Spectrometry (DPF MS) Method. *Fuel.* **2019**, 255. (*Edouard Niyonsaba and Katherine Wehde were co-authors and contributed equally to the research and writing)

5. Manheim, J.; Wehde, K.E.; Zhang, W.T.J.; Vozka, P.; Romanczyk, M.; Kilaz, G.; Kenttämaa, H.I. Identification and Quantitation of Linear Saturated Hydrocarbons in Lubricant Base Oils by Using APCI (O2, isooctane) LQIT and GC×GC/EI TOF Mass Spectrometry. *J. Am. Soc. Mass Spectrom.* **2019** (Accepted).

6. Romanczyk, M.; Velasco, J.R.; Xu, L.; Vozka, P.; Dissanayake, P.; Wehde, K.E.; Roe, N.; Keating, E.; Kilaz, G.; Trice, R.; Kenttämaa, H.I. The Capability of Different Organic Compounds to Swell Acrylonitrile Butadiene O-rings: Steric and Mechanical Properties. *Fuel* **2019**, 238, 483-492.

7. Luning Prak, D.J.; Romanczyk, M.; Wehde, K.E.; Ye, S.; McLaughlin, M.; Luning Prak, P.J.; Foley, M.P.; Kenttämaa, H.I.; Trulove, P.C.; Kilaz, G.; Xu, L.; Cowart, J.S. Analysis of Catalytic Hydrothermal Conversion Jet Fuel and Surrogate Mixture Formulation: Components, Properties, and Combustion. *Energy Fuels* **2017**, 31, 13802-13814.